

A GENERAL PATTERN FLOW THEORY FOR
MAXIMIZING WATERFLOODING RATES

by

CHRISTIAN E. HANSEN

ProQuest Number: 10794563

All rights reserved

INFORMATION TO ALL USERS

The quality of this reproduction is dependent upon the quality of the copy submitted.

In the unlikely event that the author did not send a complete manuscript and there are missing pages, these will be noted. Also, if material had to be removed, a note will indicate the deletion.



ProQuest 10794563

Published by ProQuest LLC (2018). Copyright of the Dissertation is held by the Author.

All rights reserved.

This work is protected against unauthorized copying under Title 17, United States Code
Microform Edition © ProQuest LLC.

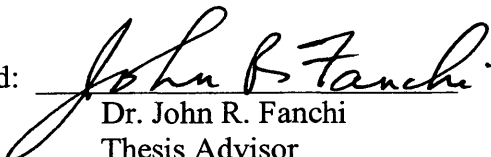
ProQuest LLC.
789 East Eisenhower Parkway
P.O. Box 1346
Ann Arbor, MI 48106 – 1346

A thesis submitted to the Faculty and the Board of Trustees of the Colorado School of Mines in partial fulfillment of the requirements for the degree of Master of Science (Petroleum Engineering).

Golden, Colorado


Date March 20, 2001

Signed: 
Christian E. Hansen

Approved: 
Dr. John R. Fanchi
Thesis Advisor

Golden, Colorado

Date March 20, 2001


Dr. Craig W. Van Kirk
Department Head,
Petroleum Engineering

ABSTRACT

This thesis unifies and completes the single-phase and non-unit mobility steady-state pattern flow theory by presenting new analytical relationships of pattern waterflooding that have not been demonstrated previously. These relationships are critical to understanding the absolute and relative flow performance of patterns in different rock-fluid (mobility) systems. These relationships show how the flow theory for injection patterns can be completed and generalized through an understanding of the mechanisms controlling pattern average reservoir pressures. It is shown how reservoir flow rates and pressures in repeated patterns after fillup (steady-state flow conditions) are governed by the pattern producer/injector ratio, P/I , and a newly defined total mobility ratio, M_T . These two variables are most important when comparing the flow capacities of different patterns, accounting for nearly all of the differences in flow capacity between different patterns within the same homogeneous, isotropic reservoir.

This thesis demonstrates for the first time how the flow capacity of patterns can vary significantly depending on the mobility ratio, and that there exists a pattern, or producer/injector ratio, that will provide maximum reservoir flow capacity relative to all other patterns for a given rock-fluid system. The producer/injector ratio providing maximum flow capacity can be found easily using the new equations. The results show that for total mobility ratios greater than one, the pattern providing the highest reservoir flow rate will have a producer/injector ratio greater than one, and vice-versa. It is shown how the skin effect translates as an adjustment to the producer/injector ratio, resulting in an *effective* producer/injector ratio, or \tilde{P}/\tilde{I} , which may be higher or lower than the physical P/I . As this thesis demonstrates, for any mobility ratio, pattern selection can have a significant effect on the flow rate, and therefore the economics of a project. The

difference in reservoir flow rates provided by the highest and lowest conductivity patterns can be particularly large for mobility ratios significantly higher or lower than unity.

The analytical equations are compared to numerical results, which show the validity of the new equations. Finally, a correlation between mobility ratio M and total mobility ratio M_T prior to water breakthrough based on numerical results is presented for a range of relative permeability curve shapes, for use in the new equations and designing the economically optimum pattern.

TABLE OF CONTENTS

	<u>Page</u>
ABSTRACT.....	iii
LIST OF FIGURES	viii
LIST OF TABLES	x
ACKNOWLEDGEMENTS	xi
1. INTRODUCTION	1
1.1 Background	1
1.2 Thesis Summary and Outline	6
2. LITERATURE REVIEW	8
3. IDEAL PATTERN RELATIONSHIPS.....	12
3.1 Average Reservoir Pressure in Ideal Patterns	12
3.2 Average Reservoir Pressure for Compressible Pattern Flow.....	17
3.3 Flow Relationships for Single-Phase (Unit-Total Mobility Ratio) Patterns.....	20
4. PATTERN RELATIONSHIPS FOR NON-UNIT TOTAL MOBILITY RATIO SYSTEMS.....	37
4.1 Average Reservoir Pressure in Non-Unit Total Mobility Ratio Patterns..	37
4.2 Flow Relationships for Non-Unit Total Mobility Ratio Patterns.....	42
4.3 Pressure and Flow Relationships Including the Skin Effect.....	46
4.4 Heterogeneous (Isotropic) Reservoirs.....	51

4.5 Anisotropic Reservoirs	52
5. APPLICATION OF NEW PATTERN RELATIONSHIPS TO DETERMINING THE HIGHEST CONDUCTIVITY PATTERN.....	54
5.1 Discussion of Methodology.....	54
5.2 Conductivity Relationship Including Skin.....	63
5.3 Conductivity Relationship in Heterogeneous, Isotropic Systems	65
5.4 Conductivity Ratio Versus Conductance Ratio.....	65
6. COMPARISON OF ANALYTICAL AND NUMERICAL PATTERN RELATIONSHIPS.....	67
6.1 Numerical Model Description.....	67
6.2 Calculating Effective Total Mobilities.....	68
6.3 Numerical vs. Analytical Results for $M = 0.20$ System.....	72
6.4 Numerical vs. Analytical Results for $M = 5.0$ System.....	79
6.5 Numerical vs. Analytical Results for $M = 0.20$ System Including Skin Effect.....	89
7. CORRELATION FOR TOTAL MOBILITY RATIO, M_T , PRIOR TO WATER BREAKTHROUGH VERSUS TOTAL MOBILITY RATIO, M	94
7.1 Description of Correlation Methodology.....	94
7.2 Correlation of M_T versus M Prior to Water Breakthrough.....	97
7.3 Consideration in Heterogeneous Reservoirs	102
8. CONCLUSIONS AND RECOMMENDATIONS.....	103
8.1 Conclusions.....	103
8.2 Recommendations.....	104

9. REFERENCES.....	105
10. APPENDIX A.....	107
11. APPENDIX B.....	123
12. APPENDIX C.....	125
13. APPENDIX D.....	134

LIST OF FIGURES

<u>Figure</u>	<u>Page</u>
3.1 Error of Eq. 3.2 when used for compressible systems versus total liquid compressibility and total system pressure drop.....	19
3.2 Inverted 9-spot pattern element of symmetry.....	22
3.3 R for equivalent side and corner well sand-face pressure vs. d/r_w	31
3.4 Dimensionless pressures of patterns at various well densities.....	35
5.1 Conductivity Ratio relationship for $M_T = 1.0$	58
5.2 Conductivity Ratio relationships for $M_T = 0.5$ and $M_T = 2.0$	60
5.3 Hybrid pattern with $P/I = 5:3$ or $3:5$	61
5.4 Conductivity Ratio relationships for $M_T = 0.2$ and $M_T = 5.0$	62
5.5 Conductivity Ratio relationships for $M_T = 0.2$, $M_T = 1.0$ and $M_T = 5.0$ where $S_{(inj)} = -2.0$ and $S_{(prod)} = 0.0$	64
6.1 41 x 41 2D simulation grid showing element of symmetry for inverted nine-spot pattern, with wells in corner cells.....	68
6.2 Graphical representation of effective total mobility calculation procedure for each pattern well.....	70
6.3 Relative permeability and total mobility relationship for $M = 0.2$ system.....	73
6.4 Total mobility ratio M_T and average effective injection total mobility $\bar{\lambda}_{Tj}$ for simulated patterns as determined from ring method for $M = 0.2$ system.....	74
6.5 Calculated vs. simulator average reservoir pressure for $M = 0.2$ patterns.....	76
6.6 Calculated vs. simulator reservoir flow rates for $M = 0.2$ patterns.....	77

6.7 Conductivity relationships for $M_T = 0.2$ & $M_T = 1.0$	78
6.8 Relative permeability and total mobility relationship for $M = 5.0$ system.....	80
6.9 Total mobility ratio M_T and average effective injection total mobility $\bar{\lambda}_{TI}$ for simulated patterns as determined from ring method for $M = 5.0$ system.....	81
6.10 Calculated vs. simulator average reservoir pressure for $M = 5.0$ patterns.....	83
6.11 Calculated vs. simulator reservoir flow rates for $M = 5.0$ patterns.....	84
6.12 Percent error in the value of \tilde{q} relative to percent error in $\bar{\lambda}_{TI}$ vs. M_T and P/I ...	86
6.13 Conductivity relationships for $M_T = 2.0$ & $M_T = 3.0$	88
6.14 41 x 41 2D simulation grid showing element of symmetry for inverted nine-spot pattern, showing skin effect applied to each pattern well.....	90
6.15 Total mobility ratio M_T , effective producer/injector ratio \tilde{P}/\tilde{I} , and average producing skin $S_{(prod)}$ as determined from numerical results for inverted nine-spot pattern with $M=0.2$ system.....	91
6.16 Calculated vs. simulator reservoir flow rates and average reservoir pressures for inverted nine-spot including skin for $M = 0.2$ system.....	93
7.1 Oil relative permeability curves as calculated from Eq. 7.1 for different m exponents, and water relative permeability as calculated from Eq. 7.2 for $n = 2$ (after Ref. 8).....	96
7.2 Average M_T before water breakthrough vs. M for oil relative permeability exponents $m=1$, $m=3$, and $m=5$	99
7.3 Average M_T before water breakthrough vs. M for oil relative permeability exponents $m=2$ and $m=4$	100

LIST OF TABLES

<u>Table</u>	<u>Page</u>
3.1 Geometry of Repeatable Injection Patterns (after Refs. 12 and 19)	14
3.2 Exact Expressions for Fully Developed Pattern Flow Rates (after Ref. 12).....	25
3.3 Pattern Dimensionless Pressures.....	29
3.4 $p_{D(9-spot)}$ as given by Eq. 3.20f for $d/r_w = 1500$ for various R values.....	32
7.1 Average M_T before water breakthrough vs. M for various oil relative permeability exponents m	98

ACKNOWLEDGEMENTS

I would like to thank my advisor, Dr. John Fanchi, for many helpful suggestions and guidance on various aspects of this thesis, and thesis committee, Dr. Erdal Ozkan and Dr. Robert Thompson for their support and helpful review. Also, thanks to Dr. Craig Van Kirk, for allowing me flexibility in meeting some of the course requirements for the Master of Science degree. Thanks are also due to my supervisor, Ken Boedeker, for his support and EOG Resources, Inc., for providing financial assistance towards this degree.

Thanks also go to teachers and colleagues, who over the years have helped me along my way and increased my understanding and appreciation of Petroleum Engineering. This list is sure to be inadequate, but must include Neil Humphreys (Mobil), R.F. Jackson (Mobil), Dr. Hossein Kazemi, Jeung Kim (Mobil), Steve Neuse (Bass Enterprises), Dr. Aziz Odeh (Mobil), Dr. Erdal Ozkan, A.W. Talash (Mobil). Gratitude should also be expressed to those that have made a tremendous influence through their writings, such as Dr. Morris Muskat, and Dr. G. Paul Willhite, who was also helpful in clarifying to me some aspects of his excellent text book on waterflooding.

Special appreciation is expressed to Duke Engineering & Services, Inc. (Calgary) and Alda Behie and Tony Settari for use of their black oil simulator (Terasim) to generate the numerical results presented in this thesis.

Finally, I would like to thank my parents, and my wife Gail, for always supporting and encouraging me in my pursuit of not only a Masters' degree, but also this thesis project, which has spanned more years than formal graduate studies at Mines. Thanks to my daughter Jennifer, who sacrificed indirectly from Dad being distracted more than he should have been when her own homework needed attention, and tying up the home computer.

CHAPTER ONE

INTRODUCTION

This thesis presents new relationships of pattern waterflooding that have not been demonstrated previously, but which are critical to understanding the absolute and relative flow performance of the various patterns in different rock-fluid (i.e. mobility) systems. These relationships show how the steady-state flow theory for injection patterns, or networks, can be completed and generalized through an understanding of the mechanisms controlling pattern average reservoir pressures. As discussed, the current two-phase pattern flow theory in the literature is incomplete, and the applicability of much of the analytical and experimental work to real reservoir systems is limited. This thesis fills a significant gap in the understanding of steady-state pattern flow behavior, especially as related to non-unit mobility ratio systems, showing how producer/injector ratio and a total mobility ratio control flow rates and reservoir pressures in waterflood patterns. The new equations apply to two-phase, steady-state, isotropic pattern flow systems of any mobility ratio, and include modifications for heterogeneity and skin effect.

This thesis also demonstrates for the first time how the reservoir flow capacity, or flux, provided by the different waterflooding patterns can vary significantly depending on the mobility ratio, and that a pattern providing maximum flow capacity exists for any rock-fluid system. The differences in flow capacity among the various patterns can be quantified easily using the equations presented.

Presented are the relationships for (1) the average reservoir pressure and (2) the individual injection well and producing well flowrates within any repeated, regularly-spaced pattern in any mobility system where the assumptions of steady-state, isotropic flow conditions apply. A normalized reservoir flow rate equation, given in terms of flow

rate per *pattern* well, or \tilde{q} , is derived which is used to demonstrate how total mobility ratio, M_T , (as defined in this thesis) and producer/injector ratio, P/I , are the two most important variables when comparing the flow capacities of different patterns within a given reservoir. A conductivity ratio is defined from the normalized flow equation that relates the reservoir flow capacities of two patterns, and which involves only these two variables. It is shown how the skin effect translates as an adjustment to the producer/injector ratio, resulting in an *effective* producer/injector ratio, or \tilde{P}/\tilde{I} , which may be higher or lower than the physical P/I . These relationships also include modifications for heterogeneous, isotropic reservoirs.

To aid in determining the most economic pattern in isotropic reservoirs, a correlation between the endpoint mobility ratio, M , and the total mobility ratio, M_T , is presented for the pre-breakthrough period, based on numerical results. Using the equations presented, the total mobility ratio derived from the correlation can be used to determine the flow rates and average pressures that will result from each of the patterns before water breakthrough. As discussed, this correlation also applies to heterogeneous, isotropic reservoirs if pore volume is homogeneous, and more approximately if pore volume is heterogeneous. The pre-breakthrough period usually has the most impact on the economics of a project, such that the optimum pattern for a project will often be the one that optimizes flow rate during this time period.

1.1 Background

The economics of a waterflooding project depend upon two primary variables which engineers must optimize when designing a waterflood scheme, (1) the total flow rate, or processing rate of the project, and (2) the amount of incremental oil recovered. Depending upon the characteristics of the reservoir, one of these variables can take a more dominant role in determining the economically optimum waterflooding pattern. For example, in reservoirs where there is a strong directional permeability component,

considerations of recovery will drive the pattern selection process because of the strong dependency of recovery on producer – injector orientation. Conversely, in reservoirs that can be considered isotropic or nearly so, optimizing the economics of the project will be driven primarily by optimizing the waterflooding flow rate, since ultimate recovery is dictated by the mobility ratio in these circumstances and not by pattern type. In both types of reservoirs, an adequate waterflooding recovery rate is paramount to an economically viable project.

However, when attempting to optimize (economically) the production rate of a waterflood project in reservoirs that can be considered isotropic, the current body of waterflooding literature is incomplete in providing the information needed to calculate and compare the flow performance of patterns in all mobility systems. Flow equations exist for “ideal” patterns, i.e. single-phase, homogeneous, isotropic, incompressible steady-state flow^{1,2}, which have also been referred to as unit-mobility systems, for virtually all of the patterns. However, the applicability of these single-phase equations is limited to a very small subset of reservoirs. A current misnomer in the literature is that “ideal” pattern equations can be applied to real reservoir systems if the endpoint mobility ratio, M , is equal to one as the sufficient criterion. As will be shown, the true condition that must exist to legitimately apply these equations is that the total mobility ratio, M_T , as defined here, is equal to one. This condition can exist in systems where M is other than one, and does not necessarily always exist when $M=1$, as shown in Chapter Seven. Only when $M_T=1$ can the single-phase equations be used with confidence.

The flow theory for non-unit total mobility systems is not nearly as well developed. Several investigators have studied non-unit mobility ratio pattern flow behavior using a variety of techniques²⁻⁸, with the five-spot being studied most frequently. These techniques have included a potentiometric model³, an X-ray shadowgraph study⁴, and a scaled flow model study⁵ of the five-spot pattern. Prats *et al.*⁶ used a potentiometric model with predetermined flood front shapes and presented corresponding mathematical formulas for predicting rates in a five-spot having an initial

gas saturation. Studies for other patterns are much less abundant. Caudle *et al.*⁷ used a flow model to study the flow performance and sweep efficiency of the skewed four-spot (seven-spot in a square well arrangement) at various mobility ratios. Hauber⁸ used the streamline concept and proposed analytical equations for the flow performance of the direct-line drive (and five-spot) patterns to show that the technique of Prats *et al.*⁶ could be extended to other patterns than the five-spot. In addition to the ideal nine-spot flow equation, Deppe² presented approximate equations for the five-spot and nine-spot patterns in non-unit mobility systems by using radial and linear flow segments to approximate the geometry of these patterns. Deppe² also shows porous-model flow study results for the nine-spot and compares these to the approximate flow equation. Other nine-spot studies have been limited to the investigation of recovery curves and sweep efficiencies⁹⁻¹¹, and not flow rates. It should be noted that all of the above methods²⁻⁸ assume an idealized displacement mechanism, i.e. there is no saturation gradient, and thus no mobility gradient within the swept region. This assumption is equivalent to the assumption of piston-like displacement, which can be valid for systems with mobility ratios much less than one, but which is a very poor assumption for mobility ratios greater than one. As shown by the correlation between M and M_T in Chapter Seven, in most cases there will be a saturation gradient in the swept region which is dependent on the shape of the relative permeability curves, even at low mobility ratios. Thus, applicability of these studies to real systems is very limited, if not invalid. Finally, none of the above studies compares the flow performance between any of the patterns with respect to mobility ratio.

Probably the most rigorous analytical treatment of non-unit mobility pattern flow is given by Willhite¹², where he presents approximate equations for non-unit mobility five-spot and line-drive patterns. Unlike previous works that discuss equations in non-unit mobility systems^{2,6,8}, Willhite considers not only piston-like displacement, but also non-piston-like displacement where there is two-phase flow behind the flood front. For the latter, he introduces a total mobility ratio, M_t , that is used to account for the mobility

gradient within the swept region. As will be shown, the total mobility ratio as defined in this thesis, M_T , is equivalent to Willhite's definition of M_i for the five-spot and line-drive patterns. However, the definition of M_i must be extended for the other patterns with producer/injector ratios other than one, and hence a new, extended definition is given in this thesis as M_T . Even though Willhite presents the most accurate method to calculate flow rates in non-unit mobility patterns, not all patterns are considered, and again, no flow performance comparisons are made between the patterns with respect to mobility ratio.

Other methods of predicting waterflooding behavior in non-unit mobility ratio, two-dimensional systems include numerical finite-difference simulation and analytical stream-tube methods¹³⁻¹⁸. These methods can account for the complete fractional flow behavior of patterns within any system without full analytical treatment. The drawback of these methods is that they do not provide the insight into the parameters governing the flow process that a representative analytical equation can provide. These simulation methods were introduced in the late 1950's and early 1960's, during the same period when much of the analytical and laboratory works on non-unit mobility systems were being pursued. It may be that these more powerful tools short-circuited the development of a more complete, analytical understanding of pattern flow behavior.

In summary, up to this point there is no consistent, unifying, analytical pattern theory that has been developed that can guide the engineer as to how the various patterns will perform in an absolute or relative sense under actual field conditions. There is no information in the literature as to which pattern will maximize the flow rate for a given mobility ratio system, and no analytical relationships that one can use to determine this. Currently, the only way to determine these relationships is through a trial and error process using reservoir simulation. To this author's knowledge, only Caudle *et al*⁷ and Craig¹⁹ hint that there should be a relationship between the producer/injector ratio and mobility ratio with respect to flow rates and pattern selection. Craig indicates that

mobility ratio is a “measure of the injectivity of a well relative to its productivity”, and that for $M > 1$, a pattern having more producers than injectors is indicated (and vice-versa), but provides no quantitative guidelines.

1.2 Thesis Summary and Outline

With this thesis, the single-phase and the non-unit mobility ratio pattern flow theory is unified and completed by showing the fundamental relationship between pattern producer/injector ratio, P/I , and a newly defined total mobility ratio, M_T , on pattern average reservoir pressures and flow rates. As will be seen, including the average pressure relationship into the flow derivation greatly simplifies the pattern flow equation, reducing all previously presented equations to a single flow relationship, either for injection wells or producing wells.

Using a normalized form of the new equation for the injection well flow rate, the producer/injector ratio that will provide the highest reservoir flow rate for any given total mobility ratio can be found easily. For total mobility ratios greater than one, the pattern providing the highest reservoir flow rate will have a producer/injector ratio greater than one, and vice-versa. At all mobility ratios, but especially when the mobility ratio is significantly higher or lower than unity, there is a substantial difference in the reservoir flow rates provided by the highest and lowest conductivity patterns. Thus, when designing a waterflood in an isotropic reservoir, it is important to understand the relationships presented here.

The theoretical presentation is divided into two sections in Chapters Three and Four. Chapter Three discusses the equations for “ideal” patterns, and develops foundational reservoir pressure and flow rate relationships. In Chapter Four, the single-phase equations are extended for non-unit total-mobility ratio systems and skin effect, along with a discussion on how the reservoir heterogeneity can be handled in the new equations. Chapter Five shows how the new relationships are applied to determine the producer/injector ratio that maximizes reservoir flow rate, for any given total mobility

ratio prior to water breakthrough. Chapter Six discusses how the total mobility ratio, M_T , is calculated and estimated, and compares numerical results from a reservoir simulator to the analytical equations for two different mobility ratio systems, $M=0.2$ and $M=5.0$, and also for the $M=0.2$ system including skin effect. In Chapter Seven, a correlation based on numerical results between mobility ratio (M) and total mobility ratio (M_T) prior to water breakthrough is presented for a range of relative permeability curve shapes, for use in the new equations and designing the economically optimum pattern. Chapter Eight summarizes the conclusions and recommendations of this thesis. Finally, an example illustrating the calculation procedures is presented in Appendix C.

CHAPTER TWO

LITERATURE REVIEW

The flow theory of waterflooding networks, or patterns, extends back to Muskat¹, who first developed exact expressions for the flow rate of the five-spot, direct and staggered line-drives, and hexagonal seven-spot patterns. Muskat's equations are limited to the assumptions of "ideal" patterns, that is, a single-phase, incompressible fluid of constant viscosity flowing in a horizontal, homogeneous and isotropic reservoir at steady-state conditions. Deppé² later presented the equation for the ideal nine-spot pattern following the method of Muskat. As shown in Chapter Seven, only in cases where the *total* mobility ratio M_T is unity can these single-phase equations be applied legitimately. For most cases these equations are inadequate for predicting flow rates in two-phase waterflooding patterns.

For non-unit mobility ratio, two-phase systems, the current waterflooding theory is limited. Several investigators have studied the variation in fluid injectivities before and after water breakthrough using a variety of techniques, mostly for the five-spot pattern. These techniques have included a potentiometric model³, a porous flow model using miscible oils⁴, and electrical resistance networks⁵ for the five-spot. Prats *et al.*⁶ used a potentiometric model with predetermined flood front shapes and presented corresponding mathematical formulas for predicting rates in a five-spot having an initial gas saturation. Other pattern studies are not as common. Caudle *et al.*⁷ used a flow model to study the flow performance and sweep efficiency of the skewed four-spot (seven-spot in a square well arrangement) at various mobility ratios. They reported that the sweep efficiency of the skewed four-spot is comparable to the five-spot for $M > 3.0$, but did not compare flow rate performance of these patterns for different mobility systems. Hauber⁸ used the

streamline concept and proposed analytical equations for the flow performance of the direct-line drive (and five-spot) patterns to show that the technique of Prats *et al.*⁶ could be extended to patterns other than the five-spot. Again, the flow performance of these patterns was not compared. As Craig¹⁹ states in his overview of the above laboratory studies³⁻⁵, all investigators found the same qualitative effects. That is, at “favorable mobility ratios ($M < 1$), the fluid injectivity declines as areal sweep increases, and at unfavorable mobility ratio ($M > 1$), fluid injectivity increases as areal sweep increases as complete areal coverage is approached”. This observation is consequence of one of the key assumptions used in these studies, i.e. an idealized displacement mechanism, where there is constant mobility within the swept region. This is equivalent to the piston-like displacement assumption, where the displacing fluid fully displaces the fluid being displaced. As discussed in Chapter One, this is a poor assumption in most cases. In most reservoir systems, there will be a saturation gradient, and thus a mobility gradient, within the swept region that is dependent on the shape of the relative permeability curves, even at low mobility ratios. As shown by the numerical results in Chapter Six, a marked decrease in flow rates occurs at water breakthrough for the $M=5.0$ system (does not continually increase) because of two-phase flow effects causing a reduced total mobility at the producing wells.

A flow model study by Rapoport *et al.*²⁰ includes the relative permeability effects in their study of the five-spot pattern, but addressed only sweep efficiency behavior and not flow rate variation as related to mobility ratio.

Deppe², in addition to the ideal nine-spot flow equation, presented approximate equations for the five-spot and nine-spot patterns in non-unit mobility, two-phase systems by using radial and linear flow segments to approximate the geometry of these patterns. Porous-model flow study results are also shown for the nine-spot and compared to the approximate flow equation. The relative flow performance of the five-spot and nine-spot as a function of mobility ratio are not investigated.

The works cited above²⁻⁸ all share the same deficiencies in that the effects of relative permeability and saturation gradients behind the flood front are not considered. This makes the direct, quantitative application of these results to real waterflood systems unclear. Also, most of these works are for flow predictions in a five-spot pattern, and no information in these studies is provided by which one may determine the relative flow performance between these patterns.

Willhite¹² also presents approximate equations for non-unit mobility five-spot and line-drive patterns. Unlike previous works^{2,6,8}, he considers both piston-like displacement and non-piston-like displacement where there is two-phase flow behind the flood front. For the latter, he introduces a total mobility ratio, M_t , that is used to account for the mobility gradient within the swept region. As will be shown, the total mobility ratio as defined in this thesis, M_T , is equivalent to Willhite's definition of M_t for the five-spot and line-drive patterns. However, the definition of M_t must be extended for the other patterns with producer/injector ratios other than one, and hence a new, extended definition is given in this thesis as M_T .

To this author's knowledge, one of the only studies comparing the flow rate performance of patterns is reported by Ziegler²¹. In this paper, the performance of the five-spot pattern and inverted nine-spot pattern for a steamflooding application in a homogeneous, heavy oil reservoir, are compared. Using a reservoir simulator, Ziegler found that oil recovery is accelerated using the inverted nine-spot compared to the five-spot on a reservoir basis for equal well spacing. These results are consistent with the results presented in this thesis, i.e. at mobility ratios greater than one (mobility ratios for heavy oil development are typically much greater than one) the producer/injector ratio providing the greatest reservoir flow rate will also be greater than one.

Up to this point it seems that the only tool available for engineers to determine the pattern providing maximum flow rate in a given mobility system is through a trial and error process using reservoir simulation. That is, only if one recognizes that the flow

performance between patterns can vary significantly depending on the characteristics of the reservoir system, which is not explained in the current waterflooding literature. Numerical and analytical¹³⁻¹⁸ simulation has been used for many years. Unlike many of the non-unit mobility flow equations currently available, these models can incorporate the effects of relative permeability and thus mobility variation in determining the flow performance of waterflood patterns. What these models fail to provide, however, is insight into the mechanisms controlling the flow process. This understanding is more readily conveyed through analytical flow equations that adequately represent the physical mechanisms involved. This understanding is provided by the equations of this thesis, which include the parameters needed to determine the relative and absolute performance of patterns.

To this author's knowledge, only Caudle *et al*⁷ and Craig¹⁹ hint that there should be a relationship between the producer/injector ratio and mobility ratio with respect to maximizing reservoir rates. For example, Craig indicates that mobility ratio is a "measure of the injectivity of a well relative to its productivity", and that for $M > 1$, a pattern having more producers than injectors is indicated (and vice-versa), but provides no quantitative guidelines.

CHAPTER THREE

IDEAL PATTERN RELATIONSHIPS

In this chapter, new “ideal” pattern relationships are presented for (1) the average reservoir pressure and (2) individual injection and producing well flow rates in repeated, regularly spaced patterns. These relationships will form the foundation for the non-unit mobility equations presented in Chapter Four. The assumptions of ideal pattern flow were first given by Muskat¹, which are a single-phase, incompressible fluid of constant viscosity flowing at steady-state conditions in a horizontal, homogeneous and isotropic reservoir. It is important to note that the assumption of single-phase flow in ideal patterns has also been referred to in the literature as being equivalent to the unit-mobility assumption, referring to the endpoint mobility ratio (M) being equal to one. As will be shown, this is not a sufficient condition to legitimately apply ideal pattern equations to two-phase systems. The sufficient condition is that the *total* mobility ratio, M_T , as defined in this thesis, is equal to one to be able to apply ideal pattern equations.

3.1 Average Reservoir Pressure in Ideal Patterns

In this section, a new equation for the average reservoir pressure in ideal patterns is introduced. Fluid flow in ideal patterns is governed by Laplace’s Equation¹, given by

$$\frac{\partial^2 p}{\partial x^2} + \frac{\partial^2 p}{\partial y^2} + \frac{\partial^2 p}{\partial z^2} = 0. \quad (3.1a)$$

The general solution of Laplace's equation in a two-dimensional, radial flow system is given by¹

$$p(r) = \frac{q\mu}{2\pi kh} \ln(r) + c, \quad (3.1b)$$

where c is a constant. As shown in Appendix A, the average reservoir pressure within uniformly spaced ideal patterns is given by

$$\bar{p}_{pat} = \frac{\sum_{i=1}^n f_i p_{wf(i)}}{\sum_{i=1}^n f_i}, \quad (3.2a)$$

where

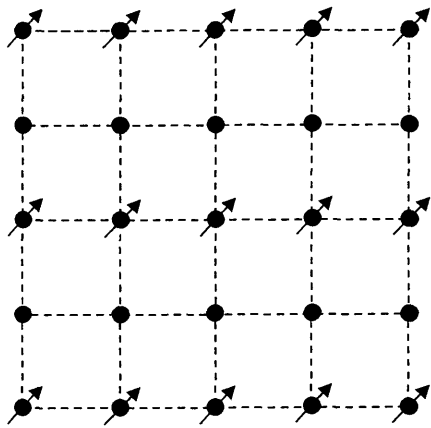
f_i = representation of element well as a fraction of total pattern wells represented by pattern element, and

$p_{wf(i)}$ = sandface pressure for each of n pattern element wells.

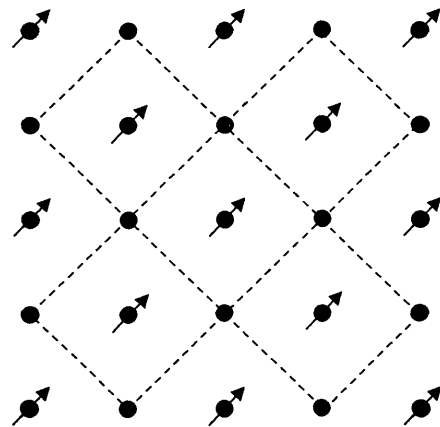
The precise definition of a uniformly spaced pattern is given in Appendix A as any pattern where an element of symmetry can be drawn where the geometric relationship between the element area and *all* of the element wells is the same. This definition thus includes any square or rectangular patterns such as the five-spot, direct and staggered-line-drives, the nine-spot, and also the hexagonal seven-spot pattern. This definition excludes the skewed four-spot, however in practicality Eq. 3.2a would very

closely approximate the average reservoir pressure for this pattern. Table 3.1 shows the well geometry for the various patterns.

Table 3.1 – Geometry of Repeatable Injection Patterns (after Refs. 12 and 19)



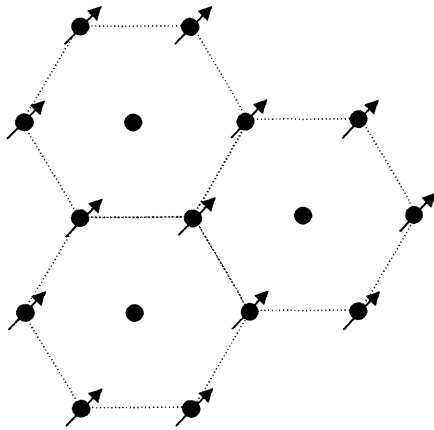
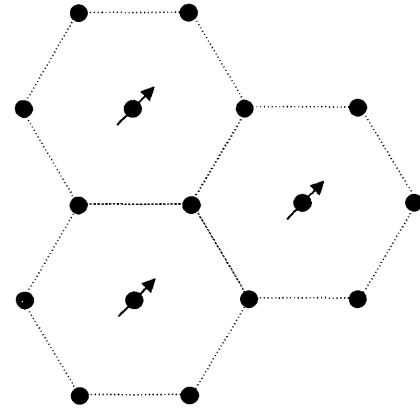
Direct Line-Drive $d/a = 1.0$ ($P/I = 1.0$)



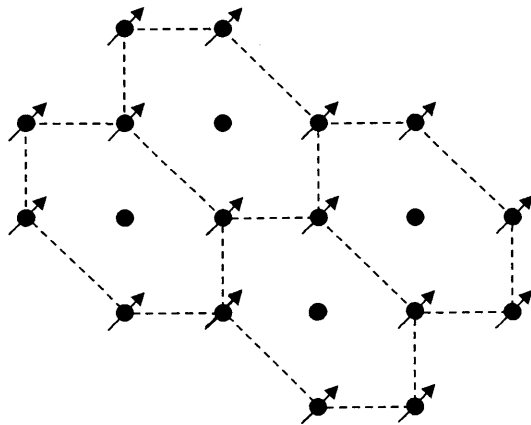
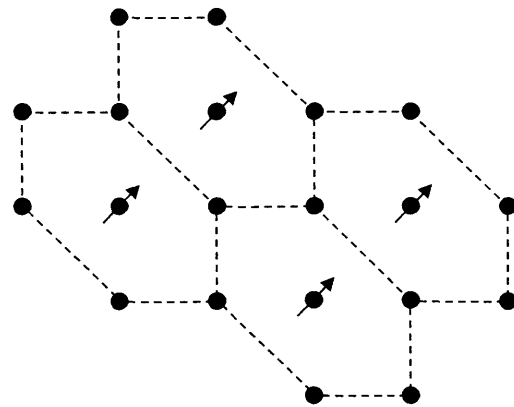
Five-Spot Pattern ($P/I = 1.0$)

(continued)

Table 3.1 (continued)

Normal Seven-Spot ($P/I = 1:2$)Inverted Seven-Spot ($P/I = 2:1$)

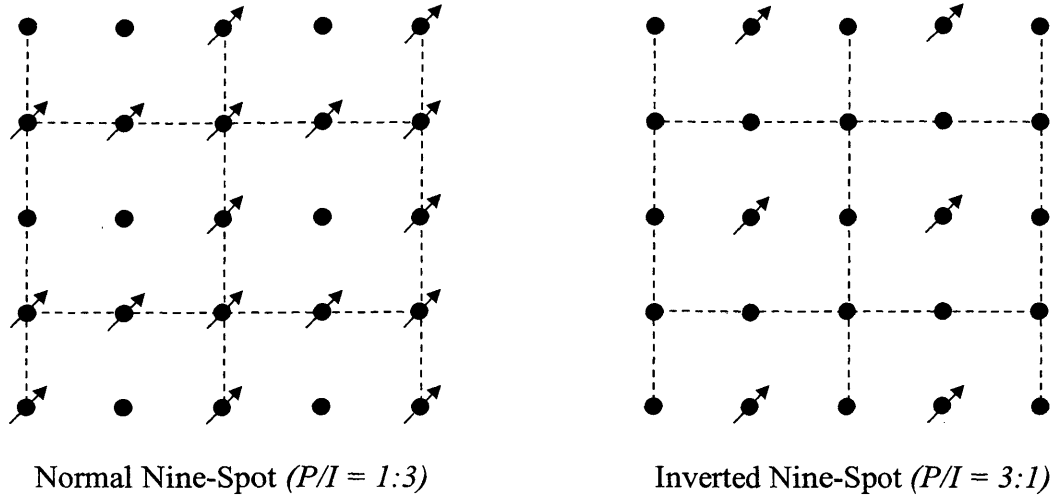
Hexagonal Well Arrangements (also known as regular four-spots)

Normal Seven-Spot ($P/I = 1:2$)Inverted Seven-Spot ($P/I = 2:1$)

Square Well Arrangements (also known as skewed four-spots)

(continued)

Table 3.1 (continued)



A more useful form of Eq. 3.2a can be expressed as

$$\bar{p}_{pat} = \frac{p_{wfl} + P/I(p_{wfp})}{1 + P/I}, \quad (3.2b)$$

where (see Appendix A for exact definitions)

\bar{p}_{pat} = average reservoir pressure of pattern,

p_{wfl} = weighted average injection well sand-face pressure,

p_{wfp} = weighted average production well sand-face pressure, and

P/I = pattern producer/injector ratio, dimensionless.

3.2 Average Reservoir Pressure for Compressible Pattern Flow

We can show that the average pressure equation can be used for compressible systems with little error for oil-water systems. For compressible systems, the governing equation is the diffusion equation¹:

$$\frac{\partial^2 \rho}{\partial x^2} + \frac{\partial^2 \rho}{\partial y^2} + \frac{\partial^2 \rho}{\partial z^2} = \frac{\phi \mu c}{k} \frac{\partial \rho}{\partial t} \quad (3.3)$$

For steady-state compressible flow, $\frac{\partial \rho}{\partial t} = 0$, and hence the right side of Eq. 3.3 is set to zero. Then we have the form of the Laplace equation in terms of densities instead of pressures. Therefore, the corresponding equation for the average density in a compressible, unit-total mobility ratio pattern is

$$\bar{\rho}_{pat} = \frac{\rho_{wf} + P/I(\rho_{wfp})}{1 + P/I} \quad (3.4)$$

Since the density relationship used in the derivation of Eq. 3.3, $\rho = \rho_0 e^{cp}$, can be well approximated by $\rho = \rho_0(1 + c\Delta p)$ for liquid-type compressibilities, we see that pressure and density are approximately linearly related. Because of this linear relationship, the average pattern pressure for compressible liquid systems can then be determined as the pressure corresponding to the average pattern fluid density, that is

$$\bar{p}_{pat} = 1/c \times \ln(\rho_{pat} / \rho_0) \quad (3.5)$$

For example, a unit-mobility inverted nine-spot pattern is operating with a sand-face injection pressure of 4800 psig, and producing well sand-face pressures of 300 psig, the average reservoir pressure according to Eq. 3.2a is

$$\bar{p}_{pat} = \frac{4800 + 3.0(300)}{1 + 3.0} = 1425 \text{ psig.}$$

Using a fluid density of 55.0 lb/cu.ft at 14.65 psia, with an average compressibility of $15 \times 10^{-6} \text{ psi}^{-1}$, we calculate the fluid densities at the injectors and producers using the injection and production sand-face pressures from the relationship $\rho = \rho_0 e^{cp}$ as follows:

Injectors:

$$\rho_{injectors} = 55.0 \times \exp(0.000015(4800)) = 59.10604 \text{ lb/cu ft}$$

Producers:

$$\rho_{producers} = 55.0 \times \exp(0.000015(300)) = 55.24806 \text{ lb/cu ft}$$

Therefore, the pattern average fluid density is calculated from Eq. 3.4 as follows:

$$\bar{\rho}_{pat} = \frac{59.10604 + 3.0(55.24806)}{1 + 3.0} = 56.21255 \text{ lb/cu ft.}$$

The pressure corresponding to this density is the average pattern pressure, calculated from Eq. 3.5 as:

$$\bar{p}_{pat} = 1 / 0.000015 \times \ln(56.21255 / 55.0) = 1453.8 \text{ psig.}$$

The average pressure in a compressible system will always be higher than in an incompressible system. Fig. 3.1 shows the error to be expected by using Eq. 3.2 to calculate the average reservoir pressure in compressible liquid systems.

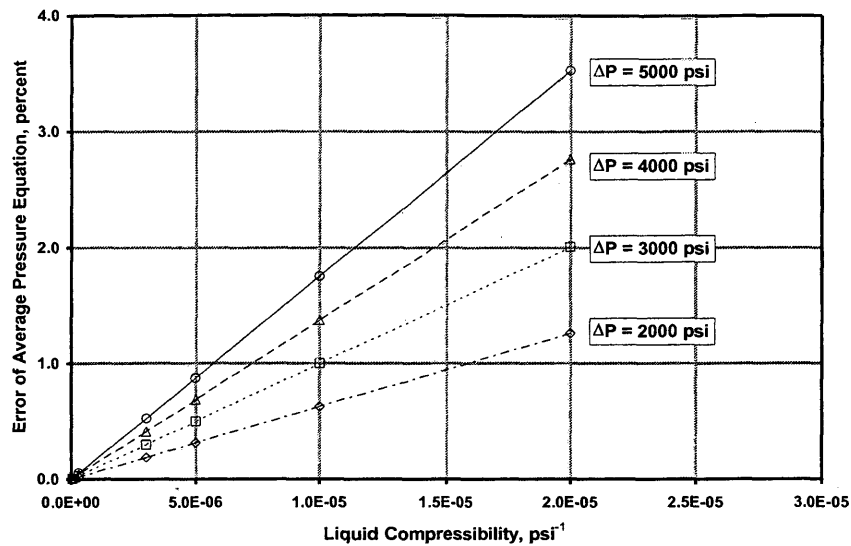


Fig. 3.1 – Error of Eq. 3.2 when used for compressible systems versus total liquid compressibility and total system pressure drop.

Note that the error of Eq. 3.2 increases with increasing total liquid compressibility and increasing total pressure drop, but for the range of compressibility typically found in oil-water systems (less than 2.0 E-5), Eq. 3.2 is still quite good, being within a few percent typically. Thus, the average pressure equation involving well pressures (Eq. 3.2) is quite

adequate for compressible waterflooding systems, and will be used as the basis for further discussions.

3.3 Flow Relationships for Single-Phase Flow (Unit-Total Mobility Ratio) Patterns

The flow equations for unit-*total* mobility ratio patterns will now be derived using the average reservoir pressure relationship (Eq. 3.2b) to a more general expression involving dimensionless pressures. In Chapter Four, the new equations will be expanded for non-unit total-mobility pattern flow, skin effect, and heterogeneous isotropic flow. These relationships are technically for incompressible liquids, but since the error due to liquids of small compressibility is small as shown above, the issue of compressibility will be ignored in the discussions that follow.

To begin, Eq. 3.2b can be written in the following form:

$$\frac{P_{wfl} - \bar{P}_{pat}}{\bar{P}_{pat} - P_{wfP}} = P / I . \quad (3.6a)$$

For steady-state pattern flow, the following identity also holds true (flowrates are in reservoir bbl/day):

$$P / I = \frac{\bar{q}_{inj}}{\bar{q}_{prod}} . \quad (3.6b)$$

Combining Eq. 3.6a and Eq. 3.6b, we can write

$$\frac{P_{wfl} - \bar{P}_{pat}}{\bar{P}_{pat} - P_{wfP}} = \frac{\bar{q}_{inj}}{\bar{q}_{prod}} . \quad (3.6c)$$

A dimensionless pressure group for steady-state pattern flow based on average reservoir pressure is defined here as:

$$P_{D(SS)} = \frac{kh}{141.2q_{ref}\mu} \Delta\bar{P}_{ref}, \quad (3.7)$$

where $\Delta\bar{P}_{ref}$ is the difference between the average reservoir pressure and well pressure, or the reference pressure drop, and q_{ref} is the reference flowrate in *reservoir* barrels per day.

As an example, Fig. 3.2 shows an element of symmetry for the inverted nine-spot pattern. The following relationships can be written for each pattern well based on Eq. 3.7:

The equation for the injector is:

$$\Delta\bar{P}_{well1} = p_{wf1} - \bar{p}_{pat} = P_{D(well1)} q_{well1} \frac{141.2\mu}{kh}. \quad (3.8a)$$

The equations for the producers are:

$$\Delta\bar{P}_{well2} = \bar{p}_{pat} - p_{wf2} = P_{D(well2)} q_{well2} \frac{141.2\mu}{kh}, \quad (3.8b)$$

$$\Delta\bar{P}_{well3} = \bar{p}_{pat} - p_{wf3} = P_{D(well3)} q_{well3} \frac{141.2\mu}{kh}, \quad (3.8c)$$

and

$$\Delta\bar{P}_{well4} = \bar{p}_{pat} - p_{wf4} = P_{D(well4)} q_{well4} \frac{141.2\mu}{kh}. \quad (3.8d)$$

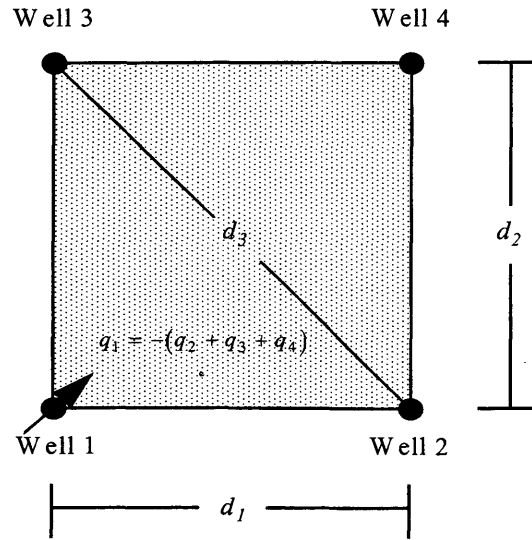


Fig. 3.2 – Inverted 9-spot pattern element of symmetry.

Note that the flow rate terms are positive since all pressure drops are expressed in the direction from injector to producer. Summing the producing well terms (Eqs. 3.8b, 3.8c, and 3.8d) we have:

$$3\bar{p}_{pai} - (p_{wf2} + p_{wf3} + p_{wf4}) = 141.2 \frac{\mu}{kh} (p_{D(\text{well}2)} q_{\text{well}2} + p_{D(\text{well}3)} q_{\text{well}3} + p_{D(\text{well}4)} q_{\text{well}4}) \quad (3.8e)$$

Rearranging Eq. 3.8e, we can write

$$\bar{p}_{pai} - \frac{(p_{wf2} + p_{wf3} + p_{wf4})}{3} = 141.2 \frac{\mu}{kh} \frac{(p_{D(\text{well}2)} q_{\text{well}2} + p_{D(\text{well}3)} q_{\text{well}3} + p_{D(\text{well}4)} q_{\text{well}4})}{3}. \quad (3.8f)$$

The average flowing sand-face pressure of the producing wells has been previously defined for Eq. 3.2b (see Appendix A) as

$$P_{wfP} = \frac{(P_{wf2} + P_{wf3} + P_{wf4})}{3}. \quad (3.9a)$$

The average dimensionless pressure-rate product of the producing wells is now defined as

$$P_{D(prod)} \bar{q}_{prod} = \frac{(P_{D(well2)} q_{well2} + P_{D(well3)} q_{well3} + P_{D(well4)} q_{well4})}{3}. \quad (3.9b)$$

Thus, we can write the following relationship for the producing wells by incorporating Eq. 3.9a and Eq. 3.9b into Eq. 3.8f:

$$\bar{P}_{pat} - P_{wfP} = P_{D(prod)} \bar{q}_{prod} 141.2 \left(\frac{\mu}{kh} \right)_{prod}. \quad (3.10a)$$

A similar expression can be obtained for the injection wells (in this case there is only one injector for the inverted nine-spot) as

$$P_{wfI} - \bar{P}_{pat} = P_{D(inj)} q_{inj} 141.2 \left(\frac{\mu}{kh} \right)_{inj}. \quad (3.10b)$$

Note that for a normal nine-spot pattern (or any normal pattern), the forms of Eq. 3.10a and Eq. 3.10b would be

$$\bar{P}_{pat} - P_{wfP} = P_{D(prod)} q_{prod} 141.2 \left(\frac{\mu}{kh} \right)_{prod} \quad (3.10c)$$

and

$$P_{wfl} - \bar{P}_{pat} = P_{D(inj)} \bar{q}_{inj} 141.2 \left(\frac{\mu}{kh} \right)_{inj}, \quad (3.10d)$$

respectively, where the equations are simply modified to show that there is a single producer (shown as single rate) and more than one injector (shown as an average rate) in the pattern. Dividing Eq. 3.10a into 3.10b and equating with Eq. 3.6c, we obtain

$$\frac{P_{wfl} - \bar{P}_{pat}}{\bar{P}_{pat} - P_{wfP}} = \frac{q_{inj}}{\bar{q}_{prod}} = \frac{P_{D(inj)} q_{inj} \left(\frac{\mu}{kh} \right)_{inj}}{P_{D(prod)} \bar{q}_{prod} \left(\frac{\mu}{kh} \right)_{prod}} = \frac{P_{D(inj)} q_{inj}}{P_{D(prod)} \bar{q}_{prod}}. \quad (3.11)$$

Since by definition the mobility of the injection well is equal to the mobility of the producing wells, we can easily deduce that

$$P_{D(prod)} = P_{D(inj)}. \quad (3.12)$$

That is, the “average” dimensionless pressure based on the definitions found in Eq. 3.7 and Eq. 3.9b for the injectors and producers are equivalent for ideal patterns of uniform spacing. This is a very important result as will be shown in the subsequent pattern derivations.

As shown by Willhite¹², the pattern flow rates for regular patterns in a single-phase, or unit-total mobility ratio (incompressible) system are given by the following

exact equations (using millidarcies here instead of darcies for permeability units) after Muskat¹ and Deppe² as shown in Table 3.2.

Table 3.2 – Exact Expressions for Fully Developed Pattern Flow Rates (after Ref. 12)

Direct Line-Drive and Staggered Line-Drive¹:

$$q = \frac{0.003541kh(\Delta P)}{\mu \left(\ln \frac{a}{r_w} + 1.571 \frac{d}{a} - 1.838 \right)} \quad (3.13a)$$

for $d/a \geq 1$.

Five-Spot¹:

$$q = \frac{0.003541kh(\Delta P)}{\mu \left(\ln \frac{d}{r_w} - 0.619 \right)} \quad (3.13b)$$

Seven-Spot¹:

$$q = \frac{0.00472kh(\Delta P)}{\mu \left(\ln \frac{d}{r_w} - 0.569 \right)} \quad (3.13c)$$

(continued)

Table 3.2 (continued)

Nine-Spot²:

$$q = \frac{0.003541kh(\Delta P_{i,c})}{\frac{1+R}{2+R} \left(\ln \frac{d}{r_w} - 0.272 \right) \mu} \quad (3.13d)$$

or

$$q = \frac{0.007082kh(\Delta P_{i,s})}{\left[\frac{3+R}{2+R} \left(\ln \frac{d}{r_w} - 0.272 \right) - \frac{0.693}{2+R} \right] \mu} \quad (3.13e)$$

where

d = inter-well distance or distance between well rows for line-drive patterns, feet

a = inter-well distance between wells within the same row for line-drive, feet

R = ratio of producing rate of corner well to side well for nine-spot

$\Delta P_{i,c}$ = pressure difference between center well and corner well for nine-spot, psi

$\Delta P_{i,s}$ = pressure difference between center well and side well for nine-spot, psi

*Note that for equivalent well density, d for the hexagonal seven-spot must be 1.0745 times d for the five-spot and nine-spot patterns.

It is important to remember that the rates calculated with the above equations are the injection well rates for inverted patterns, or the production well rates for normal

patterns. For the five-spot and line-drive patterns the producer/injector ratio is unity and there is no difference in the flow rates of producers and injectors.

Using the above exact equations and Eqs. 3.10a – 3.10e, we can now derive new, more general relationships for pattern flow rates in unit-total mobility systems that will provide the groundwork for non-unit total mobility pattern flow relationships. We begin with inverted patterns to calculate the injection rate of the injector. Taking a rearranged form of Eq. 3.10b and the five-spot flow equation Eq. 3.13b, and equating the relationships for the injection well flow rate, we obtain

$$q_{inj} = \frac{0.003541kh(\Delta P)}{\mu \left(\ln \frac{d}{r_w} - 0.619 \right)} = \frac{kh(p_{wfl} - \bar{p}_{pat})}{141.2 p_{D(inj)} \mu} . \quad (3.14)$$

From Eq. 3.2b, we can show that

$$p_{wfl} - \bar{p}_{pat} = \frac{P/I}{1 + P/I} \Delta P \quad (3.15a)$$

where

$$\Delta P = p_{wfl} - p_{wp} . \quad (3.15b)$$

Therefore, Eq. 14 is rewritten as

$$q_{inj} = \frac{0.003541kh(\Delta P)}{\mu \left(\ln \frac{d}{r_w} - 0.619 \right)} = \frac{kh(\Delta P)}{141.2 p_{D(inj)} \mu} \times \frac{P/I}{1 + P/I} . \quad (3.16)$$

For the five-spot, producer/injector ratio is 1.0. Substituting and solving for the dimensionless pressure term $p_{D(inj)}$ we obtain

$$p_{D(inj)} = \ln \frac{d}{r_w} - 0.619. \quad (3.17)$$

Thus, the new expression for the injection well rate in a five-spot pattern based on the definition of Eq. 7 becomes:

$$q_{inj} = \frac{P/I}{1+P/I} \times \frac{kh(\Delta P)}{141.2 \left(\ln \frac{d}{r_w} - 0.619 \right) \mu}. \quad (3.18)$$

In a similar way, it can be shown that the following general expression applies for the injection well flow rate in any inverted pattern:

$$q_{inj} = \frac{P/I}{1+P/I} \times \frac{kh(\Delta P)}{141.2 p_{D(inj)} \mu}, \quad (3.19)$$

where the dimensionless pressure functions of each pattern are shown below in Table 3.3. Note again from Eq. 3.12 that the dimensionless pressures for injection and production are equal for the definition of p_D found in Eq. 3.7.

 Table 3.3 – Pattern Dimensionless Pressures

Five Spot:

$$P_{D(inj)} = P_{D(prod)} = \ln \frac{d}{r_w} - 0.619 \quad (3.20a)$$

Direct Line Drive and Staggered Line Drive:

$$P_{D(inj)} = P_{D(prod)} = \ln \frac{a}{r_w} + 1.571 \frac{d}{a} - 1.838 \quad (3.20b)$$

Seven-Spot:

$$P_{D(inj)} = P_{D(prod)} = \ln \frac{d}{r_w} - 0.569 \quad (3.20c)$$

Nine-Spot:

$$P_{D(inj)} = P_{D(prod)} = \frac{3}{4} \left[\left(\frac{3+R}{2+R} \right) \left(\ln \frac{d}{r_w} - 0.272 \right) - \frac{0.693}{2+R} \right] \quad (3.20d)$$

for $\Delta P = \Delta P_{i,s}$ = pressure difference between center well and side well,

or

$$P_{D(inj)} = P_{D(prod)} = \frac{3}{2} \left[\left(\frac{1+R}{2+R} \right) \left(\ln \frac{d}{r_w} - 0.272 \right) \right] \quad (3.20e)$$

for $\Delta P = \Delta P_{i,c}$ = pressure difference between center well and corner well.

Since the difference between the sand-face pressure of the injectors and producers is defined from Eq. 3.2b as the weighted average, i.e. $\Delta P = p_{wfl} - p_{wfp}$, we see that the definitions of dimensionless pressure in Eq. 3.20d and Eq. 3.20e are based on different pressure drop terms, $\Delta P_{i,c}$ and $\Delta P_{i,s}$. Therefore, we need to write a nine-spot dimensionless pressure that is consistent with Eq. 3.2b, which uses weighted average sand-face pressures (see also Eq. 3.15b). As shown in Appendix B, this dimensionless pressure is

$$p_{D(inj)} = p_{D(prod)} = \ln \frac{d}{r_w} - 0.272 - \frac{1}{2} \times \frac{0.693}{2 + R}, \quad (3.20f)$$

for $\Delta P = p_{wfl} - p_{wfp}$ = pressure difference of weighted average injection and producing sand-face pressures.

As given above, R in Eqs. 3.20d – 3.20f is the ratio of corner-to-side well rates. The dimensionless pressures according to Eq. 3.20d and Eq. 3.20e are very sensitive to the value of R , varying by as much as a factor of two for extreme values of R . These definitions require knowledge of only one well pressure, either the corner or side well sand-face pressure. From inspection, it can be seen that the dimensionless pressure given by Eq. 3.20f is very insensitive to R , varying by less than 1.6% for even extreme values of R . However, the sand-face pressure in both the corner and side wells must be known to use this definition. Note that in formulating the definition of Eq. 3.20f, it was necessary to know how side and corner well pressures must be averaged to be consistent with the average reservoir pressure relationship of Eq. 3.2b (see Appendix B). In fact, what is actually being included indirectly by Eqs. 3.20d and 3.20e is the average reservoir pressure and its effect on flow rate, while this effect has been extracted from the dimensionless pressure given by Eq. 3.20f.

If we specify that the sand-face pressures of the corner and side wells are equivalent, then the value of R for any value of d/r_w is given by

$$R = \frac{-0.693}{\ln \frac{d}{r_w} - 0.272} + 1. \quad (3.20g)$$

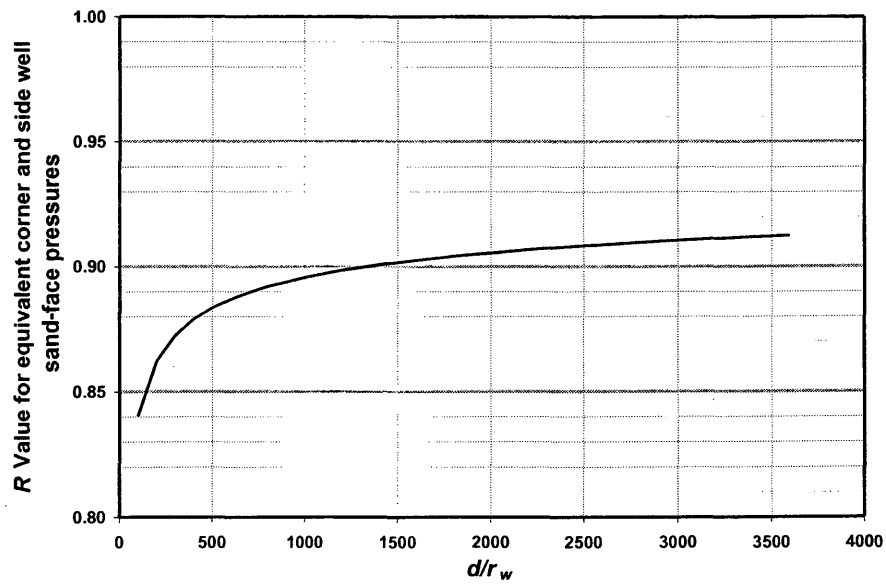


Fig. 3.3 – R for equivalent side and corner well sand-face pressures vs. d/r_w .

This result was obtained by equating the two forms of the nine-spot flow equation (Eqs. 3.13d and 3.13e) with the pressure drop terms being equivalent and solving for R . Figure 3.3 shows how R varies with d/r_w based on Eq. 20g. Note that a value of about 0.91 can be used with excellent accuracy for typical values of d/r_w .

Table 3.4 shows the dimensionless pressure calculated with Eq. 20f for $d/r_w = 1500$ at various values of R . Also shown is the relative difference from the first value of the table, namely $R = 0.9016$ for equivalent side and corner sand-face pressures as given by Eq. 20g. Table 3.4 demonstrates that dimensionless pressure for the nine-spot is insensitive to the value of R .

Table 3.4 – $p_{D(9-spot)}$ as given by Eq. 3.20f for $d/r_w = 1500$ for various R values.

R	$P_{D(9-spot)}$	<i>Relative Value</i>
0.9016	7.546601	1
1	7.550518	1.000519
2	7.579393	1.004345
5	7.616518	1.009265
10	7.637143	1.011998
1000	7.665672	1.015778
0.001	7.492855	0.992878
0.1	7.501018	0.99396
0.2	7.508518	0.994954
0.5	7.527418	0.997458

Using a similar approach as that used for inverted patterns, Eq. 3.19 is also valid to calculate the *average* injection well rate in normal patterns. Again, equating a modified form of Eq. 3.10c and Eq. 3.13b for the five-spot we have

$$q_{prod} = \frac{0.003541kh(\Delta P)}{\mu \left(\ln \frac{d}{r_w} - 0.619 \right)} = \frac{kh(\bar{p}_{pat} - p_{wfp})}{141.2 P_{D(prod)} \mu}. \quad (3.21)$$

From Eq. 3.2b, we can also show that

$$\bar{p}_{pat} - p_{wfp} = \frac{1}{1 + P/I} \Delta P. \quad (3.22)$$

Therefore, Eq. 3.21 is rewritten as

$$q_{prod} = \frac{0.003541kh(\Delta P)}{\mu \left(\ln \frac{d}{r_w} - 0.619 \right)} = \frac{kh(\Delta P)}{141.2 P_{D(prod)} \mu} \times \frac{1}{1 + P/I}. \quad (3.23)$$

Again solving for the dimensionless pressure for the five-spot where $P/I = 1.0$, we obtain the same result as the solution for the injection rate (Eq. 3.17). This result was also indicated by Eq. 3.12:

$$P_{D(prod)} = \ln \frac{d}{r_w} - 0.619. \quad (3.24)$$

Therefore, the general expression for the producing well flowrate in any normal pattern is:

$$q_{prod} = \frac{1}{1 + P/I} \times \frac{kh(\Delta P)}{141.2 p_{D(prod)} \mu}, \quad (3.25)$$

where the dimensionless pressure functions for production are given by Eqs. 3.20a – 3.20f. From Eq. 3.6b, we also know that for a normal pattern

$$\bar{q}_{inj} = P/I \times q_{prod}, \quad (3.26)$$

that is, the average injection well rate in a normal pattern equals the producer/injector ratio times the producing well flow rate. Thus, combining Eqs. 3.12, 3.25, and 3.26 we have the equation for the average injection well rate in a normal pattern,

$$\bar{q}_{inj} = \frac{P/I}{1 + P/I} \times \frac{kh(\Delta P)}{141.2 p_{D(inj)} \mu}, \quad (3.27)$$

which is equivalent to the equation for the injection well rate in an inverted pattern (Eq. 3.19). It is straightforward from here to deduce the general equation for the average producing well rate in an inverted pattern, shown here for completeness:

$$\bar{q}_{prod} = \frac{1}{1 + P/I} \times \frac{kh(\Delta P)}{141.2 p_{D(prod)} \mu}, \quad (3.28)$$

which again is the same as Eq. 3.25 for the production well rate in a normal pattern. Thus, the same equations apply to either the normal or inverted pattern cases when calculating the injection well flow rates (Eqs. 3.19 & 3.27) and production well flow rates (Eqs. 3.25 & 3.28).

The above discussion confirms the relationship of Eq. 3.12, namely, that the dimensionless pressures of injection and production, as defined by Eq. 3.7 and Eq. 3.9b, are equivalent for any regularly spaced well pattern. It can also be shown that for equivalent well density, e.g. one well per 20-acres, within the same reservoir, the dimensionless pressures given by Eqs. 3.20a – 3.20f are nearly equal, being within 5% for reasonable values of well spacing and wellbore radius. Figure 3.4 shows the dimensionless pressures for the patterns versus well density. As shown on the figure, at a

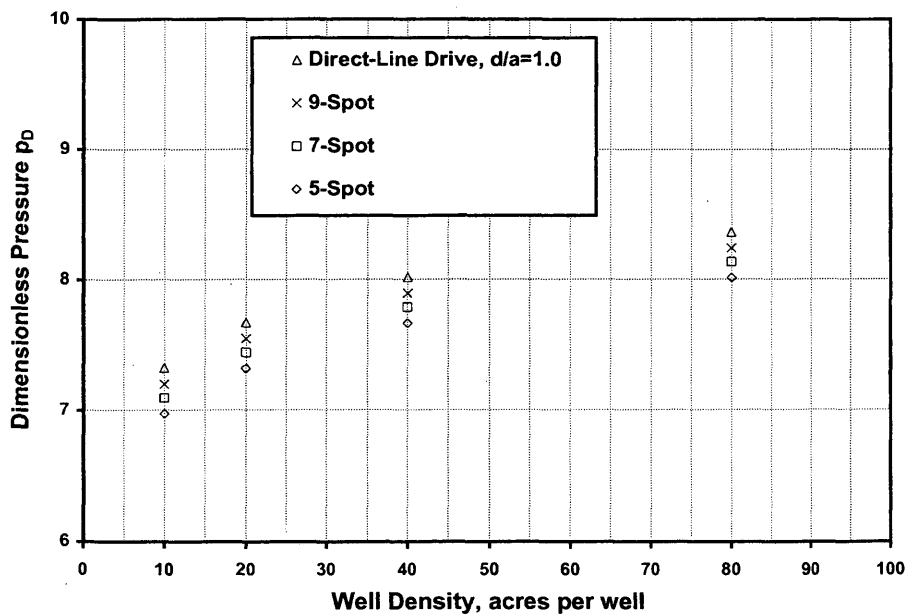


Fig. 3.4 – Dimensionless pressure of patterns at various well densities.

given well density the dimensionless pressures of all the patterns are bounded by the five-spot on the low side and the direct-line drive on the high side, where the difference between the former and the latter are within five percent. In fact, a dimensionless pressure that can be used within 2.5% for any pattern is given by

$$P_{D(inj)} = P_{D(prod)} = \ln \frac{d}{r_w} - 0.443 . \quad (3.29)$$

Since the dimensionless pressures of the patterns are within five percent for equivalent well densities, it will be shown in Chapter Four that reservoir flow rate differences between patterns in equivalent, homogeneous, isotropic, unit-*total* mobility ratio reservoir systems are due almost entirely to the pattern producer/injector ratio.

The treatment of the skin effect and heterogeneity and how these are included in the pattern equations will be presented in Chapter Four after the development of the non-unit total mobility (two-phase) equations.

CHAPTER FOUR

PATTERN RELATIONSHIPS FOR NON-UNIT

TOTAL MOBILITY RATIO SYSTEMS

The relationships for single-phase (unit-total mobility) pattern flow developed in Chapter Three will now be expanded for non-unit total mobility patterns, including the skin effect, and heterogeneous (isotropic) reservoirs.

4.1 Average Reservoir Pressure in Non-Unit Total Mobility Patterns

To expand Eq. 3.2b for non-unit mobility systems, we proceed in the same manner, except that for simplicity we assume that the sand-face pressures of the injectors are equal (p_{wfI}), and that of the producers are equal (p_{wfP}). Again referring to the element of symmetry for the inverted nine-spot pattern (Fig. 3.2), we can write the relationships for the injection and production wells for each pattern well (note that the following can be applied to any pattern with the same results. Here, the inverted nine-spot is used to more easily illustrate the equations):

The equation for the injector is

$$(p_{wfI} - \bar{p}_{pat})\lambda_{T1} = P_{D(well1)}q_{well1} \frac{141.2}{kh}. \quad (4.1a)$$

The equations for the producers are:

$$(\bar{p}_{pat} - p_{wfp})\lambda_{T2} = p_{D(well2)}q_{well2} \frac{141.2}{kh}, \quad (4.1b)$$

$$(\bar{p}_{pat} - p_{wfp})\lambda_{T3} = p_{D(well3)}q_{well3} \frac{141.2}{kh}, \quad (4.1c)$$

and

$$(\bar{p}_{pat} - p_{wfp})\lambda_{T4} = p_{D(well4)}q_{well4} \frac{141.2}{kh}, \quad (4.1d)$$

where λ_{Ti} for $i = 1, 2, 3$ and 4 , are the *effective* total mobility terms of the oil and water within the drainage region of wells 1, 2, 3 and 4, respectively, defined from the wellbore to the average reservoir pressure contour. The effective total mobility is defined as the equivalent total mobility that will result in the same pressure drop within each well region (from the well pressure to average pressure). This will be discussed in more detail in Chapter Six.

Summing Eqs. 4.1b, 4.1c, and 4.1d, and rearranging we obtain:

$$\begin{aligned} & (\lambda_{T2} + \lambda_{T3} + \lambda_{T4}) \cdot 141.2 (p_{D(well2)}q_{well2} + p_{D(well3)}q_{well3} + p_{D(well4)}q_{well4}) \\ (\bar{p}_{pat} - p_{wfp}) \frac{(\lambda_{T2} + \lambda_{T3} + \lambda_{T4})}{3} &= \frac{141.2 (p_{D(well2)}q_{well2} + p_{D(well3)}q_{well3} + p_{D(well4)}q_{well4})}{3}. \end{aligned} \quad (4.2)$$

Defining the average effective total mobility of the producing wells as

$$\bar{\lambda}_{TP} = \frac{(\lambda_{T2} + \lambda_{T3} + \lambda_{T4})}{3}, \quad (4.3)$$

and again defining the average dimensionless pressure-rate product of the producing wells as

$$P_{D(prod)} \bar{q}_{prod} = \frac{(P_{D(well2)} q_{well2} + P_{D(well3)} q_{well3} + P_{D(well4)} q_{well4})}{3}, \quad (3.9b)$$

we obtain the expression

$$(\bar{p}_{pat} - p_{wfP}) \bar{\lambda}_{TP} = \frac{141.2}{kh} P_{D(prod)} \bar{q}_{prod}. \quad (4.4a)$$

A similar expression can be obtained for the injection well(s):

$$(p_{wfl} - \bar{p}_{pat}) \bar{\lambda}_{TI} = \frac{141.2}{kh} P_{D(inj)} q_{inj}. \quad (4.4b)$$

Dividing Eq. 4.4b by Eq. 4.4a, we obtain

$$\frac{(p_{wfl} - \bar{p}_{pat}) \bar{\lambda}_{TI}}{(\bar{p}_{pat} - p_{wfP}) \bar{\lambda}_{TP}} = \frac{P_{D(inj)} q_{inj} \left(\frac{1}{kh} \right)_{inj}}{P_{D(prod)} \bar{q}_{prod} \left(\frac{1}{kh} \right)_{prod}}. \quad (4.4c)$$

The single-phase dimensionless pressure applies to non-unit total mobility flow if the flow geometry (or flow paths) do not change from that of the single-phase pattern. This is a result of the fact that dimensionless pressure is a representation of the flow resistance due to the overall flow *path* of the system, just as $p_D = \ln \frac{r_e}{r_w}$ for pure radial, steady-state, incompressible flow. The flow regimes within the different patterns vary

from radial to elliptical to linear flow, the composite flow resistance being fully accounted for with the single-phase p_D terms. Note that the conductance due to *mobility* is accounted for with $\bar{\lambda}_{TP}$ and $\bar{\lambda}_{TI}$ as defined above, where the actual calculation of these terms does depend on the flow regime, as will be shown in Chapter Six. However, as long as the varying mobilities within the system do not influence the flow geometry, i.e. flow streamlines, the single-phase dimensionless pressures apply to non-unit total mobility, two-phase flow. Porous, fluid-flow model studies^{2,4} have shown that when the mobilities of the swept and unswept regions are different, flow patterns are largely unchanged and the regions around the wells remain dominated by radial flow. Also, the dimensionless pressure of the nine-spot (Eq. 3.20f) gives important clues as to how the dimensionless pressures could change given a change in the flow geometry of the nine-spot. As discussed in Chapter Three, even when R (corner well-to-side well flow rate) varies considerably (as might occur during two-phase flow), the nine-spot dimensionless pressure varies only slightly (see Table 3.4).

Therefore, we apply the relationship of Eq. 3.12, and since $(kh)_{prod} = (kh)_{inj}$ for homogeneous, isotropic flow, we rewrite Eq. 4.4c as:

$$\frac{(P_{wfl} - \bar{P}_{pat})\bar{\lambda}_{TI}}{(\bar{P}_{pat} - P_{wfP})\bar{\lambda}_{TP}} = \frac{q_{inj}}{\bar{q}_{prod}}. \quad (4.4d)$$

Again, the relationship of Eq. 3.6b is valid, shown here specifically for the inverted nine-spot:

$$\frac{q_{inj}}{\bar{q}_{prod}} = P / I. \quad (4.5)$$

Then, a total mobility ratio is also defined as

$$M_T = \frac{\bar{\lambda}_{TI}}{\lambda_{TP}}. \quad (4.6)$$

Combining Eq. 4.4d, Eq. 4.5 and Eq. 4.6 and rearranging, we obtain the pattern average pressure equation for any mobility ratio system:

$$\bar{P}_{pat} = \frac{M_T(P_{wfl}) + P/I(P_{wfp})}{M_T + P/I}. \quad (4.7)$$

Note that when the total mobility ratio is 1.0, Eq. 4.7 reduces to Eq. 3.2b.

Based on the preceding development, it is seen that the more formal definitions of $\bar{\lambda}_{TI}$ and $\bar{\lambda}_{TP}$, the two parameters necessary to calculate the total mobility ratio, M_T , can be applied to all patterns with the definitions given below:

$$\bar{\lambda}_{TI} = \frac{\sum_{j=1}^{N_I} f_{(j)} \times \lambda_{T(j)}}{\sum_{j=1}^{N_I} f_{(j)}}, \quad (4.8a)$$

and

$$\bar{\lambda}_{TP} = \frac{\sum_{j=1}^{N_P} f_{(j)} \times \lambda_{T(j)}}{\sum_{j=1}^{N_P} f_{(j)}}, \quad (4.8b)$$

where $f_{(j)}$ is the representation of the j th producing (or injection) well in the pattern element as a fraction of the total number of producing (or injection) wells represented by

the pattern, and N_P and N_I are the number of producing and injection wells, respectively, contributing to the pattern element. Eq. 4.3 is an example of Eq. 4.8b as applied to the inverted nine-spot pattern. As shown in Appendix A, this is the same weighting procedure used when calculating p_{wfl} and p_{wfp} . These definitions apply to any pattern, and expand the definition of total mobility ratio, M_t , given by Willhite¹². The new definition for total mobility ratio, M_T , includes Willhite's definition for the 5-spot and line-drive patterns but also shows how the terms for patterns with producer/injector ratios other than one must be averaged.

4.2 Flow Relationships for Non-Unit Total Mobility Ratio Patterns

Proceeding in the same manner for single-phase, or unit-total mobility patterns, we again write the equation for the injection well rate for any inverted pattern, according to Eq. 4.4b:

$$(p_{wfl} - \bar{p}_{pat}) \bar{\lambda}_{TI} = P_{D(inj)} q_{inj} \frac{141.2}{kh}, \quad (4.9a)$$

or rearranging

$$q_{inj} = \frac{(p_{wfl} - \bar{p}_{pat}) \bar{\lambda}_{TI}}{P_{D(inj)}} \frac{kh}{141.2}. \quad (4.9b)$$

From Eq. 4.7 we can show that

$$p_{wfl} - \bar{p}_{pat} = \frac{P/I}{M_T + P/I} \Delta P. \quad (4.10)$$

Therefore, combining Eq. 4.9b and Eq. 4.10 we have

$$q_{inj} = \bar{\lambda}_{TI} \frac{P/I}{M_T + P/I} \times \frac{\Delta P}{p_{D(inj)}} \times \frac{kh}{141.2}. \quad (4.11)$$

For normal patterns, we write the expression for the production well flow rate according to Eq. 3.7 as

$$q_{prod} = \frac{(\bar{P}_{pat} - p_{wfP}) \bar{\lambda}_{TP}}{p_{D(prod)}} \frac{kh}{141.2}. \quad (4.12)$$

From Eq. 4.7 we can also show that

$$\bar{P}_{pat} - p_{wfP} = \frac{M_T}{M_T + P/I} \Delta P. \quad (4.13)$$

Combining Eq. 4.12 and Eq. 4.13 we can write

$$q_{prod} = \bar{\lambda}_{TP} \frac{M_T}{M_T + P/I} \times \frac{\Delta P}{p_{D(prod)}} \times \frac{kh}{141.2}. \quad (4.14)$$

We know from Eq. 3.6b that for inverted patterns

$$\bar{q}_{prod} = \frac{q_{inj}}{P/I}. \quad (4.15)$$

Therefore, combining Eq. 3.12, Eq. 4.11 and Eq. 4.15, we have

$$\bar{q}_{prod} = \bar{\lambda}_{TI} \frac{1}{M_T + P/I} \times \frac{\Delta P}{P_{D(inj)}} \times \frac{kh}{141.2}, \quad (4.16)$$

which is equivalent to the production rate in normal patterns given by Eq. 4.14 since $P_{D(pat)} = P_{D(inj)} = P_{D(prod)}$ (Eq. 3.12) for any pattern as defined by Eqs. 3.20a – 3.20c and Eq. 3.20f, and $\bar{\lambda}_{TI} = M_T \bar{\lambda}_{TP}$ from Eq. 4.6. Therefore, the general equation in a non-unit total mobility system for the producing well rate in a normal pattern or the average producing well rate in an inverted pattern is based on Eq. 4.14 and Eq. 4.16 as:

$$q_{prod} = \bar{q}_{prod} = \bar{\lambda}_{TP} \frac{M_T}{M_T + P/I} \times \frac{\Delta P}{P_{D(pat)}} \times \frac{kh}{141.2}. \quad (4.17)$$

Similarly, the general expression in a non-unit total mobility ratio system for the injection well rate in an inverted pattern or the average injection well rate for a normal pattern is:

$$q_{inj} = \bar{q}_{inj} = \bar{\lambda}_{TI} \frac{P/I}{M_T + P/I} \times \frac{\Delta P}{P_{D(pat)}} \times \frac{kh}{141.2}. \quad (4.18)$$

Note that Eqs. 4.17 and 4.18 reduce to the unit-mobility equations (Eqs. 3.19 & 3.27, Eqs. 3.25 & 3.28) when $M_T = 1.0$ (note that relative permeability of one is implied in the unit-total mobility equations).

Willhite¹² shows approximate equations for two-phase five-spot and staggered line-drive patterns after fillup (i.e. steady-state flow) using radial and linear flow segments in series, as Eq. 6.17 and Eq. 6.32 of Reference 12. The approximate five-spot equation in consistent units is shown as

$$q_{inj} = \frac{2\pi\lambda_o h(p_{wi} - p_{wp})}{M \ln \frac{r_f}{r_w} + \ln \frac{r_e}{r_f} + \ln \frac{r_e}{r_w}}. \quad (6.17 \text{ of Ref. 12})$$

The above cited equations are shown to be very good approximations to the single-phase (unit-mobility) equations (Eqs. 3.13a and 3.13b) for $M = 1.0$ (and piston-like displacement). For non-unit total mobility two-phase flow, these relationships are valid until the flood front radius reaches $r_e = d/\sqrt{\pi}$ from the injector ($E_A = 50\%$). Now, if we equate the approximate two-phase equation (Eq. 6.17) to the exact expression of Eq. 4.18 for the five-spot, where we equate like terms, we obtain

$$\bar{\lambda}_{TI} \frac{P/I}{M_T + P/I} \times \frac{1}{p_{D(par)}} = \frac{\lambda_o}{\frac{1}{M} \ln \frac{r_f}{r_w} + \ln \frac{r_e}{r_f} + \ln \frac{r_e}{r_w}}. \quad (4.19)$$

For true piston-like displacement and for the case where $r_f = r_e$, $M_T = M$, the endpoint mobility ratio. Also, $\lambda_o = \bar{\lambda}_{TP} = \bar{\lambda}_{TI} / M_T$. Therefore, making all the substitutions and solving for the dimensionless pressure, $p_{D(par)}$, we obtain

$$p_{D(par)} = \ln \frac{d}{r_w} - 0.572. \quad (4.20)$$

This can also be shown to be the same result as for the approximate single-phase (“unit-mobility ratio”) equation using Eq. 6.20 of Ref. 12. This approximate dimensionless pressure compares very favorably to the actual dimensionless pressure of the five-spot shown by Eq. 3.20a, and also supports the previous statements regarding the

dimensionless pressure for single-phase and non-unit total mobility flow being equivalent as long as flow geometry is preserved.

4.3 Pressure and Flow Relationships Including the Skin Effect

The pressure and flow equations for non-unit total-mobility pattern flow including skin effect will now be developed. As will be shown, the inclusion of skin can be handled as an adjustment to the producer/injector ratio.

We rewrite Eqs. 4-1a – 4.1d as follows, now including the skin effect for each pattern well.

The equation for the injector is

$$(p_{wfl} - \bar{p}_{pat})\lambda_{T1} = (p_{D(well1)} + S_{(well1)})q_{well1} \frac{141.2}{kh}. \quad (4.21a)$$

The equations for the producers are:

$$(\bar{p}_{pat} - p_{wfp})\lambda_{T2} = (p_{D(well2)} + S_{(well2)})q_{well2} \frac{141.2}{kh}, \quad (4.21b)$$

$$(\bar{p}_{pat} - p_{wfp})\lambda_{T3} = (p_{D(well3)} + S_{(well3)})q_{well3} \frac{141.2}{kh}, \quad (4.21c)$$

and

$$(\bar{p}_{pat} - p_{wfp})\lambda_{T4} = (p_{D(well4)} + S_{(well4)})q_{well4} \frac{141.2}{kh}. \quad (4.21d)$$

Summing Eqs. 4.21b, 4.21c and 4.21d for the producing wells, and rearranging we have

$$\begin{aligned}
 (\bar{p}_{pat} - p_{wfP}) \frac{(\lambda_{T2} + \lambda_{T3} + \lambda_{T4})}{3} &= \frac{141.2}{kh} \frac{(P_{D(well2)}q_{well2} + P_{D(well3)}q_{well3} + P_{D(well4)}q_{well4})}{3} \\
 &+ \frac{141.2}{kh} \frac{(S_{(well2)}q_{well2} + S_{(well3)}q_{well3} + S_{(well4)}q_{well4})}{3}. \tag{4.22}
 \end{aligned}$$

Remembering from Eq. 3.9b and Eq. 4.3 that

$$P_{D(prod)}\bar{q}_{prod} = \frac{(P_{D(well2)}q_{well2} + P_{D(well3)}q_{well3} + P_{D(well4)}q_{well4})}{3} \tag{3.9b}$$

and

$$\bar{\lambda}_{TP} = \frac{(\lambda_{T2} + \lambda_{T3} + \lambda_{T4})}{3}, \tag{4.3}$$

we also define the average rate-skin product as

$$S_{(prod)}\bar{q}_{prod} = \frac{(S_{(well2)}q_{well2} + S_{(well3)}q_{well3} + S_{(well4)}q_{well4})}{3}. \tag{4.23}$$

Combining Eq. 4.22, Eq. 3.9b, Eq. 4.3, and Eq. 4.23 we can rewrite Eq. 4.22 as

$$(\bar{p}_{pat} - p_{wfP})\bar{\lambda}_{TP} = \frac{141.2}{kh} (P_{D(prod)} + S_{(prod)})\bar{q}_{prod}. \tag{4.24a}$$

A similar equation is also written for the injector as

$$(p_{wfl} - \bar{p}_{pat}) \bar{\lambda}_{TI} = \frac{141.2}{kh} (p_{D(inj)} + S_{(inj)}) q_{inj} \quad (4.24b)$$

Dividing Eq. 4.24b by Eq. 4.24a, we obtain

$$\frac{(p_{wfl} - \bar{p}_{pat}) \bar{\lambda}_{TI}}{(\bar{p}_{pat} - p_{wfp}) \bar{\lambda}_{TP}} = \frac{(p_{D(inj)} + S_{(inj)}) q_{inj} \left(\frac{1}{kh} \right)_{inj}}{(p_{D(prod)} + S_{(prod)}) \bar{q}_{prod} \left(\frac{1}{kh} \right)_{prod}}. \quad (4.24c)$$

Again for homogeneous, isotropic flow we know that $(kh)_{prod} = (kh)_{inj}$. Also applying the relationship of Eq. 4.5, we can obtain

$$\frac{(p_{wfl} - \bar{p}_{pat}) \bar{\lambda}_{TI}}{(\bar{p}_{pat} - p_{wfp}) \bar{\lambda}_{TP}} = P/I \times \frac{(p_{D(inj)} + S_{(inj)})}{(p_{D(prod)} + S_{(prod)})}. \quad (4.25)$$

If we define an effective producer/injector ratio as

$$\tilde{P}/\tilde{I} = P/I \times \frac{(p_{D(inj)} + S_{(inj)})}{(p_{D(prod)} + S_{(prod)})}, \quad (4.26)$$

we can then write the average reservoir pressure equation including skin effect as

$$\bar{p}_{pat} = \frac{M_T (p_{wfl}) + \tilde{P}/\tilde{I} (p_{wfp})}{M_T + \tilde{P}/\tilde{I}}. \quad (4.27)$$

Note from Eq. 4.25, that if $S_{(prod)}$ is greater than $S_{(inj)}$, that the effective producer injector/ratio of the system goes down, and vice-versa, which is intuitively correct. Also

note that if $S_{(prod)} = S_{(inj)}$, then the skin effect cancels and the reservoir pressure behaves as if there was no skin, so that the effective producer/injector ratio is equal to the physical producer/injector ratio, or $\tilde{P}/\tilde{I} = P/I$. Flow rates, however, will still be influenced by skin effect, as will be shown below. Taking an example, assume we have an inverted nine-spot pattern on 20-acre spacing with $r_w = 0.33$ ft. Then, using Eq. 3.20f, we calculate the dimensionless pressure for the nine-spot as (with $R=0.91$)

$$p_{D(inj)} = p_{D(prod)} = \ln \frac{933.38}{0.33} - 0.272 - \frac{1}{2} \times \frac{0.693}{2 + 0.91} = 7.547.$$

If the individual producing wells all have a skin effect of +5.0, then from Eq. 4.23

$$S_{(prod)} = 5.0.$$

Then, if $S_{(inj)} = 0$, we calculate the effective producer injector ratio from Eq. 4.26 as

$$\tilde{P}/\tilde{I} = 3.0 \times \frac{(7.547 + 0)}{(7.547 + 5.0)} = 1.804.$$

Therefore, this system will have a reservoir pressure that reflects a producer/injector ratio of 1.8 instead of 3.0, i.e. it will be higher.

The generalized pattern flow equations including skin effect can thus be written according to Eqs. 4.17 and 4.18 as

$$q_{prod} = \bar{q}_{prod} = \bar{\lambda}_{TP} \frac{M_T}{M_T + \tilde{P}/\tilde{I}} \times \frac{\Delta P}{(p_{D(pat)} + S_{(prod)})} \times \frac{kh}{141.2} \quad (4.28)$$

and

$$q_{inj} = \bar{q}_{inj} = \bar{\lambda}_{TI} \frac{\tilde{P}/\tilde{I}}{M_T + \tilde{P}/\tilde{I}} \times \frac{\Delta P}{(p_{D(pat)} + S_{(inj)})} \times \frac{kh}{141.2}. \quad (4.29)$$

Note from Eq. 4.23 that a more formal definition for calculating the average rate-skin product for application to other patterns can be written as

$$S_{(inj)} = \frac{\sum_{j=1}^{N_I} f_{(j)} \times S_{(j)} \times q_{(j)}}{\sum_{j=1}^{N_I} f_{(j)} \times q_{(j)}}, \quad (4.30a)$$

and

$$S_{(prod)} = \frac{\sum_{j=1}^{N_P} f_{(j)} \times S_{(j)} \times q_{(j)}}{\sum_{j=1}^{N_P} f_{(j)} \times q_{(j)}}, \quad (4.30b)$$

where $f_{(j)}$ is the representation of the j th producing (or injection) well in the pattern element as a fraction of the total number of producing (or injection) wells represented by the pattern, and N_P and N_I are the number of producing and injection wells, respectively, contributing to the pattern element. Note that if the producing wells in the above inverted nine-spot example have differing skins, then a knowledge of the individual producing well rates is necessary to calculate an accurate value of $S_{(prod)}$ as given by Eq. 4.30b. If the flow rates are nearly the same, then a straight average of skin can be sufficient. If however, the flow rates are significantly different between the producing wells, a knowledge of these rates or their fractional contribution among the wells becomes crucial

to determining the effective skin, $S_{(prod)}$. The same comments apply to determining $S_{(inj)}$ for the normal nine-spot. The individual well flow rates can be estimated with the following equation, for the inverted nine-spot shown in Fig. 3.2. Applying Eqs. 4.21b – 4.21d to Eq. 4.30b, assuming that the individual producing well dimensionless pressures are approximately equal to the value defined in Eq. 3.9b, that is

$$P_{D(prod)} \cong P_{D(well2)} \cong P_{D(well3)} \cong P_{D(well4)}, \quad (4.31)$$

we can write

$$S_{(prod)} \cong \frac{\sum_{j=1}^{N_p} f_{(j)} \times S_{(j)} \times q_{(j)}}{\sum_{j=1}^{N_p} f_{(j)} \times q_{(j)}} = \frac{\frac{\lambda_2 S_2}{(P_{D(well2)} + S_2)} + \frac{\lambda_3 S_3}{(P_{D(well3)} + S_3)} + \frac{\lambda_4 S_4}{(P_{D(well4)} + S_4)}}{\frac{\lambda_2}{(P_{D(well2)} + S_2)} + \frac{\lambda_3}{(P_{D(well3)} + S_3)} + \frac{\lambda_4}{(P_{D(well4)} + S_4)}}. \quad (4.32)$$

Eq. 4.32 can be used with excellent results at any stage of the waterflood, before and after water breakthrough, as will be shown in Chapter Six. In practice, however, the mobility terms in Eq. 4.32 will be known most accurately before breakthrough. In this case, as Eq. 4.32 shows, the producing well mobility terms will be the same and the weighted average skin of production, $S_{(prod)}$, will simply be equal to the arithmetic average of the individual well skin factors.

4.4 Heterogeneous (Isotropic) Reservoirs

If the permeability is different around individual wells, as might be determined from well tests, then permeability of each pattern well can be incorporated into the average effective *relative* total mobility calculation (Eqs. 4.8a and 4.8b) to result in an average effective *absolute* total mobility for injection and production as

$$\bar{\lambda}_{TI(abs)} = \frac{\sum_{j=1}^{N_I} f_{(j)} \times \lambda_{T(j)} \times k_{(j)}}{\sum_{j=1}^{N_I} f_{(j)}}, \quad (4.33a)$$

and

$$\bar{\lambda}_{TP(abs)} = \frac{\sum_{j=1}^{N_I} f_{(j)} \times \lambda_{T(j)} \times k_{(j)}}{\sum_{j=1}^{N_I} f_{(j)}}, \quad (4.33b)$$

where the permeability, k , has now been included with mobility. Then, these average absolute effective mobilities are used in the equations just as those defined in Eqs. 4.8a and 4.8b. For example, Eq. 4.18 becomes

$$q_{inj} = \bar{q}_{inj} = \bar{\lambda}_{TI(abs)} \frac{P/I}{M_T + P/I} \times \frac{\Delta P}{P_{D(pat)}} \times \frac{h}{141.2}, \quad (4.34)$$

where total mobility ratio M_T is also calculated with the average absolute effective total mobilities, $\bar{\lambda}_{TI(abs)}$ and $\bar{\lambda}_{TP(abs)}$, with Eq. 4.6.

In the same way, thickness h can also be included with the average effective total mobility calculation as kh instead of just permeability, k . Note that heterogeneity here still must include the assumption of isotropic permeability for these equations to be valid.

4.4 Anisotropic Reservoirs

The equations presented in this chapter, while strictly applicable to isotropic reservoirs, should provide good first order approximations to the behavior of mildly anisotropic systems, becoming less accurate with increasing anisotropy. If anisotropy is significant, then flow rate concerns tend to become overshadowed by recovery

considerations. In these cases, a reservoir simulation study should be performed to study the effects of anisotropy.

CHAPTER FIVE

APPLICATION OF NEW PATTERN RELATIONSHIPS

TO DETERMINING THE HIGHEST

CONDUCTIVITY PATTERN

This chapter applies the pattern equations developed in Chapter Three and Chapter Four to the development of a method that can be used easily to determine the pattern with the highest flow capacity for any mobility ratio system, by defining a conductivity ratio. A discussion of the skin effect is included and how this impacts the conductivity ratio, and the conditions for applying this concept to heterogeneous reservoirs. Finally, a discussion on the relationship between conductivity ratio defined in this thesis, with a previously defined conductance ratio, γ , is shown as a reference with previous work. Example calculations using the equations presented in this chapter and Chapter Four, to determine the highest conductivity pattern are presented in Appendix C.

5.1 Discussion of Methodology

Referring to Eqs. 4.18 and Eq. 4.29, since the dimensionless pressures of the different patterns (Eqs. 3.20a – 3.20c, Eq. 3.20f) are within five percent for equivalent well spacing as stated earlier, comparing the individual injection *well* flow rates between the different patterns in a two-phase system can be based solely on the comparison of the term

$$\bar{\lambda}_T \frac{P/I}{M_r + P/I} \tag{5.1a}$$

or

$$\bar{\lambda}_{TII} \frac{\tilde{P}/\tilde{I}}{M_T + \tilde{P}/\tilde{I}}. \quad (5.1b)$$

for each of the patterns, since all other terms are the same or approximately so. Note that in the case where a skin effect is involved, a comparison using only Eq. 5.1b assumes that the terms $S_{(inj)}$ and $S_{(prod)}$ would be the same between the patterns, which is unlikely. If the skin factor is the same for all the pattern wells, which seems to be a more likely assumption, then the effective and the physical producer/injector ratios, \tilde{P}/\tilde{I} and P/I , will be the same as discussed in Chapter Four. Thus it seems that the most practical assumption is that the skin factors amongst all of the wells are similar, and the comparison of flow rates can then be made based on Eq. 5.1a. A special case involving different skin factors will be considered later, where the injection skin $S_{(inj)}$ is consistent relative to the producing skin $S_{(prod)}$. This might happen, for example, where injection is taking place near parting pressure such that the injectors will have a fracture and will always have a negative skin as compared to the producers for any given pattern.

Since the number of total wells associated to each injector is given by $1 + P/I$, we can define a normalized injection rate as the injection rate *per pattern well* as

$$\tilde{q} = \frac{q_{inj}}{1 + P/I}. \quad (5.2)$$

Therefore, we can now compare the total *reservoir* flow rate that will be provided by each of the patterns using Eq. 5.2. From the previous remarks related to Eq. 5.1, this comparison can be made simply by comparing the following term for each of the patterns (dividing Eq. 5.1 by Eq. 5.2):

$$\bar{\lambda}_{TI} \frac{P/I}{(M_T + P/I)(1 + P/I)}, \quad (5.3a)$$

or

$$\bar{\lambda}_{TI} \frac{\tilde{P}/\tilde{I}}{(M_T + \tilde{P}/\tilde{I})(1 + P/I)}. \quad (5.3b)$$

Note that in Eq. 5.3b, both the effective and physical producer/injector ratios are involved. A reservoir conductivity ratio can then be defined using Eq. 5.3 for two different patterns as

$$\frac{\tilde{q}_{(1)}}{\tilde{q}_{(2)}} = \frac{(\bar{\lambda}_{TI})_1 (P/I)_1 (M_T + P/I)_2 (1 + P/I)_2}{(\bar{\lambda}_{TI})_2 (P/I)_2 (M_T + P/I)_1 (1 + P/I)_1}, \quad (5.4a)$$

or

$$\frac{\tilde{q}_{(1)}}{\tilde{q}_{(2)}} = \frac{(\bar{\lambda}_{TI})_1 (\tilde{P}/\tilde{I})_1 (M_T + \tilde{P}/\tilde{I})_2 (1 + P/I)_2}{(\bar{\lambda}_{TI})_2 (\tilde{P}/\tilde{I})_2 (M_T + \tilde{P}/\tilde{I})_1 (1 + P/I)_1}, \quad (5.4b)$$

where subscripts 1 and 2 refer to the parameters of any two patterns, 1 and 2. Eq. 5.4 provides an easy method to quickly determine the optimum pattern for the maximum waterflooding flow rate in a given reservoir by comparing the producer/injector ratios of all the patterns relative to a base pattern. Since producer/injector ratio is known for each pattern, using Eq. 5.4 involves only estimating the parameters $\bar{\lambda}_{TI}$ and $\bar{\lambda}_{TP}$ (where $M_T = \frac{\bar{\lambda}_{TI}}{\bar{\lambda}_{TP}}$). As will be shown with numerical results in Chapter Six, $\bar{\lambda}_{TI}$ will be approximately the same for each pattern in a given reservoir-fluid system among all the patterns so that a single value for $\bar{\lambda}_{TI}$, and thus M_T , can be used to compare all the patterns, or producer/injector ratios. As will be shown, the assumption of $\bar{\lambda}_{TI}$ being the same for any given pattern is especially good when $M < 1$, and is quite acceptable when

$M > 1$. Thus, a more simplified form of Eq. 5.4 for comparisons involving the same injection fluid where $(\bar{\lambda}_{TI})_1 = (\bar{\lambda}_{TI})_2$ is given by

$$\frac{\tilde{q}_{(1)}}{\tilde{q}_{(2)}} = \frac{(P/I)_1 (M_T + P/I)_2 (1 + P/I)_2}{(P/I)_2 (M_T + P/I)_1 (1 + P/I)_1}, \quad (5.5a)$$

or

$$\frac{\tilde{q}_{(1)}}{\tilde{q}_{(2)}} = \frac{(\tilde{P}/\tilde{I})_1 (M_T + \tilde{P}/\tilde{I})_2 (1 + P/I)_2}{(\tilde{P}/\tilde{I})_2 (M_T + \tilde{P}/\tilde{I})_1 (1 + P/I)_1}. \quad (5.5b)$$

The reservoir conductivity relationship for $M_T = 1$ is shown by Figure 5.1, where each of the pattern producer/injector ratios is compared with a base reference pattern $(P/I)_2 = 1.0$. That is, the conductivity of all producer/injector ratios are compared to a producer/injector ratio of one.

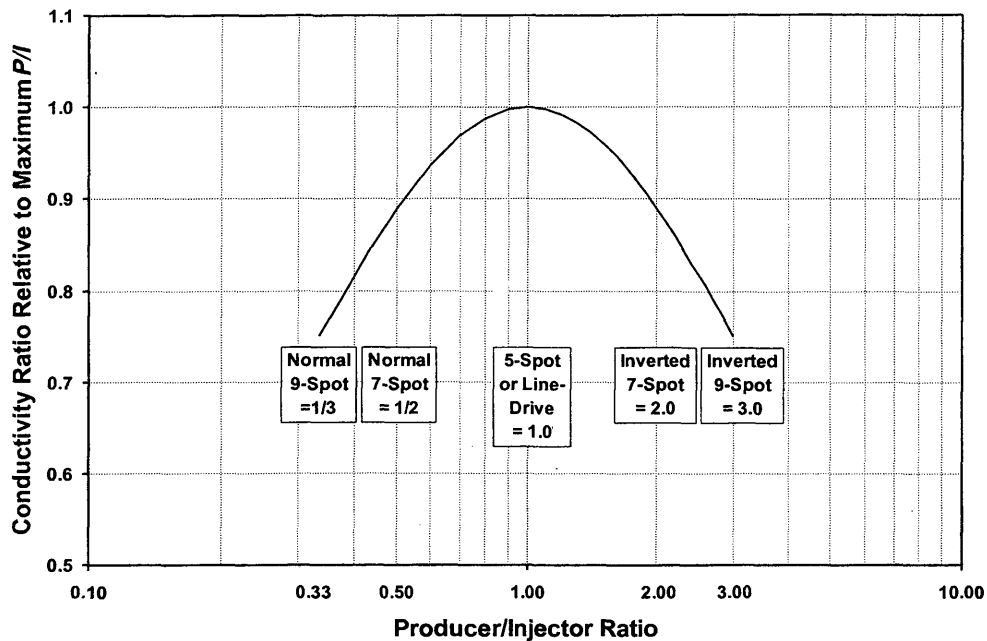


Fig. 5.1 – Conductivity Ratio relationship for $M_T = 1.0$.

As shown on Fig. 5.1, when $M_T = 1$, a producer/injector ratio of 1.0 also provides the maximum reservoir flow rate, that is, a five-spot or a line-drive pattern with $d/a=1.0$. The seven-spot and nine-spot patterns, either normal or inverted, provide 88% and 75% of the capacity of the five-spot or line-drive patterns ($d/a=1.0$), respectively. In actuality, the line-drive patterns with $d/a=1.0$ will provide 95% of the flow capacity of the five-spot, since the dimensionless pressure of the line-drive pattern is about 5% higher (see Figure 3.4).

Note that the base producer/injector ratio used in Eq. 5.5 as *pattern 2* also provides the maximum conductivity. This convention will be followed for subsequent

comparisons of other total mobility ratios, i.e. the producer/injector ratio providing the highest conductivity will be the base pattern, $(P/I)_2 = (P/I)_{max}$ as also indicated on the ordinate axis of Figure 5.1.

Next, the conductivity relationships for $M_T = 0.5$ and $M_T = 2.0$ are shown on Figure 5.2. These total mobility ratios are plotted on the same graph to illustrate a few of the important relationships of Eq. 5.5. Note how the conductivity relationships are symmetrical around the $P/I = 1.0$ axis for these two total mobility ratios, which are reciprocals of one another. The producer/injector ratios corresponding to the maximum flow capacity, $(P/I)_{max}$, are also reciprocals. That is, when $M_T = 0.5$, $(P/I)_{max} = 0.7$, while for $M_T = 2.0$, $(P/I)_{max} = 1/0.7$, or 1.428. Notice that the producer/injector ratios providing the minimum reservoir flow rates, or $(P/I)_{min}$, only provide 62% of that provided by $(P/I)_{max}$.

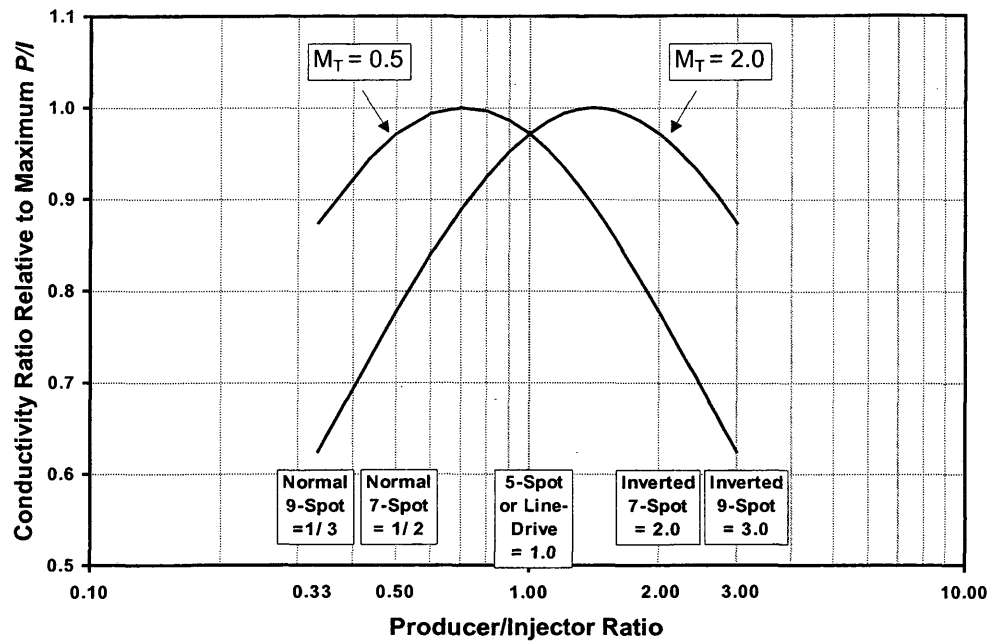


Fig. 5.2 – Conductivity Ratio relationships for $M_T = 0.5$ and $M_T = 2.0$.

Even though no repeatable pattern corresponds exactly to these values of $(P/I)_{max}$ for $M_T = 0.5$ and $M_T = 2.0$, they are sufficiently close to an actual pattern. In this case, a hybrid pattern that fills the gap between a five-spot and seven-spot will provide the highest flow capacity. This pattern is a combination five-spot, skewed four-spot (or seven-spot in a rectangular well arrangement) as shown on Figure 5.3.

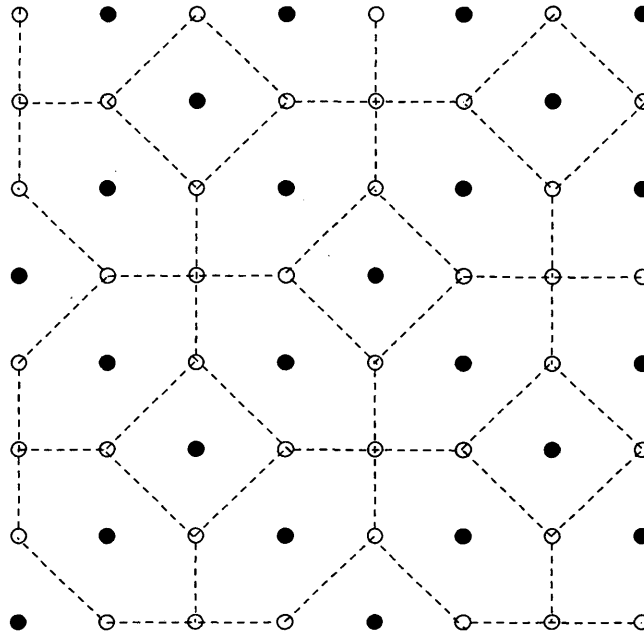


Fig. 5.3 – Hybrid pattern with $P/I = 5:3$ or $3:5$.

The producer/injector ratio of this pattern is either 1.67 (5:3) for an inverted pattern or 0.60 (3:5) for a normal pattern. This pattern arrangement will provide slightly more rate than a seven-spot for the total mobility ratios in Fig. 5.2. Even though an ideal flow equation has not been written for this pattern, we know from Chapter Three that dimensionless pressure is largely independent of pattern geometry. Thus, we can calculate the flow rate according to Eq. 4.17 or Eq. 4.18, using the dimensionless pressure of either the five-spot or seven spot (Eq. 3.20a or Eq. 3.20c), or perhaps an average of these p_D values.

Figure 5.4 shows the conductivity relationships for $M_T = 0.2$ and $M_T = 5.0$. Here, for $M_T = 0.2$, $(P/I)_{max} = 0.45$, and for $M_T = 5.0$, $(P/I)_{max} = 1/0.45$, or 2.22. Note from

Figures 5.2 and 5.4, when $M_T > 1.0$, $(P/I)_{max} > 1.0$, and when $M_T < 1.0$, $(P/I)_{max} < 1.0$. Also, as the total mobility ratio, M_T , gets further away from 1.0, the difference between the conductivity at $(P/I)_{max}$ and $(P/I)_{min}$ gets larger. For $M_T = 0.2$ and $M_T = 5.0$, the conductivity ratio is about one-half between the highest and lowest conductivity patterns.

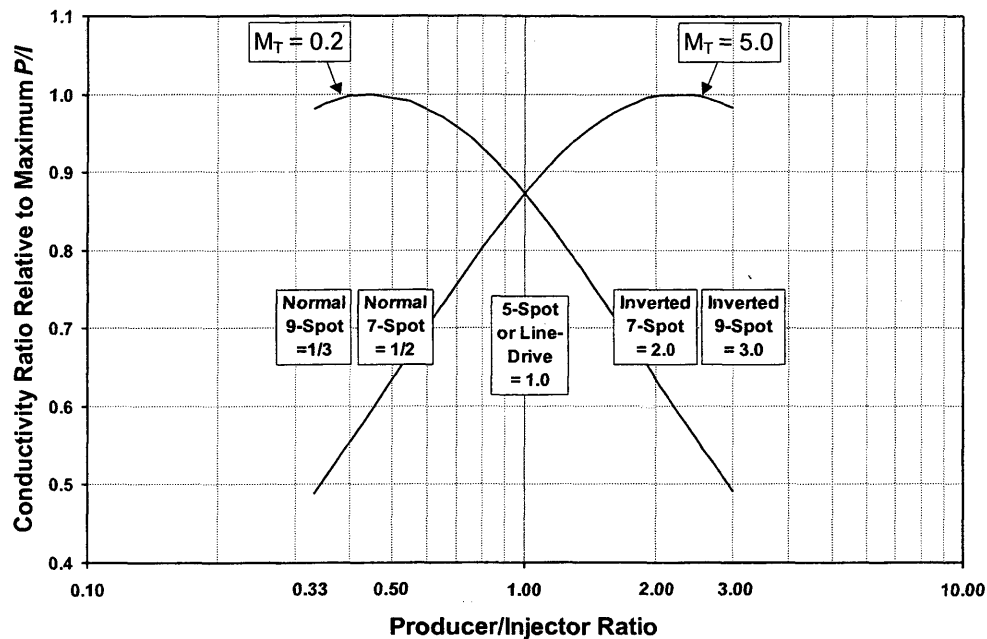


Fig. 5.4 – Conductivity Ratio relationships for $M_T = 0.2$ and $M_T = 5.0$.

The preceding discussion has very significant implications for the economics of a flood. For example, if the total mobility ratio $M_T = 0.2$, then the economically optimum

pattern will probably not be an inverted nine-spot, since this would provide about one-half the rate that could be achieved with a normal seven-spot. The economically optimum pattern ultimately may not be a normal seven-spot, depending on the capital investment required to convert wells to injection and/or install the necessary fluid handling facilities. Note that a five-spot will in most cases provide over 85% of the capacity of $(P/I)_{max}$. At the same time, for a reservoir system with $M_T = 5.0$ it would not be necessary to add more injection wells than required for an inverted nine-spot (for a five-spot), since this pattern provides 98% of the maximum possible reservoir flow rate.

The conductivity relationship for any total mobility ratio can be determined easily with the procedure outlined above. The relative cost/benefit of implementing any given pattern can then be evaluated easily in homogeneous, isotropic reservoirs.

5.2 Conductivity Relationship Including Skin

The effects of skin on the conductivity ratio will now be examined for an example case where the injection skin $S_{(inj)}$ and production skin $S_{(prod)}$ are the same for all patterns. A plausible scenario where this might occur would be where the injection wells will be operated at formation parting pressure such that the injectors will always have a negative skin as compared to the producers for any given pattern. For this example, a comparison of the patterns will be made where

$$S_{(inj)} = -2.0$$

and

$$S_{(prod)} = 0.0.$$

Figure 5.5 shows the conductivity relationships for $M_T = 0.2$, $M_T = 1.0$ and $M_T = 5.0$, with the above skin factors. Note how the relationships for $M_T = 0.2$ and $M_T = 5.0$ are no longer symmetrical about the $P/I=1.0$ axis, but are skewed. Comparing Fig. 5.5

with previous figures, we see that the conductivity relationships are expanded at higher total mobility ratios, and vice-versa. That is, since the injectors have a negative skin, there is a larger difference in conductivity between $(P/I)_{max}$ and $(P/I)_{min}$ at larger total mobility ratios. If the producers had a negative skin, or the injectors had a positive skin, there would be more difference between $(P/I)_{max}$ and $(P/I)_{min}$ at *lower* total mobility ratios.

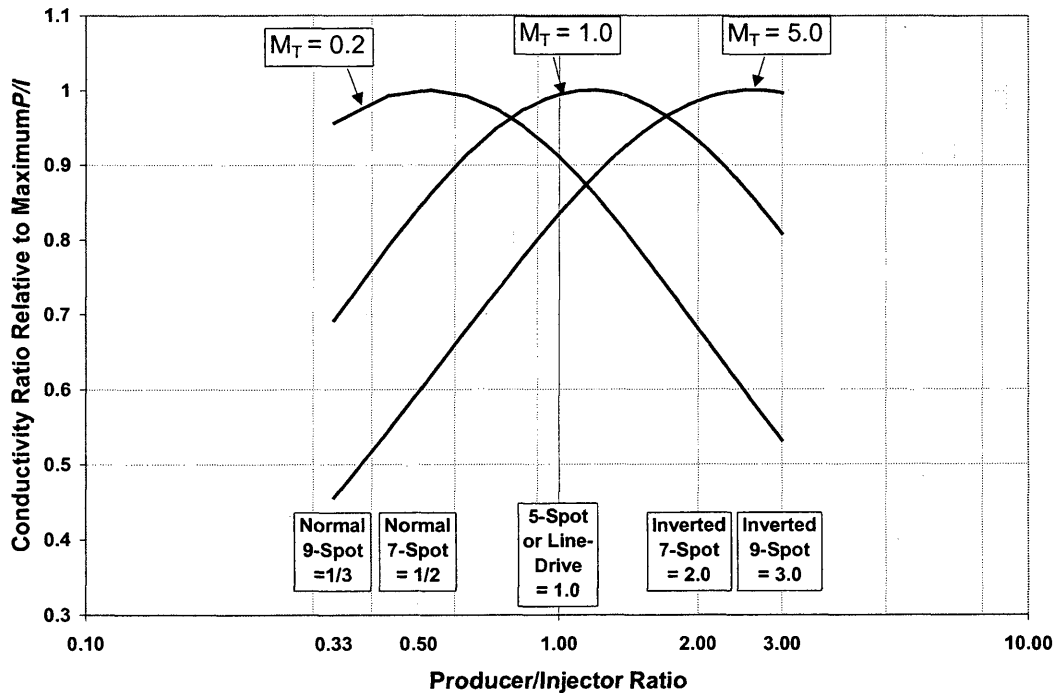


Fig. 5.5 – Conductivity Ratio relationships for $M_T = 0.2$, $M_T = 1.0$, and $M_T = 5.0$ where $S_{(inj)} = -2.0$ and $S_{(prod)} = 0.0$.

5.3 Conductivity Relationship in Heterogeneous, Isotropic Systems

If the reservoir heterogeneity is limited to variable formation permeability-thickness, kh , and variable porosity-thickness, ϕh , (i.e. not anisotropy), then the conductivity relationships presented for homogeneous systems can be used with good results if the following condition applies:

$$P/I = \frac{\sum_{j=1}^{N_P} f_{(j)} \times kh_{(j)}}{\sum_{j=1}^{N_I} f_{(j)} \times kh_{(j)}}, \quad (5.6)$$

that is, the total permeability-thickness of the producers to the total permeability-thickness of the injectors is approximately equal to the producer/injector ratio for any pattern that might be implemented in a given reservoir. This is probably a very good assumption for most reservoirs.

5.4 Conductivity Ratio Versus Conductance Ratio

As a final comparison of the conductivity ratio as defined by Eq. 5.4 or 5.5 with previous work, Aronofsky and Ramey³, in developing a flow correlation for a five-spot using a potentiometric flow model, defined a conductance ratio, γ . This is the ratio of the pattern flow rate at a given percentage of area swept by the displacing fluid, to the pattern flow rate with only the displaced fluid flowing. At areal sweep less than 50%, the conductance ratio can be related to the conductivity ratio given by Eq. 5.4, where $(\bar{\lambda}_{TI})_1 \neq (\bar{\lambda}_{TI})_2$, $(\bar{\lambda}_{TP})_1 = (\bar{\lambda}_{TP})_2$, and $(P/I)_1 = (P/I)_2$, as

$$\gamma = \frac{(\bar{\lambda}_{TI})_1 (M_T + P/I)_2}{(\bar{\lambda}_{TI})_2 (M_T + P/I)_1}. \quad (5.7)$$

At an areal sweep efficiency, E_A , equal to 50%, $\frac{(\bar{\lambda}_{TI})_1}{(\bar{\lambda}_{TI})_2} = M_t$, $(M_T)_1 = M_t$, and $(M_T)_2 = 1.0$. Willhite¹², in Tables 6.6 & 6.7, shows for a mobility ratio $M=1.0$, the total mobility ratio, $M_t = 0.932$ for $E_A = 0.50$ (Table 6.6). Using Eq. 5.6, the conductance ratio is calculated as

$$\gamma = 0.932 \frac{(1+1)}{(0.932+1)} = 0.9648.$$

This compares with a value of 0.965 reported in Table 6.7 of Ref. 12.

CHAPTER SIX

COMPARISON OF ANALYTICAL AND NUMERICAL PATTERN RELATIONSHIPS

The relationships developed analytically in Chapter Three, Chapter Four, and Chapter Five will now be compared with numerical results. It will be shown how the individual well effective total mobilities, λ_{Ti} , and the total mobility ratio, M_T , are estimated, and then calculated from the numerical results. The results will be compared for two different mobility ratio systems, $M=0.2$ and $M=5.0$, and also for the $M=0.2$ system including skin effect. A commercial, black oil reservoir simulator (TeraSim, Duke Engineering, Calgary) was used to generate the numerical results.

6.1 – Numerical Model Description

Fig. 6.1 shows the 41 x 41, 2D-grid used for modeling 20-acre, two-phase patterns. With a well in each corner, pattern elements of the nine-spot, direct line-drive, and five-spot patterns can be simulated. In modeling an element of symmetry for a given pattern, the grid porosities and transmissibilities in the corner and edge cells are modified in the standard way such that lines of symmetry pass through the well centers. The well productivity indices are also adjusted by a factor of one quarter. The producers and injectors are operated at a constant sand-face pressure constraint, so that any pressure and flow rate variations predicted in the model are the result of changing total mobilities within the reservoir. These model parameters are consistent with the assumptions used in the analytical equations.

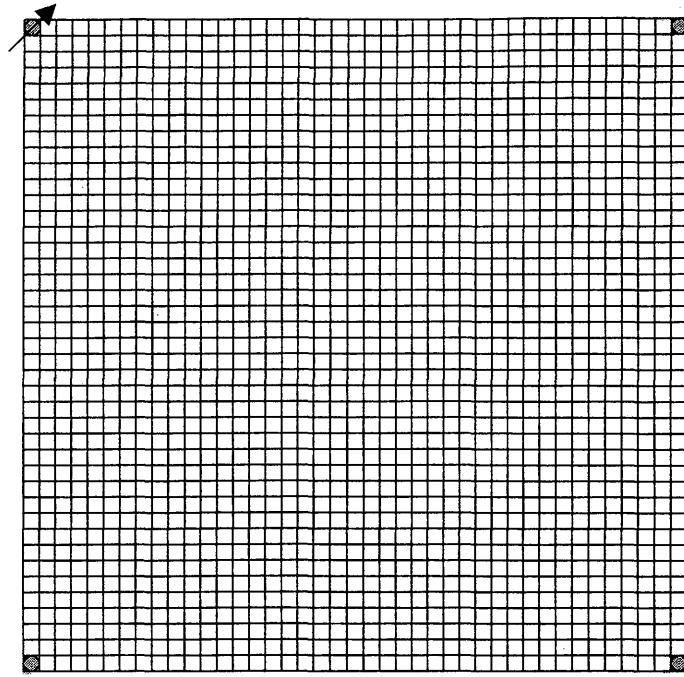


Fig. 6.1 – 41 x 41 2D simulation grid showing element of symmetry for inverted nine-spot pattern, with wells in corner cells.

6.2 - Calculating Effective Total Mobilities

As discussed in Chapter Four, the individual well effective total mobilities are the equivalent total mobilities that will result in the same pressure drop within each well region from the wellbore radius to average pressure contour. Since most of the flow in patterns can adequately be described as radial or nearly radial^{2,4}, especially near the wells, the effective total mobilities for each pattern well as defined for Eqs. 4.1a – 4.1d can be determined using the same approach outlined by Willhite¹² for calculating an “average apparent viscosity”, $\bar{\lambda}_f^{-1}$, near the injection well:

$$\bar{\lambda}_{rf}^{-1} = \frac{\int_{r_w}^{r_f} \lambda_r^{-1} dr / r}{\ln(r_f / r_w)}. \quad (6.1a)$$

This is simply the reciprocal of the formula for radial series averaging of total mobility from the well out to an effective radius r_f . For the modeling results to be presented, this formula was applied with a numerical integration of the simulation output (oil and water relative permeabilities and viscosities for each grid cell) at numerous timesteps. Figure 6.2 graphically illustrates the procedure used. Since radial flow dominates, arcs of increasing radius are superimposed on the cartesian grid to delineate rings beginning at the wellbore. The average total mobility for each ring is determined by weighting the mobility of every cell that has a portion of its area in the ring, and summing the results. The weighting factor for a given cell is equal to the proportion that the cell's area within the ring bears to the total ring area. Once the average total mobility is calculated for all rings (out to a certain radial distance from the well), the *effective* total mobility is calculated for each well as

$$\lambda_{r_{eff}} = \frac{\ln(r_n / r_w)}{\sum_{j=1}^n \left(\frac{\ln(r_j / r_{j-1})}{\lambda_{Tj}} \right)}, \quad (6.1b)$$

where

$r_j \equiv$ outer radius of ring j , feet.

$r_{j-1} \equiv$ inner radius of ring j , feet.

$\lambda_{Tj} \equiv$ total mobility of ring j , cp^{-1} , and

λ_{Teff} \equiv effective near-well total mobility, cp^{-1} .

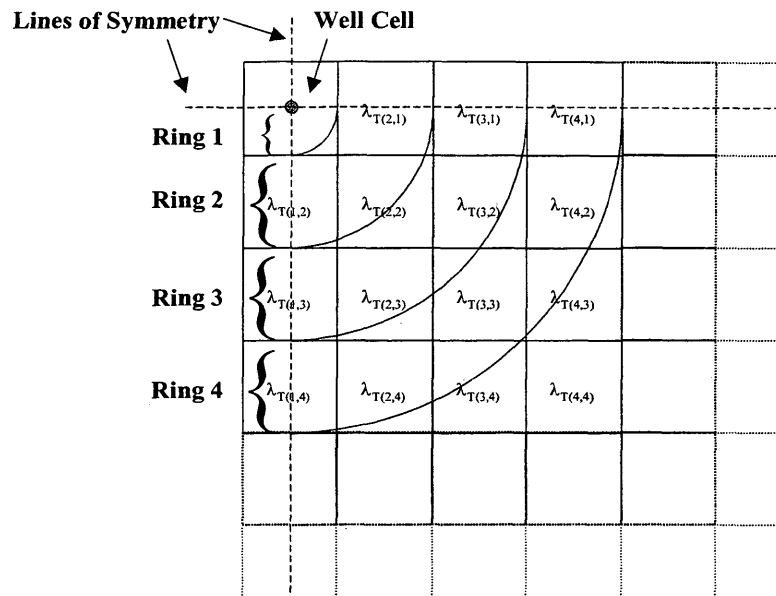


Fig. 6.2-Graphical representation of effective near-well total mobility calculation procedure for each pattern well.

A study of Eq. 6.1 will reveal that the mobilities closer to the well have the larger impact on the effective total mobility calculation for a well, which is a characteristic of radial flow. As a result, it is not essential to account for mobilities further away from a well since these have an increasingly smaller impact on the effective total mobility

calculation. We can therefore very closely approximate the effective total mobility for an individual well by employing Eq. 6.1b out to a sufficiently large radial distance from the well. For the numerical results presented here, twenty rings were used for each well, i.e. $n=20$ in Eq. 6.1b, which is about halfway between wells, or $0.5d$. This number of rings accounts for total mobilities within 75% of the simulation area, i.e. that portion being closest to the wells.

As an example, Ring 3 in Fig. 6.2 contains portions of 8 cells. When calculating the total mobility within Ring 3, the area that each of these cells contains within the ring is calculated. Then, the total area of the ring is determined by summing these areas for the eight cells. Finally, the fraction of the total area that each cell contributes to the ring is multiplied by the mobility of the cell, then summed to obtain the total mobility of the ring. Note that even with significantly different mobilities within each cell of a given ring, the total amount of fluid conducted by the ring will be related to the weighted average total mobility of the ring as described above. This is because the pressures on the inner and outer radius of a ring coincide with pressure contours in the reservoir, and thus the same pressure drop occurs across the entire ring. After the effective near-well total mobility is calculated for each well using Eq. 6.1b, the average injection and producing well effective total mobilities $\bar{\lambda}_{Ti}$ and $\bar{\lambda}_{Tp}$ are calculated according to Eq. 4.8a and Eq. 4.8b. A listing of a computer program which calculates the cell areas in the rings, extracts the relative permeabilities and viscosities from the simulator output and performs the above calculations is included in Appendix D. This expands the definition of total mobility ratio as presented by Willhite¹²,

$$M_t = \frac{1}{\bar{\lambda}_{rf}^{-1} \lambda_{ro}},$$

where λ_{ro} is the relative mobility of the oil phase (water is at irreducible). In contrast to λ_{ro} , $\bar{\lambda}_{TP}$ in Eq. 4.6 is defined for all patterns, and includes the total mobility of both phases to allow for the calculation of pressures and flow rates after breakthrough. Also, Eq. 4.8a and Eq. 4.8b show how $\bar{\lambda}_{TI}$ and $\bar{\lambda}_{TP}$ are calculated for producer/injector ratios other than one. The methodology shown by Willhite¹² using M_I to predict pattern flow rates in non-unit total mobility systems is developed for the pre-breakthrough period for the five-spot and line-drive patterns only, whereas the equations presented here apply to all patterns before and after breakthrough.

6.3 – Numerical vs. Analytical Results for $M = 0.20$ System

The numerical results will now be compared to the analytical equations using the procedure outlined above for estimating the effective total mobilities of each well. Figure 6.3 shows the relative permeability relationship and the oil and water viscosities representing a system with $M=0.20$.

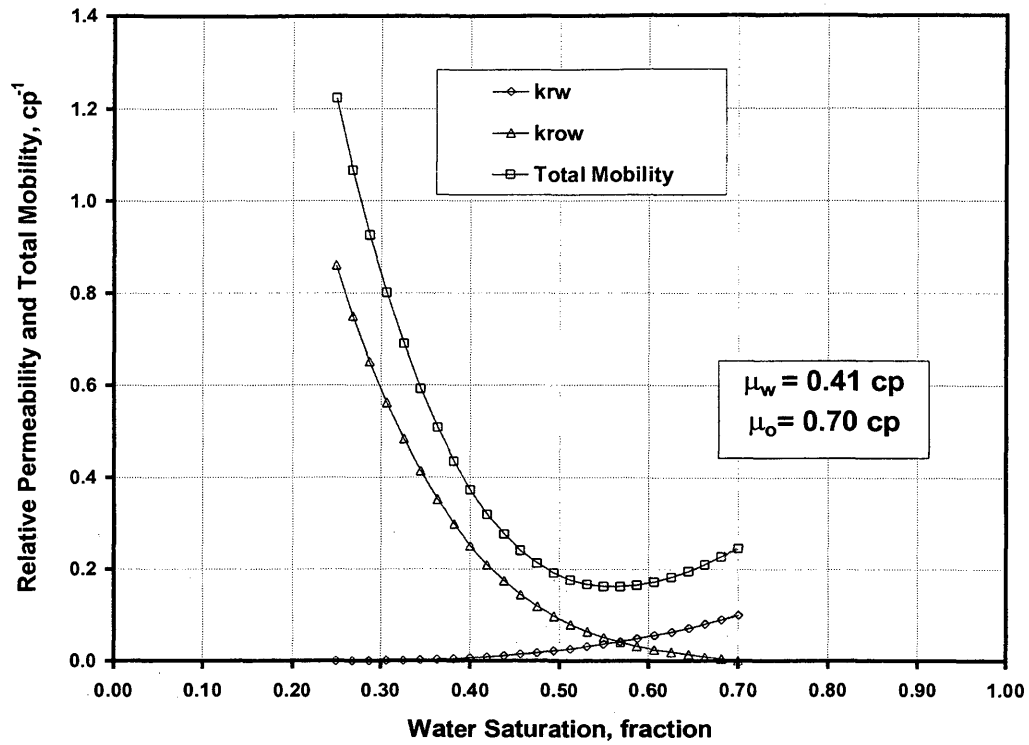


Figure 6.3 – Relative permeability and total mobility relationship for $M=0.2$ system.

Using the relative permeability relationship shown in Fig. 6.3, the numerical results were generated for the normal nine-spot, the five-spot, and inverted nine-spot. In the simulation, the sand-face pressures are held constant, where $p_{wfI} = 5000$ psi, and $p_{wfP} = 100$ psi. The wells had no skin effect.

Figure 6.4 shows the average effective injection well total mobility, $\bar{\lambda}_{TI}$, and the total mobility ratio, M_T , calculated from the simulation output at regular simulation intervals using the “ring” method described above, and Eq. 4.8 and Eq. 4.6.

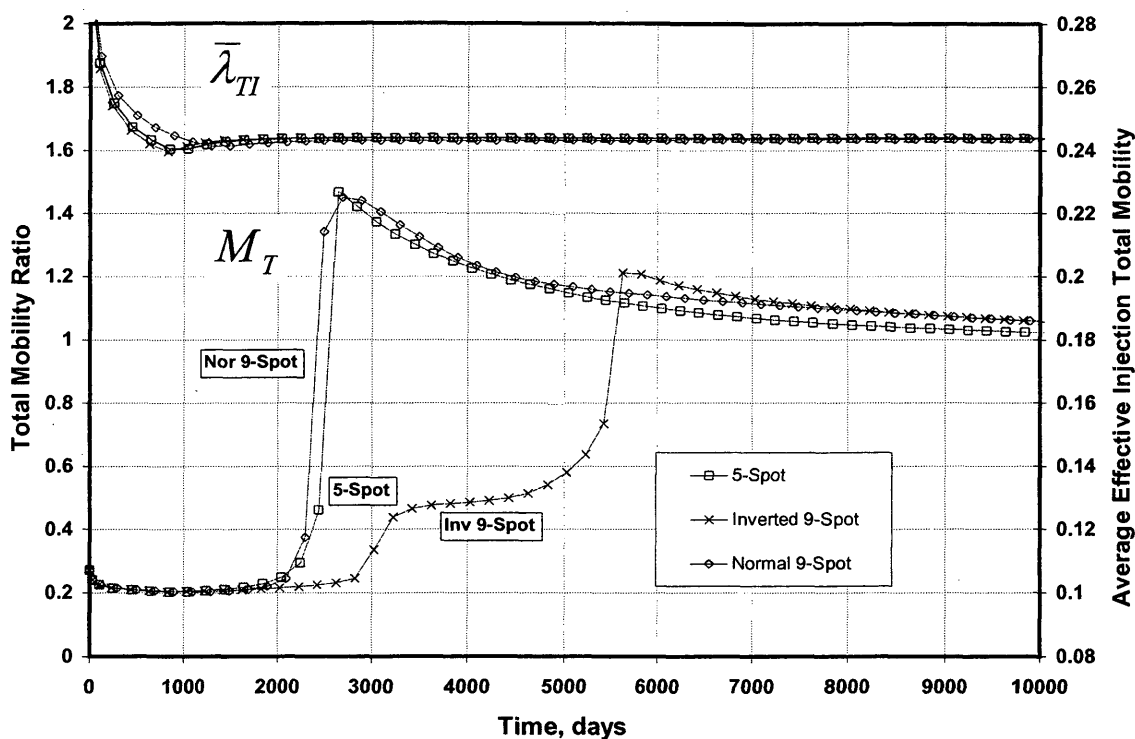


Fig. 6.4 – Total mobility ratio M_T and average effective injection total mobility $\bar{\lambda}_{TI}$ for simulated patterns as determined from ring method for $M=0.2$ system.

Note how $\bar{\lambda}_{Tt}$ changes almost identically for all the patterns, quickly settling at the endpoint mobility of water. This behavior is typical of systems with $M < 1$, or “favorable” mobility ratios, as the water is increasingly efficient at displacing the oil with decreasing M . At very low M , the displacement approaches “pistonlike” displacement. As will be shown, at $M > 1$, the displacement is less efficient and $\bar{\lambda}_{Tt}$ changes more gradually with time.

The values shown in Fig. 6.4 are then used to calculate the average reservoir pressure and reservoir flowrate using Eq. 4.7, and Eq. 4.18 and Eq. 5.2, respectively. Note that for non-unit total mobility ratios, steady-state flow technically does not exist because of the constantly changing mobilities resulting from ever changing saturations within the reservoir. However, the flood can be treated as a series of steady-states that can be described by the above equations at discrete points, or snapshots in time.

Figure 6.5 shows the average pressures calculated using Eq. 4.7 and the values shown in Fig. 6.4 for several points in time for the three pattern simulations. The simulated results are shown as continuous lines, while the calculated values are shown as

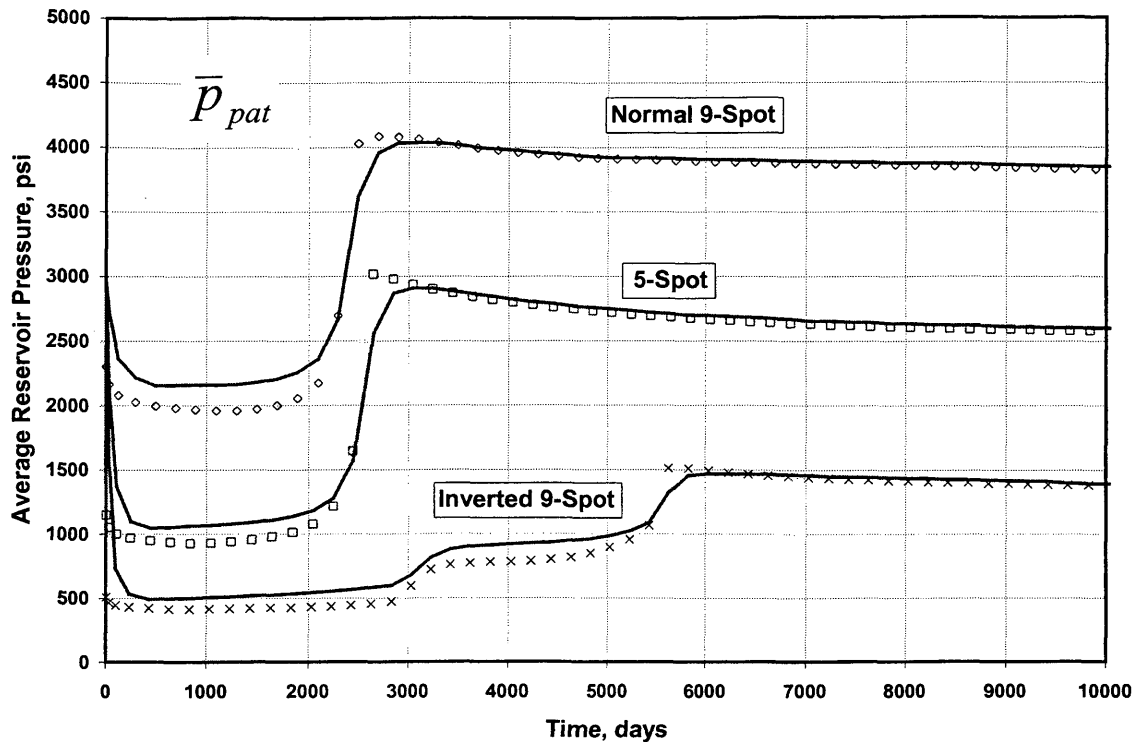


Fig. 6.5 – Calculated vs. simulator average reservoir pressures for $M=0.2$ patterns.

individual points. Referring to Fig. 6.5, prior to water breakthrough the calculated results are lower than the simulated results, within about 10% or less typically (breakthrough can be seen as the abrupt change in reservoir pressures at approximately 2500 days for the 5-spot and normal nine-spot – for the inverted nine-spot the side well breakthrough and corner well breakthrough can be seen separately at 3000 days and 5500 days). However, after water breakthrough, the calculated results are much closer, typically within 1-2 percent. The larger discrepancy prior to breakthrough is probably due to the rapid changing of saturations near the flood front, resulting in the assumption of steady-state

being somewhat less valid. After breakthrough, the saturations are changing much more gradually, and hence the steady-state assumption would apply with more validity.

Figure 6.6 shows the comparison between the calculated and simulated reservoir flow rates \tilde{q} , again using the parameters shown in Fig. 6.4 with Eq. 4.18 and Eq. 5.2. Again, the calculated values are shown as points while the simulator rates are shown as continuous lines. Note the excellent agreement between the calculated and simulator values before and after water breakthrough.

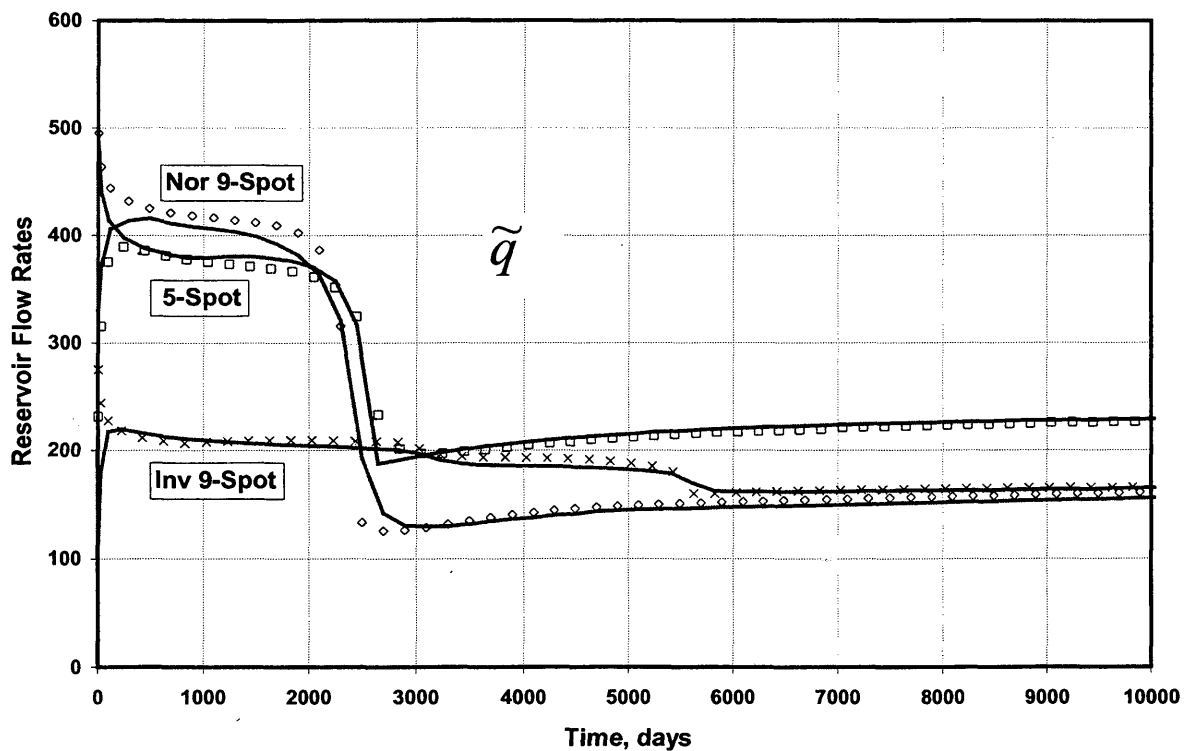


Fig. 6.6 – Calculated vs. simulator reservoir flow rates for $M=0.2$ patterns.

Using a few reference points, we can compare the relative rates shown on Fig. 6.6 with the conductivity ratio method described in Chapter Five using the conductivity relationships shown on Fig. 6.7. From Fig. 6.4, at 1,000 days all patterns have $M_T = 0.2$ and equivalent $\bar{\lambda}_{PI}$, such that Eq. 5.5a describes the conductivity relationship. Comparing

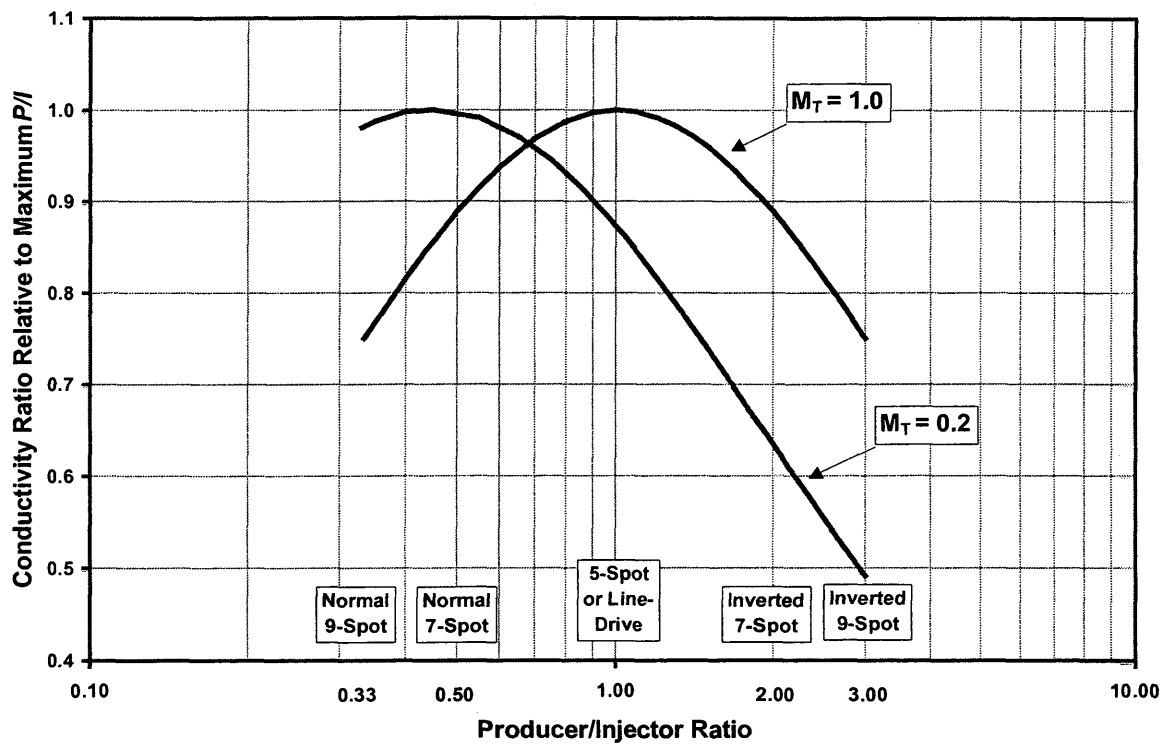


Fig. 6.7 – Conductivity relationships for $M_T = 0.2$ & $M_T = 1.0$.

the reservoir flow rates in Fig. 6.6 to the conductivity relationship for $M_T = 0.2$ in Fig. 6.7, we see that the flow rates are aligned according to this relationship. As another reference, at 8,000 days and after M_T is approximately equal to 1.0 for all patterns, and the rates have realigned according to the $M_T = 1.0$ conductivity relationship.

6.4 – Numerical vs. Analytical Results for $M = 5.0$ System

Following the same procedure as in the previous section, the numerical results for an “unfavorable” mobility ratio system with $M=5.0$ are compared to the analytical equations. Figure 6.8 shows the relative permeability relationship and viscosities for this rock-fluid system. Using the relationship shown in Fig. 6.8, the numerical results were generated for the normal nine-spot, the five-spot, and inverted nine-spot, where the sand-face pressures are held constant with $p_{wf} = 5000$ psi and $p_{wp} = 100$ psi, and the wells had no skin effect.

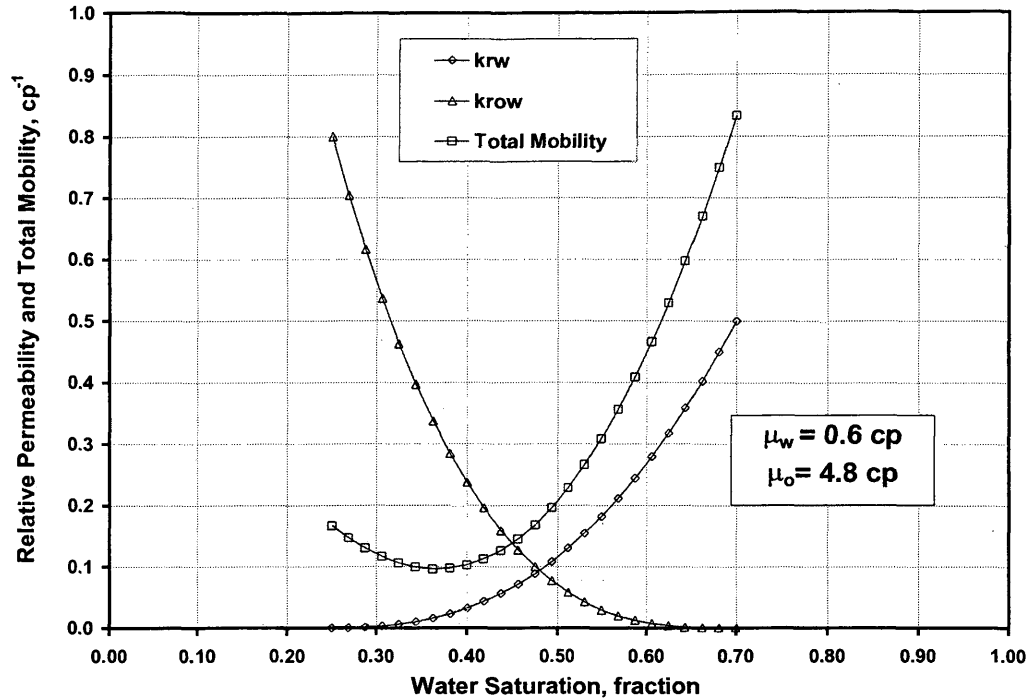


Figure 6.8 – Relative permeability and total mobility relationship for $M=5.0$ system.

Figure 6.9 shows the average effective injection well total mobility, $\bar{\lambda}_{TI}$, and the total mobility ratio, M_T , calculated from the simulation output at regular simulation intervals again using the “ring” method. Note how $\bar{\lambda}_{TI}$ changes at different rates between all the patterns. This relative difference in $\bar{\lambda}_{TI}$ is the result of the differences in injection rates among the patterns. For systems with $M > 1.0$ prior to breakthrough, as producer/injector ratio decreases, reservoir flowrates decrease and individual injection

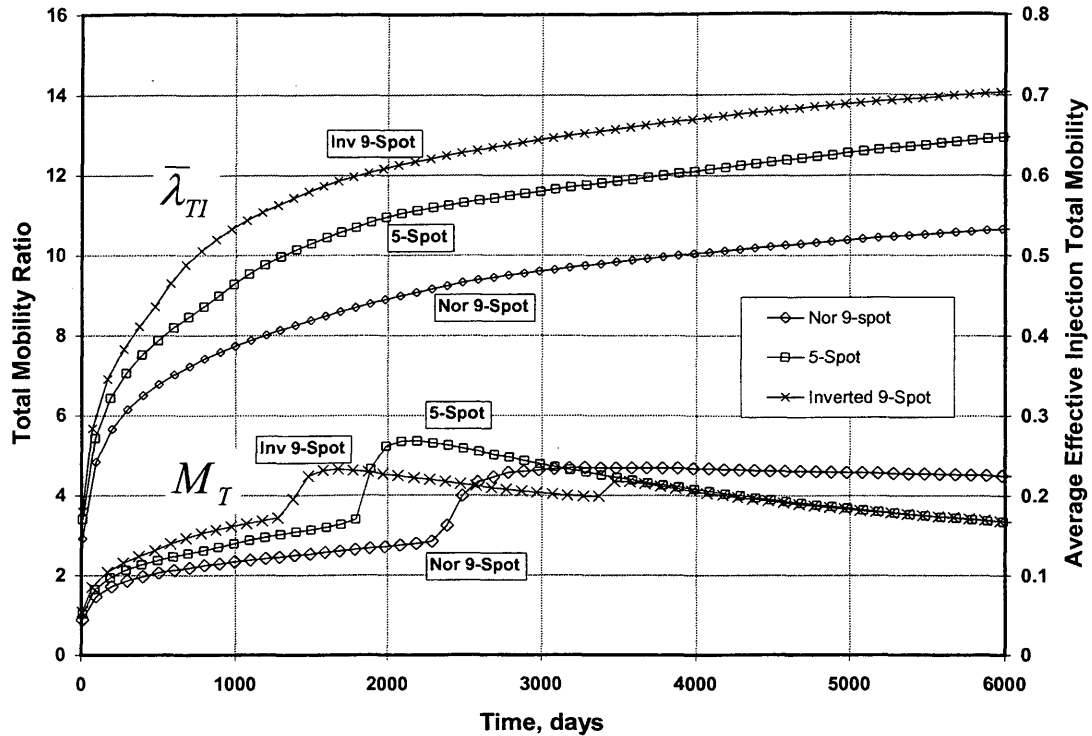


Fig. 6.9 – Total mobility ratio M_T and average effective injection total mobility $\bar{\lambda}_{TI}$ for simulated patterns as determined from ring method for $M=5.0$ system.

well rates decrease even more because the reservoir flowrate is distributed amongst an increasing number of injectors. This compounding effect on the individual injection well rate as P/I decreases results in a much slower advance in the flood front around individual injectors, and a correspondingly slower increase in $\bar{\lambda}_{TI}$. This behavior is typical of systems with $M > 1$, or “unfavorable” mobility ratios, as the water is increasingly less efficient at displacing the oil with increasing M . For all of the patterns,

$\bar{\lambda}_T$ continues to increase throughout the flood life (asymptotically toward the endpoint mobility of water) because oil is continuing to be swept from the water contacted portion of the reservoir. Note also how M_T continually increases prior to breakthrough, and approaches but is less than the endpoint mobility ratio M . As will be shown below and also in Chapter Seven, even though there are not insignificant differences in $\bar{\lambda}_T$ and M_T between the patterns, Eq. 5.5 can be used with excellent results to compare the relative conductivities of the patterns prior to water breakthrough.

Figure 6.10 shows the average pressures calculated using Eq. 4.7 and the values shown in Fig. 6.9 for several points in time for the three pattern simulations. The simulated results are shown as continuous lines, while the calculated values are shown as individual points. In contrast to when $M = 0.2$, any differences between the calculated and simulated average pressures are in the reverse direction, with post-breakthrough results typically in closer agreement, which again could be due to a deviation from the steady-state assumption. In any case, the comparisons between the numerical and analytical results are quite good.

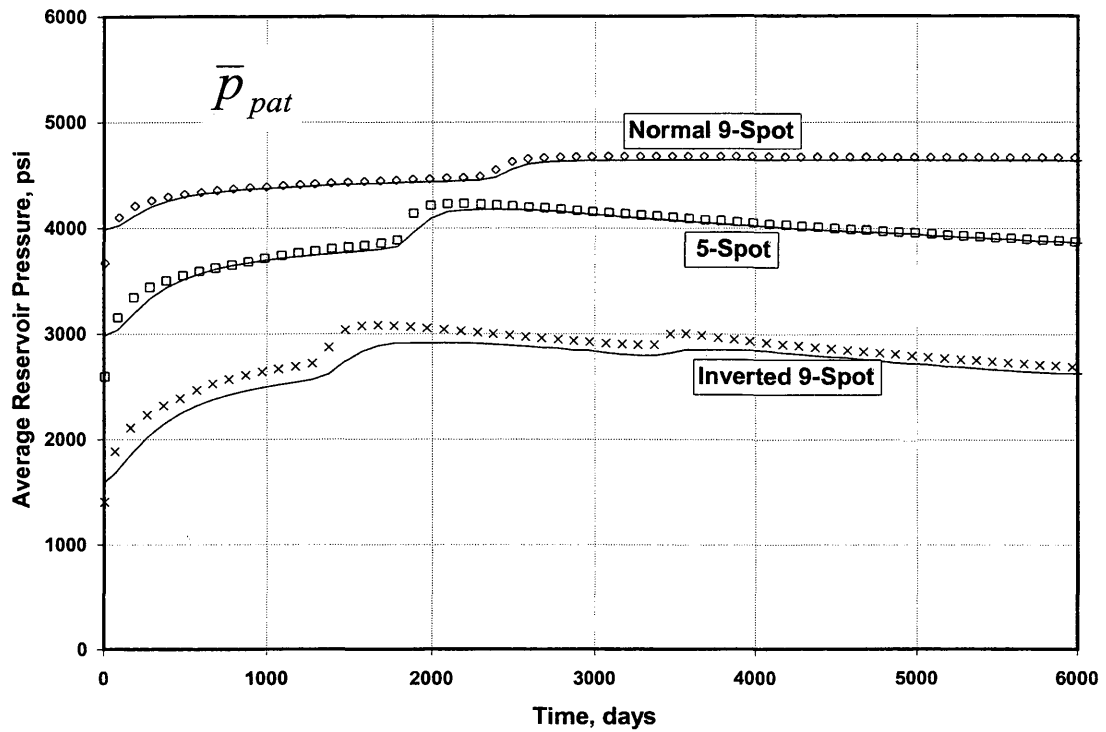


Fig. 6.10 – Calculated vs. simulator average reservoir pressures for $M=5.0$ patterns.

Figure 6.11 shows the comparison between the calculated reservoir flow rates \tilde{q}_{inj} , again using the parameters shown in Fig. 6.4 with Eq. 4.18 and Eq. 5.2. As before, the calculated values are shown as points while the simulator rates are shown as continuous lines. Again there is excellent agreement between the calculated and simulator values.

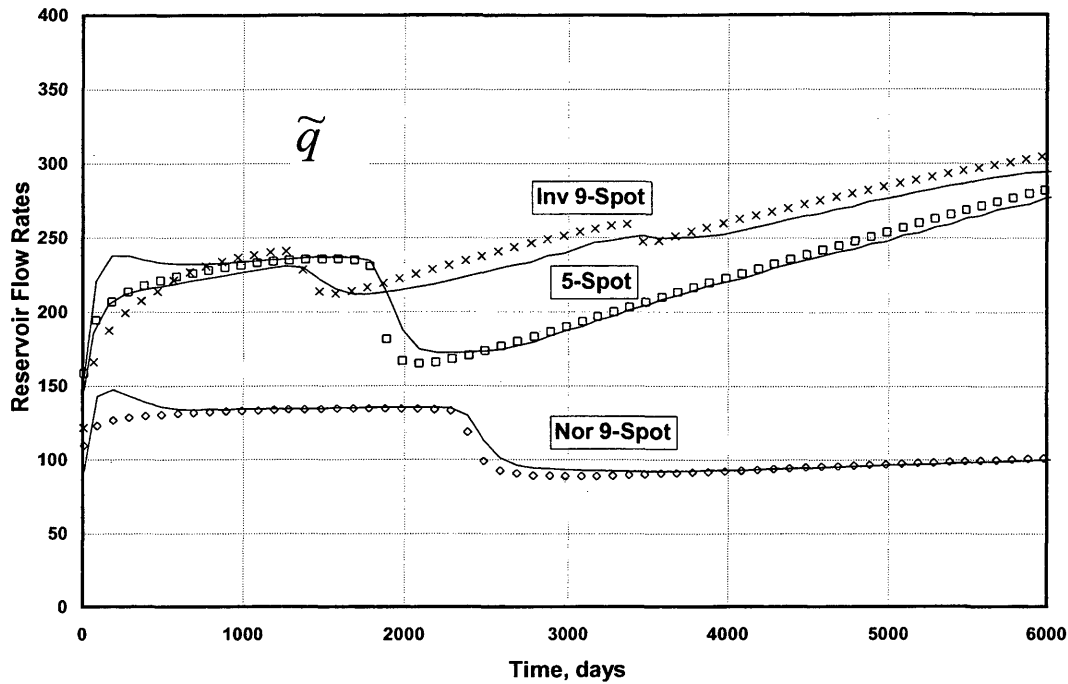


Fig. 6.11 – Calculated vs. simulator reservoir flow rates for $M=5.0$ patterns.

We can once again compare the numerical results shown in Fig. 6.11 with the conductivity relationship presented in Chapter Five. Referring to Fig. 6.9, prior to water breakthrough (<1268 days for inverted nine-spot), M_T increases from 1.0 to approximately 3.0 for all patterns during this period. At the same time, $\bar{\lambda}_{T1}$ increases from the endpoint mobility of oil to approximately 0.50 for the five-spot, with the other patterns being within 15-20% of the five-spot value at any given point in time. Even though there is a significant difference in these parameters between the patterns, a valid comparison can still be made using a single, average value for each of these parameters in

Eq. 5.4. The reason for this is that as M_T increases, reservoir flow rate \tilde{q} as given by Eq. 5.2 becomes less sensitive to the variable $\bar{\lambda}_{TI}$. In fact, it can be shown in a straightforward manner by taking the partial differential of Eq. 5.2 that

$$\frac{\partial \tilde{q} / \tilde{q}}{\partial \bar{\lambda}_{TI} / \bar{\lambda}_{TI}} = \frac{P/I}{M_T + P/I}, \quad (6.2)$$

that is, the percent error in the value of \tilde{q} relative to the percent error in $\bar{\lambda}_{TI}$ is given by the right hand side of Eq. 6.2. Figure 6.12 shows the behavior of Eq. 6.2, where it can be seen that as P/I decreases and M_T increases, the percent change in \tilde{q} relative to the percent change in $\bar{\lambda}_{TI}$ goes down. For example, when $M_T = 5.0$ and $P/I = 1.0$, a 10% error in $\bar{\lambda}_{TI}$ will translate into about a 2% error in \tilde{q} . Of course, the values given by Eq. 6.2 are tangents, and changing $\bar{\lambda}_{TI}$ will automatically change M_T such that the absolute change in \tilde{q} will also depend on the magnitude of change in $\bar{\lambda}_{TI}$. Note that for all

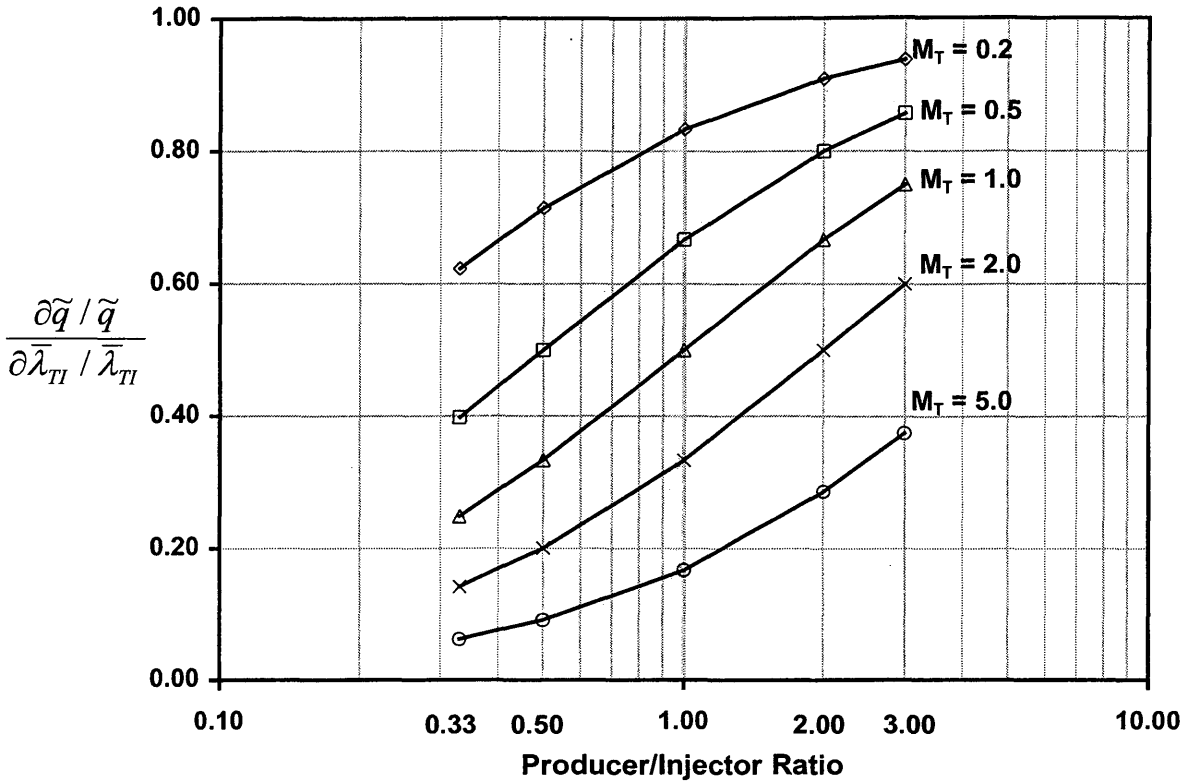


Fig. 6.12 – Percent error in the value of \tilde{q} relative to percent error in $\bar{\lambda}_{TI}$ vs. M_T and P/I .

values, the percent change in \tilde{q} is always less than the percent change in $\bar{\lambda}_{TI}$. This is because in Eq. 5.2, $\bar{\lambda}_{TI}$ appears in the numerator as well as the denominator (in M_T), so there is not a one-to-one correspondence.

Fig. 6.12 shows why a larger degree of uncertainty in $\bar{\lambda}_{TI}$ at larger total mobility ratios can be tolerated when calculating absolute rates, and how a comparison between patterns based on Eq. 5.5 for the numerical results shown above will yield very acceptable results. Note that this comparison applies best prior to breakthrough, i.e. when

$\bar{\lambda}_{Tp}$ is the same between all patterns. Thus, referring again to Fig. 6.9, since prior to breakthrough an average M_T for all the patterns is approximately 2.5, and as stated above $\bar{\lambda}_{Tl}$ (and thus M_T) does not vary by more than 20% from the average value any point in time, we can estimate from Fig. 6.12 that the largest error that can be expected by ignoring $\bar{\lambda}_{Tl}$ in the conductivity ratio comparison (Eq. 5.5) is approximately

$$\frac{3.0}{2.5 + 3.0} = 0.55 \left(\frac{\partial \tilde{q} / \tilde{q}}{\partial \bar{\lambda}_{Tl} / \bar{\lambda}_{Tl}} \text{ at } P/I = 3.0 \right)$$

minus

$$\frac{0.33}{2.5 + 0.33} = 0.12 \left(\frac{\partial \tilde{q} / \tilde{q}}{\partial \bar{\lambda}_{Tl} / \bar{\lambda}_{Tl}} \text{ at } P/I = 0.33 \right)$$

times 20% (variance in $\bar{\lambda}_{Tl}$), that is $(0.55 - 0.12)0.2$, or 8.6%. Of course, if we know $\bar{\lambda}_{Tl}$ for each pattern then we can use Eq. 5.4 with even better results. As will be shown in Chapter Seven, the value of $\bar{\lambda}_{Tl}$ that corresponds to the average flow rate before water breakthrough is within 10% for all of the patterns at any given mobility ratio, and thus an even smaller error is expected by ignoring $\bar{\lambda}_{Tl}$ in the conductivity ratio comparison given by Eq. 5.5.

Figure 6.13 shows the conductivity relationships for $M_T = 2.0$ & $M_T = 3.0$. Interpolating between these relationships, we see from Fig. 6.11 that prior to water breakthrough the pattern rates are aligned very closely according to these relationships. That is, the inverted nine-spot and five-spot have about equal rates, and the normal nine-spot has about 60% of these rates.

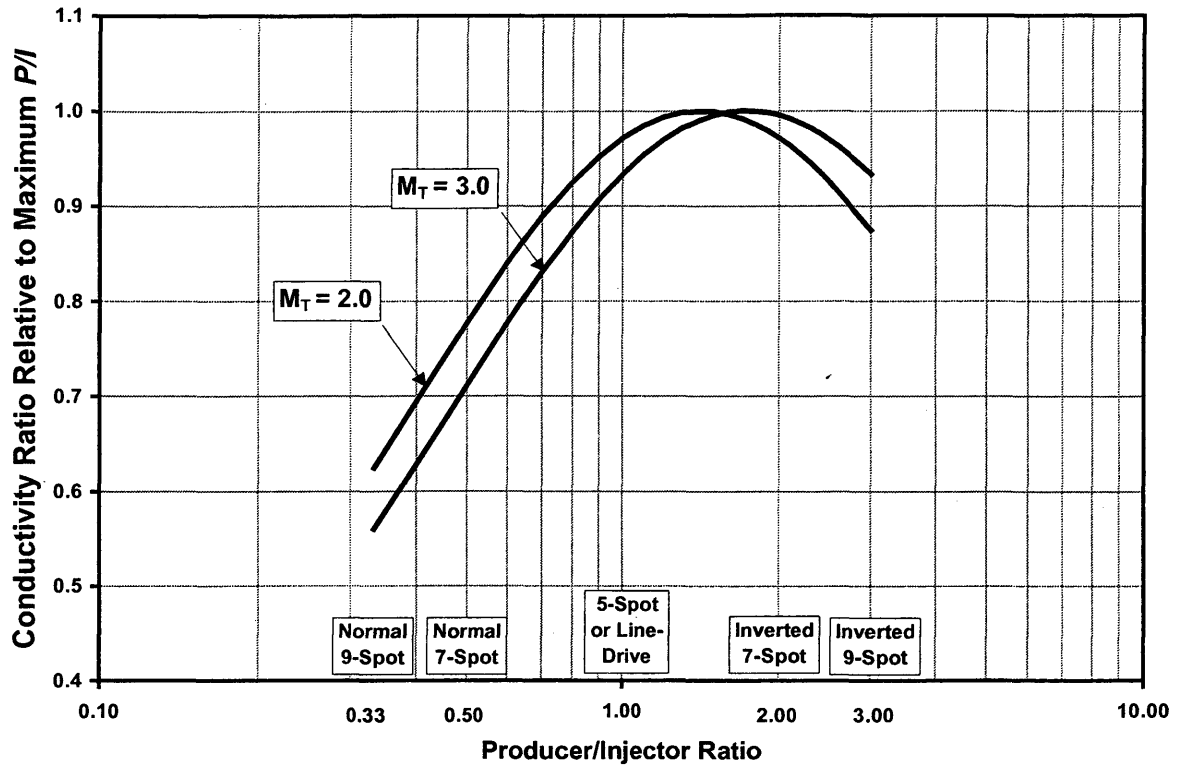


Fig. 6.13 – Conductivity relationships for $M_T=2.0$ & $M_T=3.0$.

The above discussion shows the difficulty that can exist predicting M_T prior to breakthrough for systems with $M > 1.0$, since unlike systems with $M < 1.0$, M_T can be significantly different from M and harder to predict. However, Eq. 6.2 shows how this difficulty in predicting $\bar{\lambda}_{Tf}$ (and thus M_T) as M increases is offset to a large degree by the characteristics of the flow rate calculation. If we know a good average value for these parameters for all the patterns we can predict absolute and relative reservoir flow rates with good accuracy. In Chapter Seven, a correlation between M and M_T is presented for

the pre-breakthrough period for use in the equations presented in this thesis for a range of relative permeability curve shapes.

6.5 – Numerical vs. Analytical Results for $M = 0.20$ System Including Skin Effect

The numerical results and the analytical equations will be compared for the system where $M=0.2$ (Fig. 6.3), now also including skin effect for the pattern wells of an inverted nine-spot pattern, to compare to the equations presented in Chapter Four (Eqs. 4.23 through 4.32). This comparison will show how $S_{(prod)}$ and \tilde{P}/\tilde{I} are not constant, but vary with time according to changes in relative producing well flow rates. As with prior simulations, the sand-face pressures are held constant, where $p_{wf} = 5000$ psi, and $p_{wfp} = 100$ psi.

Fig. 6.14 again shows the simulation grid use for the numerical modeling, and also the skin effect that was applied to each of the element wells for an inverted nine-spot pattern. The two side well producers have a skin effect of $S = +5$ and $S = +10$, respectively, and the corner producing well has a skin effect of $S = +20$. The injection well skin was set to zero. The large variation in skin effect for the producing wells was chosen to show the application of Eq. 4.26 and Eq. 4.32, and the variation that can occur in $S_{(prod)}$ and \tilde{P}/\tilde{I} with the inverted-nine spot, due to the flow rates of the side-and-corner producers changing differently with time.

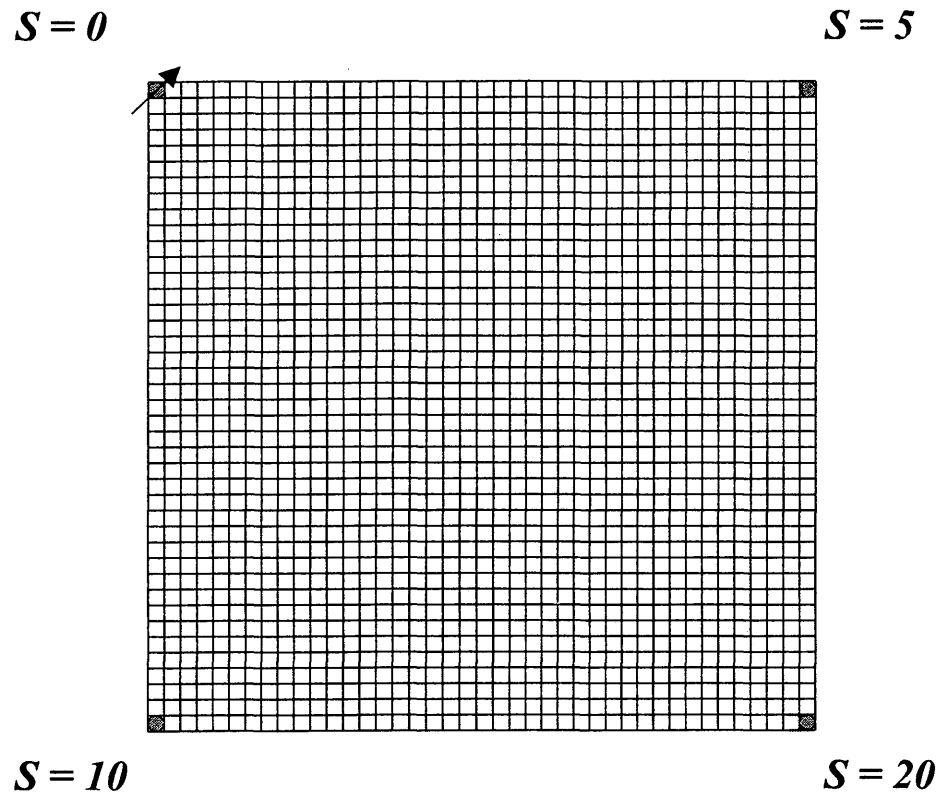


Fig. 6.14 – 41 x 41 2D simulation grid showing element of symmetry for inverted nine-spot pattern, showing skin effect applied to each pattern well.

Figure 6.15 shows the average producing skin $S_{(prod)}$ calculated with Eq. 4.30b and estimated with Eq. 4.32, the effective producer injector ratio, \tilde{P}/\tilde{I} , calculated from Eq. 4.26, and the total mobility ratio M_T (Eq. 4.6). These quantities were determined at several times from simulation output parameters. The dimensionless pressure for the 20-

acre inverted nine-spot for use in Eq. 4.26 and Eq. 4.32 was calculated using Eq. 3.20f, as

$P_{D(9-spot)} = 7.547$ for equal side and corner producing sand-face pressures. Note

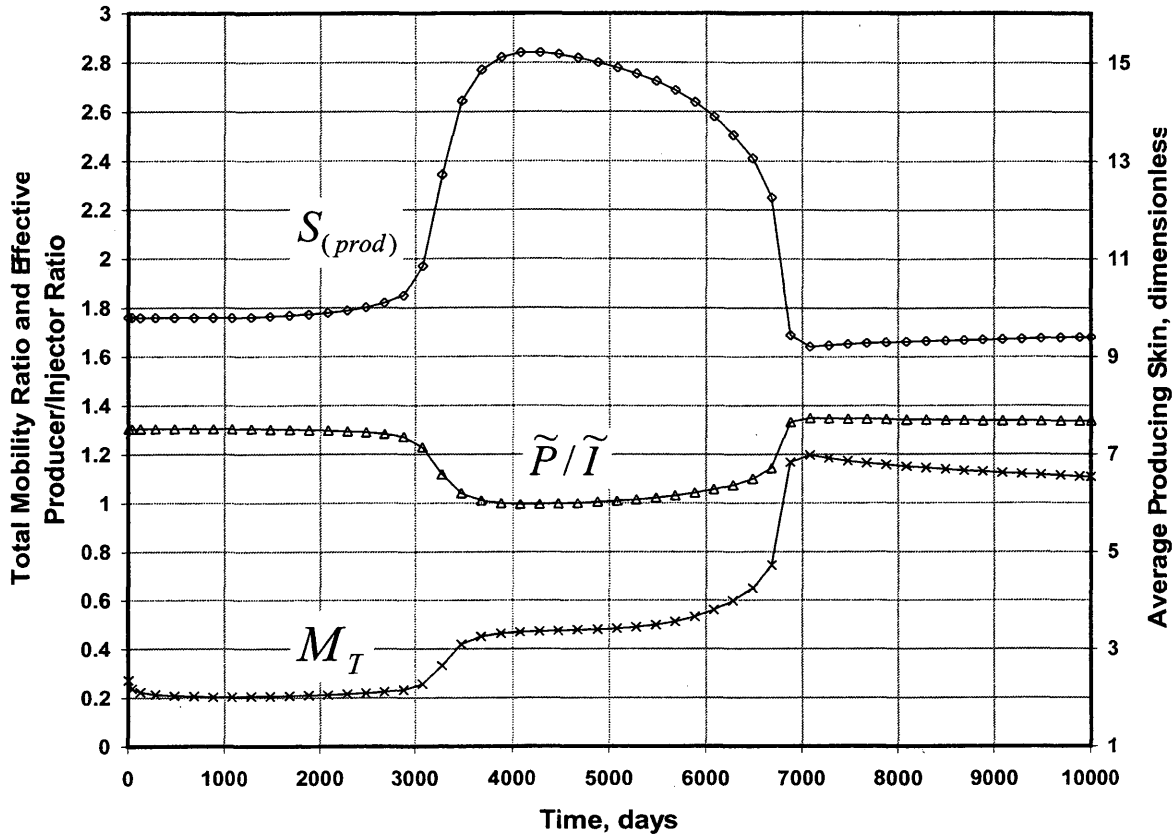


Fig. 6.15 – Total mobility ratio M_T , effective producer/injector ratio \tilde{P}/\tilde{I} , and average producing skin $S_{(prod)}$ as determined from numerical results for inverted nine-spot pattern with $M=0.2$ system.

from Fig. 6.15 that the average producing skin $S_{(prod)}$ changes as a result of flow rate differences in the side and corner producers as breakthrough occurs first in the side producers. As discussed in Chapter Four, the relative magnitude of these flow rates are

estimated with the effective total mobilities (as determined from ring method) of the side-and-corner wells as shown by Eq. 4.32. The rate changes result in corresponding changes in the effective producing skin, $S_{(prod)}$ and the effective producer injector ratio, \tilde{P}/\tilde{I} , as indicated by Eq. 4.26 and Eq. 4.32. These parameters were used to calculate the average reservoir pressure \bar{p}_{pat} (Eq. 4.27) and reservoir flowrate \tilde{q} (Eq. 4.29 and Eq. 5.2) as shown on Fig. 6.16. As with prior comparisons, the simulated results are shown as continuous lines, while the calculated values are shown as individual points. Note the excellent agreement between the calculated and simulator results.

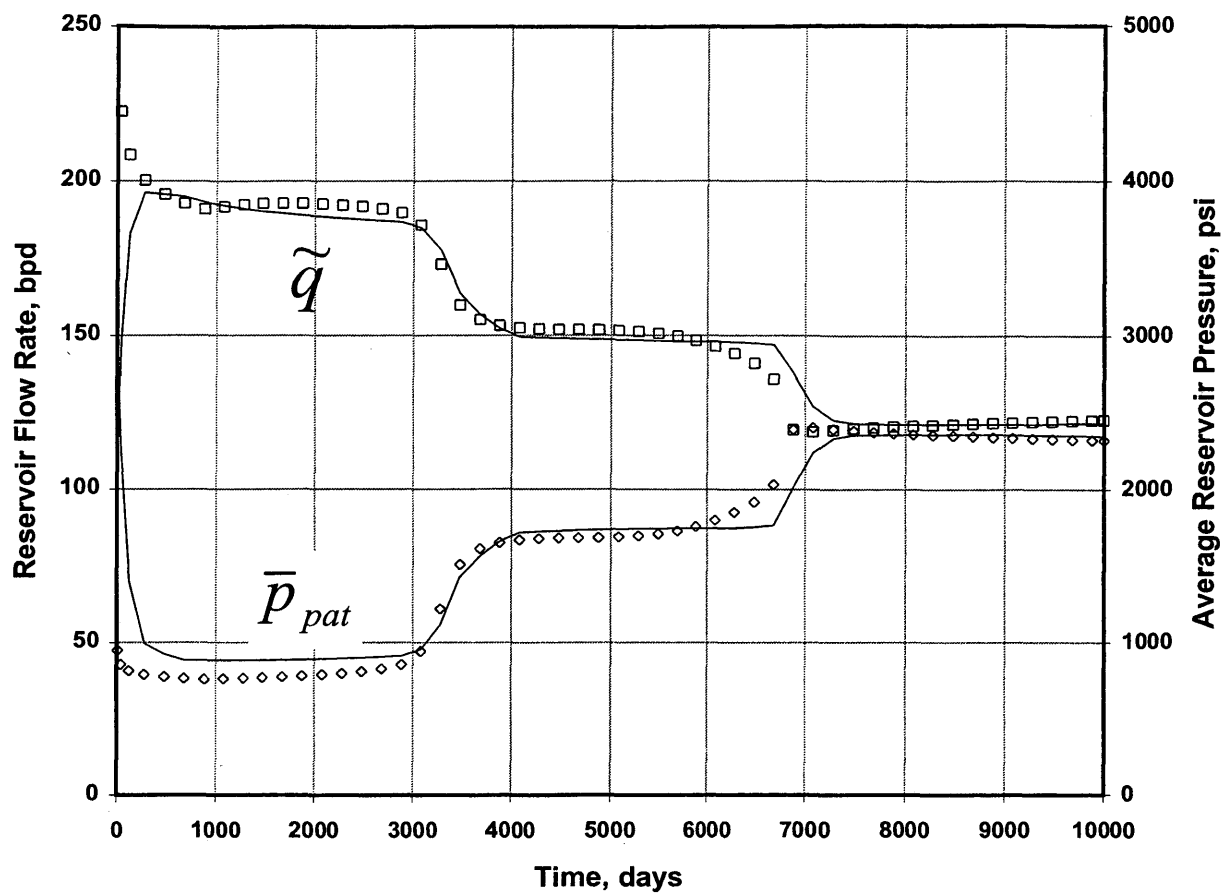


Fig. 6.16 – Calculated vs. simulator reservoir flow rates and average reservoir pressures for inverted nine-spot including skin for $M=0.20$ system.

CHAPTER SEVEN
CORRELATION FOR TOTAL MOBILITY RATIO, M_T ,
PRIOR TO WATER BREAKTHROUGH
VERSUS MOBILITY RATIO, M

In this chapter, a correlation for the total mobility ratio, M_T , versus the endpoint mobility ratio, M , is presented for a range of relative permeability curve shapes. This correlation is for the pre-breakthrough period, and was developed from simulation results. The correlation can be used to accurately predict reservoir flow rates and reservoir pressures in homogeneous, isotropic, non-unit total mobility ratio systems prior to water breakthrough. The pre-breakthrough performance is treated because of the significance that this period has on the economics of a project. Example calculations are shown in Appendix C, where the absolute and relative flow performance of patterns is compared to determine the highest flow capacity pattern before water breakthrough using the equations presented in Chapters Four and Five.

7.1 – Description of Correlation Methodology

Willhite¹² presents a range of relative permeability curves based on varying the exponent m in the relative permeability relationship given by

$$k_{ro} = \alpha_1(1 - S_{wD})^m, \quad (7.1)$$

where

k_{ro} = oil relative permeability in presence of water,

α_1 = end-point oil relative permeability in presence of water,

$$S_{wD} = \frac{S_w - S_{iw}}{1 - S_{or} - S_{iw}},$$

S_{iw} = irreducible water saturation,

and

S_{or} = residual oil saturation.

The water relative permeability is given by the relationship

$$k_{rw} = \alpha_2 S_{wD}^n, \quad (7.2)$$

where

k_{rw} = water relative permeability,

and

α_2 = end-point water relative permeability.

Figure 7.1 shows the oil relative permeability curves calculated with Eq. 7.1 for $m = 1, 2, 3, 4,$ and 5 , for $\alpha_1 = 1.0$, as also presented in Ref. 8. The water relative permeability curve calculated from Eq. 7.2 for $n = 2$ is also shown on the figure, where $\alpha_2 = 0.10$. Note that the endpoint relative permeabilities are not characteristic to the correlation to be presented, but rather only the exponents m and n . That is, the endpoint relative permeabilities are simply scaling factors, and any endpoint relative permeabilities can be used in the correlation. For the correlation to be presented, only the oil exponent m was varied, while the water exponent n was fixed, at $n = 2.0$.

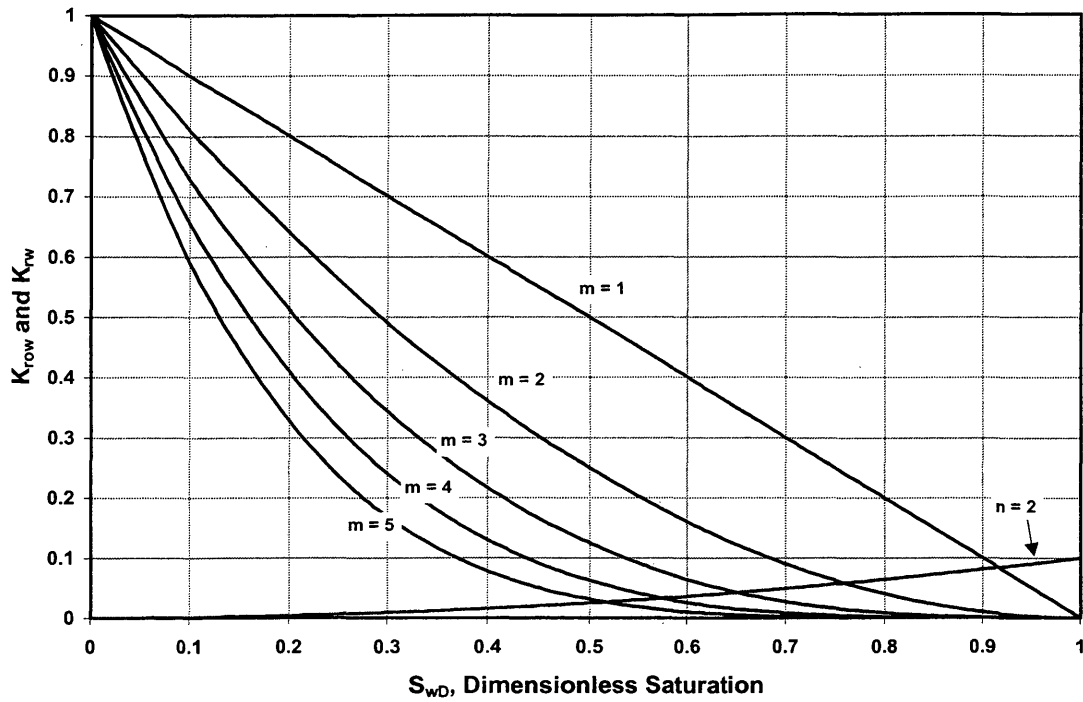


Fig. 7.1 – Oil relative permeability curves as calculated from Eq. 7.1 for different m exponents, and water relative permeability as calculated from Eq. 7.2 for $n = 2$ (after Willhite¹²).

The correlation to be shown is based on the average reservoir flow rate prior to water breakthrough, where the total mobility ratio was back-calculated according to a rearranged form of Eq. 4.18, also substituting $\bar{\lambda}_{TI} = M_T \bar{\lambda}_{TP}$ (Eq. 4.6) to calculate M_T as

$$M_T = \frac{P/I}{\left[\frac{kh\Delta P(P/I)\bar{\lambda}_{TP}}{141.2 p_{D(inj)} q_{ave}} - 1 \right]} \quad (7.3)$$

Note that the average effective injection total mobility is calculated from the correlation value of M_T and the specific value of $\bar{\lambda}_{TP}$ for a given reservoir with $\bar{\lambda}_{TI} = M_T \bar{\lambda}_{TP}$, for use in the equations presented in Chapter Four and Chapter Five. Note also that the correlation total mobility ratio can be used when skin effect is present.

7.2 - Correlation M_T versus M Prior to Water Breakthrough

Table 7.1 shows the correlation for between M_T and M for the oil relative permeability exponents shown in Fig. 7.1, $m=1, 2, 3, 4$, and 5 , for the five-spot, the inverted nine-spot, and the normal nine-spot. Figure 7.2 shows graphically the information shown on Table 7.1 for exponents $m = 1, 3$, and 5 , while Fig. 7.3 shows the relationships for exponents $m = 2$ and 4 .

Table 7.1 – Average M_T before water breakthrough vs. M for various oil relative permeability exponents m .

m	M	5-spot	<i>Inverted</i> 9-spot	<i>Normal</i> 9-spot
1	0.2	0.2069	0.2121	0.2110
2	0.2	0.2046	0.2103	0.2034
3	0.2	0.1843	0.1891	0.1804
4	0.2	0.1589	0.1663	0.1536
5	0.2	0.1375	0.1456	0.1330
1	0.5	0.5122	0.5186	0.5228
2	0.5	0.4809	0.4849	0.4745
3	0.5	0.4188	0.4307	0.4087
4	0.5	0.3543	0.3679	0.3396
5	0.5	0.3056	0.3144	0.2890
1	0.7	0.7114	0.7152	0.7241
2	0.7	0.6483	0.6570	0.6459
3	0.7	0.5645	0.5760	0.5449
4	0.7	0.4720	0.4864	0.4529
5	0.7	0.3993	0.4129	0.3814
1	1.0	0.9833	0.9795	0.9874
2	1.0	0.8861	0.8977	0.8763
3	1.0	0.7652	0.7758	0.7238
4	1.0	0.6453	0.6485	0.6045
5	1.0	0.5388	0.5484	0.5085
1	2.0	1.835	1.813	1.756
2	2.0	1.602	1.592	1.503
3	2.0	1.328	1.333	1.234
4	2.0	1.093	1.100	1.025
5	2.0	0.920	0.920	0.850
1	3.0	2.572	2.444	2.365
2	3.0	2.218	2.129	1.979
3	3.0	1.772	1.773	1.615
4	3.0	1.453	1.470	1.332
5	3.0	1.218	1.233	1.106
1	5.0	3.628	3.494	3.238
2	5.0	3.071	2.989	2.727
3	5.0	2.536	2.468	2.210
4	5.0	2.079	2.075	1.835
5	5.0	1.755	1.748	1.564

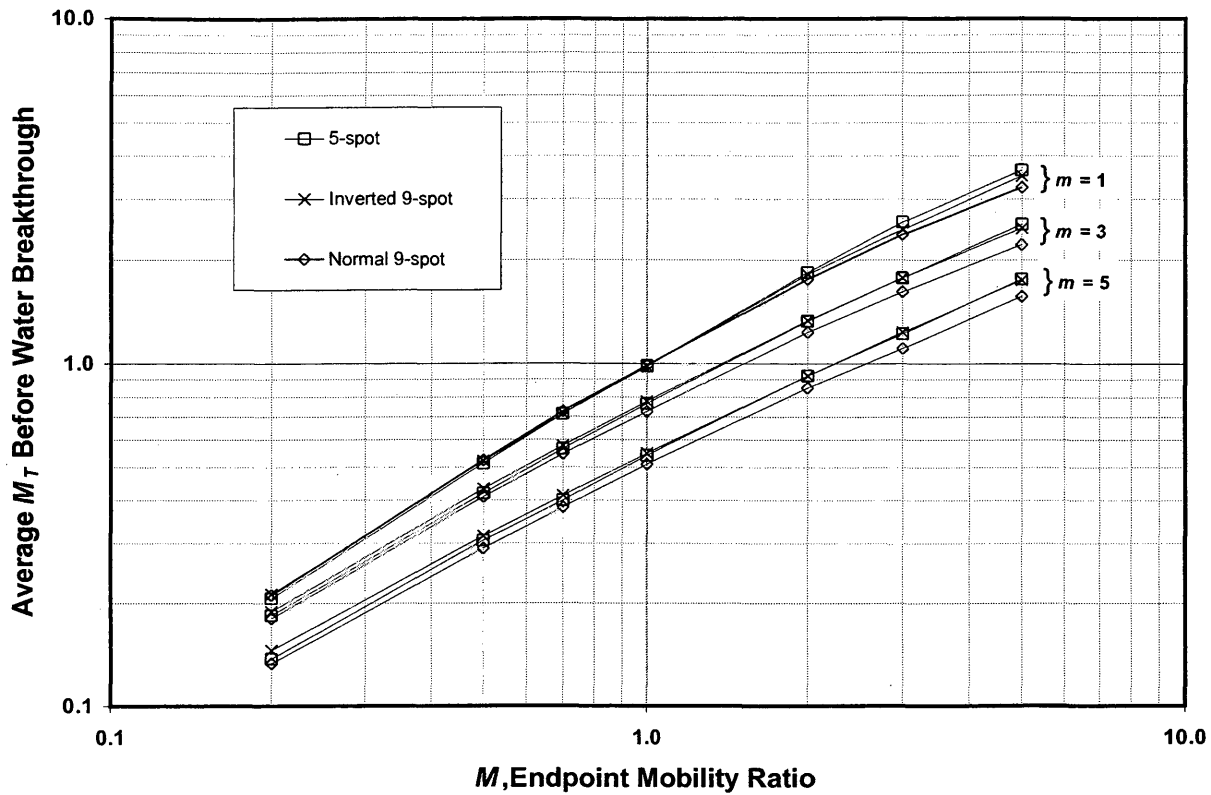


Fig. 7.2 – Average M_T before water breakthrough vs. M for oil relative permeability exponents $m=1$, $m=3$, and $m=5$.

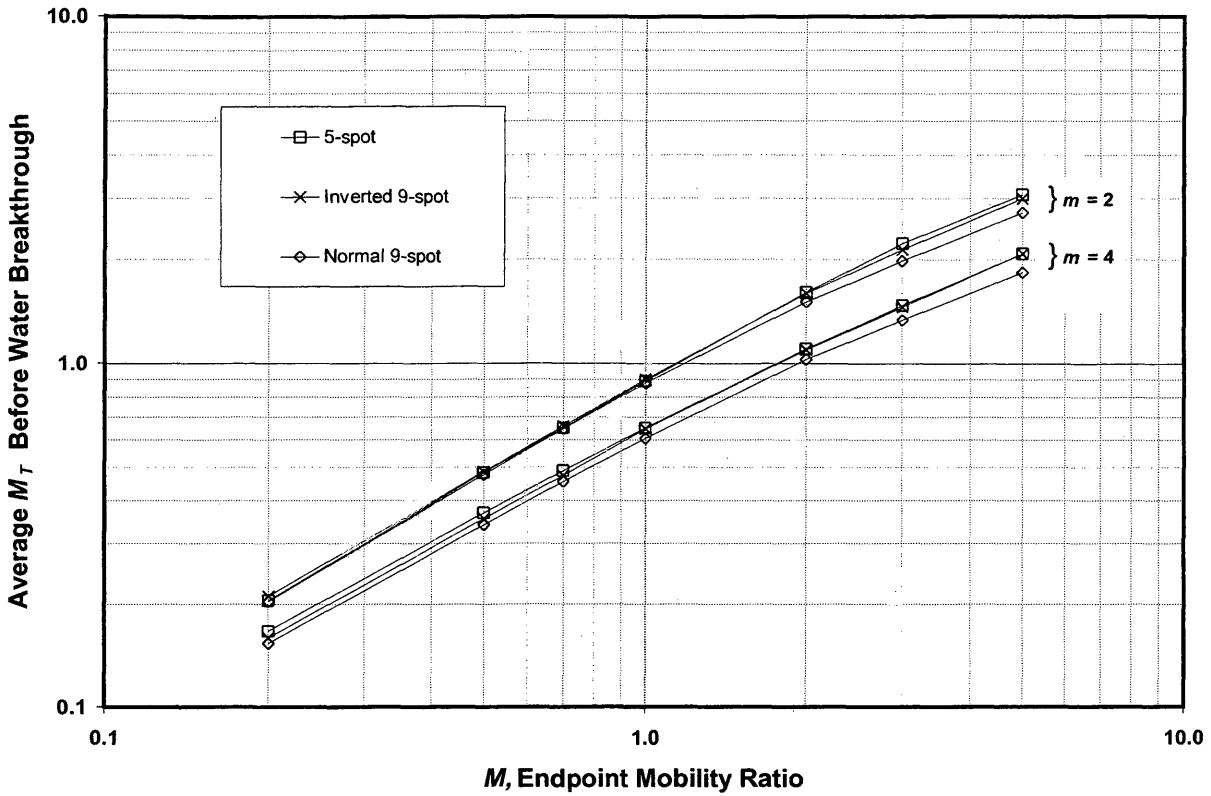


Fig. 7.3 – Average M_T before water breakthrough vs. M for oil relative permeability exponents $m=2$ and $m=4$.

Referring to Table 7.1 and Figures 7.2 and 7.3, note how M_T becomes increasingly less than M as M increases and the oil relative permeability exponent m increases. Also note how the values of M_T for the five-spot and inverted nine-spot are almost identical at any given combination of M and m , while the normal nine-spot is less.

However, the values at any given mobility ratio are always within 10% or less. As discussed in Chapter Six and referring to Fig. 6.12 and Eq. 6.2, at total mobility ratios greater than 2.0, the expected error in the calculated rate relative to the error in $\bar{\lambda}_T$ is given by Eq. 6.2 as

$$\frac{0.33}{2.0 + 0.33} = 0.14.$$

Therefore, using the values of M_T for the five-spot or inverted nine-spot in Table 7.1 to calculate the rates for all of the patterns results in an expected error of about $(0.14)(0.10)$, or 1.4%. This also applies to the conductivity ratio using Eq. 5.5. Note that if the value of M_T given in Table 7.1 for the normal nine-spot was used for all patterns, the error in the inverted nine-spot flow rate would be

$$\frac{3.0}{2.0 + 3.0} \times 0.10 = 0.06,$$

or 6% error. Thus, M_T for the five-spot or inverted nine-spot in Table 7.1 should be used in calculating the absolute rates of all the patterns, or in the conductivity relationship using Eq. 5.5.

The data in Table 7.1 and Fig. 7.1 shows why the single phase equations given in Table 3.1 are in most cases inadequate for calculating flow rates. Only in the case where $M = 1$ and $m = 1$ can they be used with good results. However, it is probably a rare instance where the oil relative permeability curves are defined by $m = 1$. As a general rule, m is usually between 2 and 4.

7.3 – Considerations In Heterogeneous Reservoirs

The correlation presented above can be used for any homogeneous, isotropic reservoir system to determine the flow rates and average pressures that will result from each of the patterns before water breakthrough. This correlation also applies to heterogeneous, isotropic reservoirs if pore volume is homogeneous, using the adjustments to the flow equations discussed in Chapter Four. However, the correlation becomes more approximate if pore volume is heterogeneous, especially in systems where $M > 1.0$. This is because the pore volume around each injector determines how quickly the flood front moves away from the well, which in turn affects how the total mobility profile changes as a function of time, and the calculation of $\bar{\lambda}_{Tf}$. Thus this mobility profile and the resulting calculation for M_T can be somewhat different depending on the degree of pore volume heterogeneity. This is not a concern where $M < 1.0$, because the total mobility of the injection wells, or $\bar{\lambda}_{Tf}$, is established quickly in these systems as discussed in Chapter Six.

CHAPTER EIGHT

CONCLUSIONS AND RECOMMENDATIONS

The conclusions and recommendations of this thesis are presented in this chapter.

8.1 Conclusions

1. This thesis presents new equations for the average reservoir pressure and flow rate in repeated, uniform patterns after fillup when steady-state conditions apply, in homogeneous, isotropic reservoirs. Also shown is how skin and reservoir heterogeneity effects can be included in the new relationships. These equations complete and unify the single-phase and non-unit mobility pattern flow theory.
2. The new equations show how producer/injector ratio and a total mobility ratio, as defined in this thesis, control reservoir pressures and flow rates.
3. The new, generalized flow equation using the dimensionless pressure concept reveals that the dimensionless pressures defined relative to the average reservoir pressure for each of the patterns are within 5% at equal well density.
4. Comparisons of the conductivity of various patterns within the same reservoir can be based solely on the comparison of terms involving the producer/injector ratio and total mobility ratio of the patterns. These variables account for most all of the differences in flow capacities between the various patterns. This method also can be applied to heterogeneous isotropic permeability reservoirs as outlined in this thesis.
5. For total mobility ratios greater than one, the pattern providing the greatest reservoir flowrate will have a producer/injector ratio greater than one, and vice-versa.
6. The difference in reservoir flow rates provided by the highest and lowest conductivity patterns is significant in all mobility systems, but especially when the mobility ratio is

significantly higher or lower than unity. When the total mobility ratio is either 5.0 or 0.2, the difference is a factor of two between the highest and lowest conductivity patterns.

7. The skin effect can be translated as an adjustment to the physical producer/injector ratio, resulting in an effective producer/injector ratio.
8. The correlation presented between the endpoint mobility ratio M and the total mobility ratio M_T based on numerical results for several oil relative permeability curve shapes prior to water breakthrough can be used to accurately predict average pressures and flow rates in patterns using the equations presented. This correlation also applies to heterogeneous, isotropic reservoirs if pore volume is homogeneous, using the adjustments to the flow equations discussed in Chapter Four. However, the correlation becomes more approximate if pore volume is heterogeneous, especially in systems where $M > 1.0$.

8.2 Recommendations

1. When designing waterfloods in reservoirs that can be considered homogeneous and isotropic, an understanding of the relationships presented in this thesis is recommended so that the economically optimum flooding pattern can be determined.
2. An economic analysis of the optimum pattern should include the costs of conversion, operating, fluid handling requirements, etc., which will be pattern specific.
3. The relationships presented in this thesis should provide adequate results in mildly anisotropic reservoirs. If a significant degree of anisotropy exists, pattern selection based on a simulation study is recommended.

REFERENCES

1. Muskat, M.: *Flow of Homogeneous Fluids*, IHRDC, Boston (1982).
2. Deppe, J.C.: "Injection Rates – the Effect of Mobility Ratio, Area Swept, and Pattern," *Society of Petroleum Engineers Journal* (June, 1961) 81-91.
3. Aronofsky, J.S. and Ramey, H.J., Jr.: "Mobility Ratio – Its Influence on Injection and Production Histories in Five-Spot Water Flood", *Trans.*, AIME (1956) **207**, 205-210.
4. Caudle, B.H. and Witte, M.D.: "Production Potential Changes During Sweepout in a Five-Spot System," *J. Pet. Tech.* (Dec. 1959) 63-65; *Trans.*, AIME, **216**.
5. Nobles, M.A. and Janzen, H.B.: "Application of a Resistance Network for Studying Mobility Ratio Effects," *Trans.*, AIME (1958) **213**, 356-358.
6. Prats, M., Matthews, C.S., Jewett, R.L., and Baker, J.D.: "Prediction of Injection Rate and Production History for Multifluid Five-Spot Floods," *J. Pet. Tech.* (May 1959) 98-105; *Trans.*, AIME, **216**.
7. Caudle, B.H., Hickman, B.M., and Silberberg, I.H.: "Performance of the Skewed Four-Spot Injection Pattern," *J. Pet. Tech.* (Nov. 1968) 1315-19; *Trans.*, AIME, **243**.
8. Hauber, W.C.: "Prediction of Waterflood Performance for Arbitrary Well Patterns and Mobility Ratios," *J. Pet. Tech.* (Jan. 1964) 95-103.
9. Cotman, N.T., Still, G.R., and Crawford, P.B.: "Laboratory Comparison of Oil Recovery in Five-Spot and Nine-Spot Waterflood Patterns," *Prod. Monthly* (Dec. 1962) **27**, No. 12, 10-13.
10. Watson, R.E., Silberberg, I.H., and Caudle, B.H.: "Model Studies of the Inverted Nine-Spot Injection Pattern," *J. Pet. Tech.* (July, 1964) 801-804.
11. Muskat, M.: "The Theory of Nine-Spot Flooding Networks," *Prod. Monthly* (March 1948) **12**, 14.

12. Willhite, G.P.: *Waterflooding*, Textbook Series, Society of Petroleum Engineers, Richardson, TX (1986) 3.
13. Douglas, J. Jr., Peaceman, D.W., and Rachford, H.H.: "A Method for Calculating Multi-Dimensional Immiscible Displacement," *Trans. AIME*, (1959) **216**, 297-308.
14. Higgins, R.V. and Leighton, A.J.: "A Computer Method of Calculating Two-Phase Flow in Any Irregularly Bounded Porous Medium," *J. Pet. Tech.* (June 1962) 679-83; *Trans.*, AIME, **225**.
15. Fanchi, J.F.: *Principles of Applied Reservoir Simulation*, Boston: Butterworth-Heinemann (2001).
16. LeBlanc, J.L. and Caudle, B.H.: "A Streamline Model for Secondary Recovery," *Soc. Pet. Eng. J.* (March 1971) 7-12.
17. Martin, J.C. and Wegner, R.E.: "Numerical Solution of Multiphase, Two-Dimensional Incompressible Flow Using Stream-Tube Relationships," *Soc. Pet. Eng. J.* (Oct. 1979) 313-23; *Trans.*, AIME, **267**.
18. Datta-Gupta, A.: "Streamline Simulation: A Technology Update," *J. Pet. Tech.* (Dec. 2000) 68-73.
19. Craig, F.F. Jr.: *The Reservoir Engineering Aspects of Waterflooding*, Monograph Series, SPE, Richardson, TX (1971) 3, 78-95.
20. Rapaport, L.A., Carpenter, C.W., Jr., and Leas, W.J.: "Laboratory Studies of Five-Spot Waterflood Performance," *Trans.*, AIME (1958) **213**, 113-120.
21. Ziegler, V.M.: "A Comparison of Steamflood Strategies: Five-Spot Pattern vs. Inverted Nine-Spot," *SPE Reservoir Engineering*, (Nov. 1987) 549-558.
22. Craft, B.C. and Hawkins, M.F.: *Applied Petroleum Reservoir Engineering*, Prentice-Hall, Inc., Englewood Cliffs, N.J. (1959) 283-289.
23. Collins, R.E.: *Flow of Fluids Through Porous Media*, McGraw-Hill Book Company, Inc., New York (1937).
24. Honarpour, M., Koederitz, L., and Harvey, A.H.: *Relative Permeability of Petroleum Reservoirs*, CRC Press, LLC (1986).

APPENDIX A

MATHEMATICAL DEVELOPMENT OF STEADY-STATE

PATTERN AVERAGE PRESSURE EQUATION

The derivation of Eq. 3.2 is presented in this Appendix. Muskat¹ defined ideal flow assumptions as a single phase, incompressible fluid of constant viscosity flowing at steady-state conditions in a homogeneous, isotropic, horizontal flow medium. For an ideal injection pattern of uniform spacing, Eq. 3.2 describes the average reservoir pressure within any element of symmetry:

$$\bar{P}_{pat} = \frac{p_{wfl} + P/l(p_{wfp})}{1 + P/l}. \quad (3.2b)$$

The pressure distribution for a single well in a two-dimensional, ideal radial flow system is given by the general solution of the Laplace equation¹:

$$p(r) = \frac{q\mu}{2\pi kh} \ln(r) + c. \quad (A.1)$$

It can be shown using the same approach as Craft and Hawkins²² that the average pressure between an external radius, r_e , and the wellbore radius, r_w , in an ideal radial flow system is given by:

$$\bar{P}_{re} = P_{wf} + \frac{q\mu}{2\pi kh} \left(\frac{r_e^2}{r_e^2 - r_w^2} \right) \left(\ln \frac{r_e}{r_w} + \frac{r_w^2}{2r_e^2} - \frac{1}{2} \right). \quad (A.2)$$

Fig. A.1 shows an ideal radial pressure distribution between r_w and r_e , where Eq. A.2 describes the average reservoir pressure. Note that in the above equations q is positive for production and negative for injection.

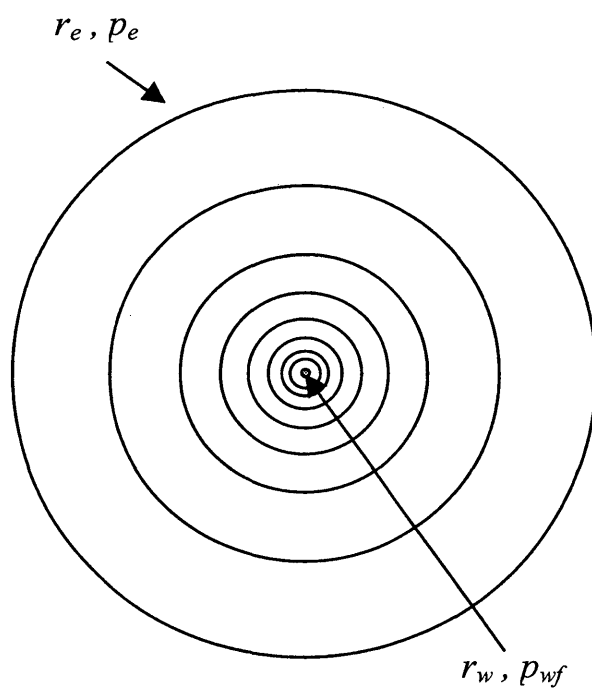


Fig. A.1 – Ideal radial pressure distribution.

Fig. A.2 shows a square shape within an ideal radial pressure distribution. The average pressure \bar{p}_s within the square shape due to the flow conditions at the well can be derived as follows.

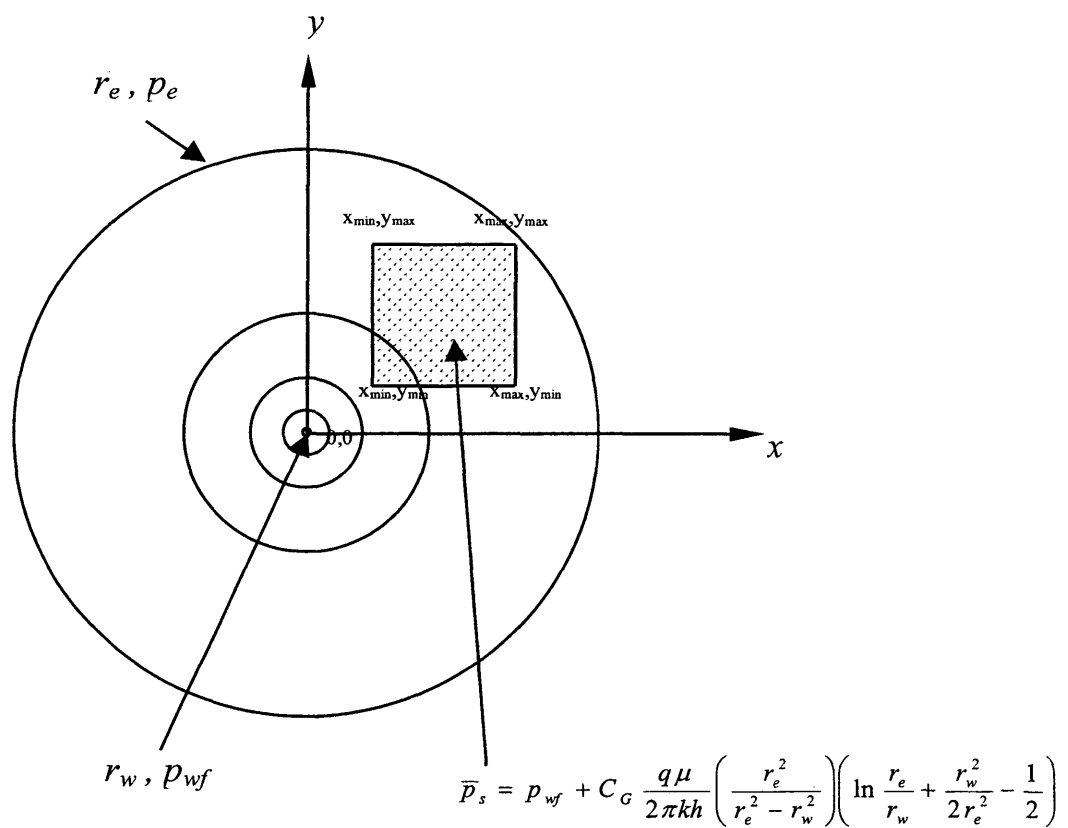


Fig. A.2 – Ideal radial pressure distribution with square shape located between r_w and r_e .

If a cartesian coordinate system is defined where the center of the well is located at the origin (0,0), and the four corners of the square shape are defined as (x_{min}, y_{min}) , (x_{max}, y_{min}) , (x_{min}, y_{max}) and (x_{max}, y_{max}) then the expression for the average pressure within the shape can be written as:

$$\bar{p}_s = \frac{\int_{x_{min}}^{x_{max}} \int_{y_{min}}^{y_{max}} p_{(x,y)} dy dx}{\int_{x_{min}}^{x_{max}} \int_{y_{min}}^{y_{max}} dy dx}$$

where

$$p_{(x,y)} = p_{wf} + \frac{q\mu}{2\pi kh} \ln \frac{\sqrt{x^2 + y^2}}{r_w} .$$

Therefore,

$$\bar{p}_s = p_{wf} + \frac{\frac{q\mu}{2\pi kh} \int_{x_{min}}^{x_{max}} \int_{y_{min}}^{y_{max}} \left[\ln \frac{\sqrt{x^2 + y^2}}{r_w} \right] dy dx}{\int_{x_{min}}^{x_{max}} \int_{y_{min}}^{y_{max}} dy dx} . \quad (A.3)$$

Rearranging Eq. A.3, we have

$$\bar{p}_s - p_{wf} = \frac{\frac{q\mu}{2\pi kh} \int_{x_{min}}^{x_{max}} \int_{y_{min}}^{y_{max}} \left[\ln \frac{\sqrt{x^2 + y^2}}{r_w} \right] dy dx}{\int_{x_{min}}^{x_{max}} \int_{y_{min}}^{y_{max}} dy dx} . \quad (A.4)$$

Rearranging Eq. A.2 we obtain:

$$\bar{p}_{re} - p_{wf} = \frac{q\mu}{2\pi kh} \left(\frac{r_e^2}{r_e^2 - r_w^2} \right) \left(\ln \frac{r_e}{r_w} + \frac{r_w^2}{2r_e^2} - \frac{1}{2} \right). \quad (\text{A.5})$$

Dividing Eq. A.4 by Eq. A.5, we obtain the following expression:

$$\frac{\bar{p}_s - p_{wf}}{\bar{p}_{re} - p_{wf}} = \frac{\int_{x_{\min}}^{x_{\max}} \int_{y_{\min}}^{y_{\max}} \left[\frac{\ln \sqrt{x^2 + y^2}}{r_w} \right] dy dx}{\int_{x_{\min}}^{x_{\max}} \int_{y_{\min}}^{y_{\max}} dy dx \left(\frac{r_e^2}{r_e^2 - r_w^2} \right) \left(\ln \frac{r_e}{r_w} + \frac{r_w^2}{2r_e^2} - \frac{1}{2} \right)}. \quad (\text{A.6})$$

Since the right hand side of Eq. A-6 is constant for a given combination of (x_{\min}, y_{\min}) , (x_{\max}, y_{\max}) , r_w and r_e , this constant expression is defined as the *geometrical constant* C_G :

$$\frac{\bar{p}_s - p_{wf}}{\bar{p}_{re} - p_{wf}} = C_G. \quad (\text{A.7})$$

Note that geometrical constant C_G is independent of flow rate. Combining Eq. A.5 and Eq. A.7, the general expression for the average pressure within any shape located within an ideal radial pressure distribution (in like manner to Fig. A.2) from r_w to r_e is given by:

$$\bar{p}_s = p_{wf} + C_G \frac{q\mu}{2\pi kh} \left(\frac{r_e^2}{r_e^2 - r_w^2} \right) \left(\ln \frac{r_e}{r_w} + \frac{r_w^2}{2r_e^2} - \frac{1}{2} \right), \quad (\text{A.8})$$

where the geometrical constant depends upon the shape dimensions, the geometric relationship between the shape and the well, and the radii r_w and r_e .

Figure A.3 shows a portion of an infinite well array for the inverted nine-spot pattern, where an element of symmetry is shown as the shaded portion involving four wells. The surrounding infinite array of image wells is necessary to mathematically generate the pressure distribution within the element area. Note that the lines connecting well centers are no-flow boundaries – the rates are assigned to the image wells to accomplish this mathematically. Several wells are also labeled on the figure as Wells 1-24. Because of the symmetry of radial flow, note how element Wells 1–4 have the same geometric relationship with respect to the element area, and thus for the same values of r_w and r_e would all have the same geometrical constant C_G . In the same way, image wells 5-12 would share the same C_G , as would image Wells 13-16 and image Wells 17-24, and so forth.

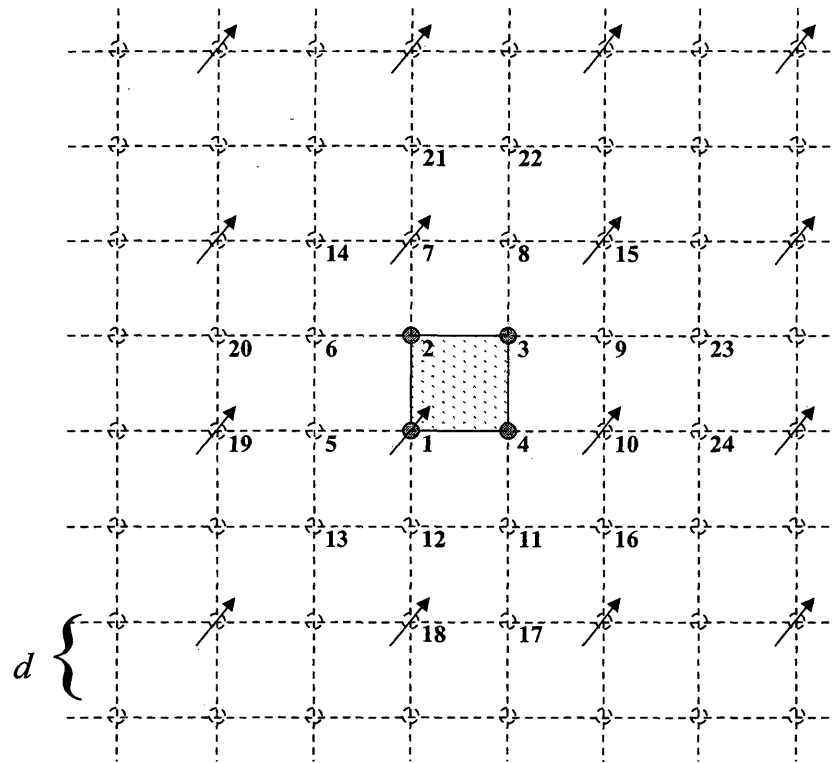


Fig. A.3 – Inverted nine-spot element of symmetry and infinite array of image wells.

The relationship in Eq. 3.2 is valid for any pattern shape where the geometrical relationship between each of the element wells to the element area is the same, however, the specific case of an inverted nine-spot will be developed here for simplicity. Also, at this point in the derivation, it will be understood that the r_e associated with a given geometrical constant C_G is equal to the minimum distance from a well necessary to encompass the shape, or pattern element area. For example, referring to Fig. A.3, in

calculating C_G for Well 5 with respect to the element area, r_e will be equal to the distance between Well 5 and Well 3. Using this convention, Well 6 would automatically have the same C_G as Well 5, since the distance between Well 6 and Well 4 would be taken for r_e , which is the same as for Well 5. Finally, all wellbore radii will be assumed equal.

As will be seen, it will not be necessary to evaluate the geometrical constant C_G for each image well or set of image wells that share the same C_G , because this term cancels in the derivation. It will only be necessary to devise a scheme to properly account for each image well and its associated geometrical constant. This accounting can be done by observing that for wells that have the same C_G with respect to the pattern element, the minimum distance between the well and the element area is also the same. For example, Wells 5-12 have the same C_G , and the minimum distance between these wells and the element area is one well spacing, or d . Similarly, the minimum distance between Wells 13-16 and the element area is $\sqrt{d^2 + d^2}$, while that for Wells 17-24 is $2d$, and so forth. The notation for the geometrical constant associated with a given well will here be given the form of $C_{G(m,n)}$, where m and n are coefficients of the term $\sqrt{(md)^2 + (nd)^2}$ which describes the minimum distance between the well and the element area. In the same way, the r_e associated with a given geometrical constant will be denoted $r_{e(m,n)}$.

In writing the equation for the average pressure for the element of symmetry of the inverted nine-spot as represented in Fig. A.3, the effect of all element wells and the infinite array of image wells on the element area is added using an incremental approach with the principle of superposition, where the average pressure in the element area will be given by:

$$\bar{P}_{pat} = \bar{P}_1 + \Delta\bar{P}_2 + \Delta\bar{P}_3 + \Delta\bar{P}_4 + \Delta\bar{P}_{image} \quad (A.9)$$

The contribution to the average pressure within the pattern element due to Well 1 is (Eq. A.8):

$$\bar{p}_1 = p_{wf1(q_1)} + C_{G(0,0)} \frac{q_1 \mu}{2\pi kh} \left(\frac{r_{e(0,0)}^2}{r_{e(0,0)}^2 - r_w^2} \right) \left(\ln \frac{r_{e(0,0)}}{r_w} + \frac{r_w^2}{2r_{e(0,0)}^2} - \frac{1}{2} \right), \quad (\text{A.10})$$

where

$$p_{wf1(q_1)} = \frac{\mu}{2\pi kh} q_1 \ln(r_w) + c \equiv \text{flowing sand-face pressure of Well 1 due to the flow of only Well 1, and where } c \text{ is a constant to be determined.}$$

The incremental contribution to the average pressure within the pattern element due to Well 2 will be:

$$\Delta \bar{p}_2 = \Delta p_{wf2(q_2)} + C_{G(0,0)} \frac{q_2 \mu}{2\pi kh} \left(\frac{r_{e(0,0)}^2}{r_{e(0,0)}^2 - r_w^2} \right) \left(\ln \frac{r_{e(0,0)}}{r_w} + \frac{r_w^2}{2r_{e(0,0)}^2} - \frac{1}{2} \right), \quad (\text{A.11})$$

where

$$\Delta p_{wf2(q_2)} = \frac{\mu}{2\pi kh} q_2 \ln(r_w) \equiv \text{incremental change in flowing sand-face pressure of Well 2 due to the flow of Well 2.}$$

Similarly, the incremental contribution to the average pressure within the pattern element due to Well 3 and Well 4 will be:

$$\Delta\bar{p}_3 = \frac{\mu}{2\pi kh} q_3 \ln(r_w) + C_{G(0,0)} \frac{q_3 \mu}{2\pi kh} \left(\frac{r_{e(0,0)}^2}{r_{e(0,0)}^2 - r_w^2} \right) \left(\ln \frac{r_{e(0,0)}}{r_w} + \frac{r_w^2}{2r_{e(0,0)}^2} - \frac{1}{2} \right) \quad (\text{A.12})$$

and

$$\Delta\bar{p}_4 = \frac{\mu}{2\pi kh} q_4 \ln(r_w) + C_{G(0,0)} \frac{q_4 \mu}{2\pi kh} \left(\frac{r_{e(0,0)}^2}{r_{e(0,0)}^2 - r_w^2} \right) \left(\ln \frac{r_{e(0,0)}}{r_w} + \frac{r_w^2}{2r_{e(0,0)}^2} - \frac{1}{2} \right). \quad (\text{A.13})$$

respectively. A condition of steady-state, incompressible pattern flow is given by

$$\sum q_I = -\sum q_P \quad (\text{A.14a})$$

that is, total injection equals total production within an element of symmetry. Specifically for the inverted nine-spot pattern, this relationship is

$$q_1 = -(q_2 + q_3 + q_4). \quad (\text{A.14b})$$

Summing Eqs. A.10 through A.13 and combining Eq. A.14 results in

$$\bar{p}_{pat} = c + \Delta\bar{p}_{image}, \quad (\text{A.15})$$

where

$$\Delta\bar{p}_{image} = \Delta\bar{p}_{image_prod} + \Delta\bar{p}_{image_inj}. \quad (\text{A.16})$$

As will be shown next, the contribution of the image wells to the average pressure of the pattern element cancel in their effect, such that the contribution of the image wells to the average pressure is zero. The following equation involving single and double summation terms describes the incremental contribution of the injectors in the infinite

array of image wells to the average pressure of the pattern element, using the convention $C_{G(m,n)}$ as described above:

$$\Delta \bar{p}_{image_inj} = 2 \sum_{m=1}^{\infty} \left[\sum_{n=0}^{m-1} \left\{ \frac{\mu}{2\pi kh} q_I \ln(r_w) + C_{G(m,n)} \frac{q_I \mu}{2\pi kh} \left(\frac{r_{e(m,n)}^2}{r_{e(m,n)}^2 - r_w^2} \right) \left(\ln \frac{r_{e(m,n)}}{r_w} + \frac{r_w^2}{2r_{e(m,n)}^2} - \frac{1}{2} \right) \right\} \right] +$$

$$\sum_{n=1}^{\infty} \left[\frac{\mu}{2\pi kh} q_I \ln(r_w) + C_{G(m,m)} \frac{q_I \mu}{2\pi kh} \left(\frac{r_{e(m,m)}^2}{r_{e(m,m)}^2 - r_w^2} \right) \left(\ln \frac{r_{e(m,m)}}{r_w} + \frac{r_w^2}{2r_{e(m,m)}^2} - \frac{1}{2} \right) \right], \quad (A.17)$$

where (m,n) are coefficients of the term $\sqrt{(md)^2 + (nd)^2}$, and where (m,m) are also coefficients of the term $\sqrt{(md)^2 + (md)^2}$.

Next, the incremental contribution of the producers in the infinite array of image wells to the average pressure of the pattern element is given by the following summation terms:

$$\Delta \bar{p}_{image_prod} = 6 \sum_{m=1}^{\infty} \left[\sum_{n=0}^{m-1} \left\{ \frac{\mu}{2\pi kh} q_P \ln(r_w) + C_{G(m,n)} \frac{q_P \mu}{2\pi kh} \left(\frac{r_{e(m,n)}^2}{r_{e(m,n)}^2 - r_w^2} \right) \left(\ln \frac{r_{e(m,n)}}{r_w} + \frac{r_w^2}{2r_{e(m,n)}^2} - \frac{1}{2} \right) \right\} \right] +$$

$$3 \sum_{m=1}^{\infty} \left[\frac{\mu}{2\pi kh} q_P \ln(r_w) + C_{G(m,m)} \frac{q_P \mu}{2\pi kh} \left(\frac{r_{e(m,m)}^2}{r_{e(m,m)}^2 - r_w^2} \right) \left(\ln \frac{r_{e(m,m)}}{r_w} + \frac{r_w^2}{2r_{e(m,m)}^2} - \frac{1}{2} \right) \right]. \quad (A.18)$$

Given that the relationship of Eq. A.14 must apply for steady-state conditions, we also impose the restriction for this derivation that each producing well produces at exactly one-third the rate of the injector, i.e.

$$q_P = q_2 = q_3 = q_4 = -\left(\frac{1}{3}\right)q_I. \quad (\text{A.19})$$

This restriction is not necessary for the relationship in Eq. 3.2 to be valid, but merely simplifies the accounting of producing well terms for this derivation (i.e. note how the production rate terms in Eq. A.18 involves only q_P , without regard to a specific producing well of the pattern element Well 2, 3, or 4). Summing Eq. A.17 and Eq. A.18, and substituting the relationship of Eq. A.19, we can write the contribution of the infinite array of injectors and producers on the average pressure of the pattern element as:

$$\Delta\bar{p}_{image} = \Delta\bar{p}_{image_prod} + \Delta\bar{p}_{image_inj} = 0. \quad (\text{A.20})$$

Therefore, combining Eq. A.15 and Eq. A.20, we have the equation for the average pressure within the pattern element:

$$\bar{p}_{pat} = c. \quad (\text{A.21})$$

Presently, because the constant c in Eq. A.21 is not known, an expression must be found which relates c to some known variable(s). This is accomplished by developing an expression for the flowing bottomhole pressure of each element well, $p_{wf(i)}$, and summing the results. The principle of superposition is applied with the equation²³:

$$p(x, y) = \frac{-\mu}{4\pi kh} \sum_{i=1}^n q_i \ln[(x - x_i)^2 + (y - y_i)^2] + c, \quad (\text{A.22})$$

where the contribution of each well in the array including the element wells is accounted for to determine the flowing bottomhole pressure of each element well. In a strict mathematical sense, since Eq. A.22 is based on the line source solution, the interwell distances are measured from well center to well center, where the implied wellbore pressures are located at infinitesimal well radii. However, in practicality, the interwell distances are measured from the center of one well to r_w of the next, where the equivalent well pressure can be taken as if the wellbore were at a single point by noting that r_w is very small compared with the well spacing¹. Therefore, referring again to Fig. A.3, the expression for element injector Well 1 is:

$$\begin{aligned}
p_{wfl} = & \frac{-\mu}{4\pi kh} \left\{ q_I \ln(r_w)^2 + q_P (4 \ln d^2) + q_P (4 \ln(2d^2)) + \right. \\
& q_P \sum_{m=1}^{\infty} \left(4 \ln \left\{ [(2m+1)d]^2 + [(2m+1)d]^2 \right\} \right) + q_P \sum_{m=1}^{\infty} \left(4 \ln [(2m+1)d]^2 \right) + \\
& q_P \sum_{m=1}^{\infty} \left[\sum_{n=1}^m \left(8 \ln \left\{ (2n-1)d]^2 + [(2m+1)d]^2 \right\} \right) \right] + q_P \sum_{m=1}^{\infty} \left[\sum_{n=1}^m \left(8 \ln \left\{ 2nd]^2 + [(2m+1)d]^2 \right\} \right) \right] + \\
& q_P \sum_{m=1}^{\infty} \left[\sum_{n=1}^m \left(8 \ln \left\{ (2n-1)d]^2 + [2md]^2 \right\} \right) \right] + q_I \sum_{m=1}^{\infty} \left[\sum_{n=1}^m \left(8 \ln \left\{ 2nd]^2 + [(2m+2)d]^2 \right\} \right) \right] + \\
& \left. q_I \sum_{m=1}^{\infty} \left(4 \ln [2md]^2 \right) + q_I \sum_{m=1}^{\infty} \left(4 \ln \left\{ 2md]^2 + [2md]^2 \right\} \right) \right\} + c. \tag{A.23}
\end{aligned}$$

Similarly, the equations for the flowing bottomhole pressures of element producing Wells 2 and 4 are:

$$\begin{aligned}
p_{wf2} = p_{wf4} = & \frac{-\mu}{4\pi kh} \left\{ q_P \ln(r_w)^2 + q_P (2 \ln d^2) + q_P (4 \ln(2d^2)) + q_P \sum_{m=1}^{\infty} \left(2 \ln [(2m+1)d]^2 \right) + \right. \\
& q_P \sum_{m=1}^{\infty} \left(4 \ln \left\{ [(2m+1)d]^2 + [(2m+1)d]^2 \right\} \right) + q_P \sum_{m=1}^{\infty} \left(4 \ln [2md]^2 \right) + q_P \sum_{m=1}^{\infty} \left(4 \ln \left\{ 2md]^2 + [2md]^2 \right\} \right) + \\
& \left. q_P \sum_{m=1}^{\infty} \left[\sum_{n=1}^m \left(8 \ln \left\{ (2n-1)d]^2 + [(2m+1)d]^2 \right\} \right) \right] + q_P \sum_{m=1}^{\infty} \left[\sum_{n=1}^m \left(4 \ln \left\{ 2nd]^2 + [(2m+1)d]^2 \right\} \right) \right] + \right.
\end{aligned}$$

$$\begin{aligned}
& q_P \sum_{m=1}^{\infty} \left[\sum_{n=1}^m \left(4 \ln \left\{ [(2n-1)d]^2 + [2md]^2 \right\} \right) \right] + q_P \sum_{m=1}^{\infty} \left[\sum_{n=1}^m \left(8 \ln \left\{ [2nd]^2 + [(2m+2)d]^2 \right\} \right) \right] + q_I (2 \ln d^2) + \\
& q_I \sum_{m=1}^{\infty} \left(2 \ln [(2m+1)d]^2 \right) + q_I \sum_{m=1}^{\infty} \left[\sum_{n=1}^m \left(4 \ln \left\{ [2nd]^2 + [(2m+1)d]^2 \right\} \right) \right] + \\
& q_I \sum_{m=1}^{\infty} \left[\sum_{n=1}^m \left(8 \ln \left\{ [(2n-1)d]^2 + [2md]^2 \right\} \right) \right] \} + c. \tag{A.24}
\end{aligned}$$

Finally, the flowing bottomhole pressure equation for element producer Well 3 is:

$$\begin{aligned}
p_{wf3} &= \frac{-\mu}{4\pi kh} \left\{ q_P \ln(r_w)^2 + q_P (4 \ln d^2) + q_P \sum_{m=1}^{\infty} \left(4 \ln [2md]^2 \right) + q_P \sum_{m=1}^{\infty} \left(4 \ln \left\{ [2md]^2 + [2md]^2 \right\} \right) \right. \\
&+ q_P \sum_{m=1}^{\infty} \left(4 \ln [(2m+1)d]^2 \right) + q_P \sum_{m=1}^{\infty} \left[\sum_{n=1}^m \left(8 \ln \left\{ [(2n-1)d]^2 + [2md]^2 \right\} \right) \right] + \\
&q_P \sum_{m=1}^{\infty} \left[\sum_{n=1}^m \left(8 \ln \left\{ [2nd]^2 + [(2m+2)d]^2 \right\} \right) \right] + q_P \sum_{m=1}^{\infty} \left[\sum_{n=1}^m \left(8 \ln \left\{ [2nd]^2 + [(2m+1)d]^2 \right\} \right) \right] + q_I (4 \ln (2d^2)) \\
&+ q_I \sum_{m=1}^{\infty} \left(4 \ln \left\{ [(2m+1)d]^2 + [(2m+1)d]^2 \right\} \right) + q_I \sum_{m=1}^{\infty} \left[\sum_{n=1}^m \left(8 \ln \left\{ [(2n-1)d]^2 + [(2m+1)d]^2 \right\} \right) \right] \} + c. \tag{A.25}
\end{aligned}$$

Summing Eq. A.23, Eq. A.24 (for Wells 2 and 4), and Eq. A.25, and again substituting the relationship of Eq. A.19, we can write:

$$p_{wf1} + p_{wf2} + p_{wf3} + p_{wf4} = 4c. \tag{A.26}$$

Combining Eq. A.21 and Eq. A.26 the expression for the average pattern pressure can now be written in terms of the pattern element well flowing bottomhole pressures as

$$\bar{p}_{pat} = \frac{p_{wf1} + p_{wf2} + p_{wf3} + p_{wf4}}{4}, \tag{A.27a}$$

or in more general terms,

$$\bar{P}_{pat} = \frac{\sum_{i=1}^n P_{wf(i)}}{n} \quad (\text{A.27b})$$

For patterns with a producer/injector ratio ≥ 1 , i.e. $P/I \geq 1$,

$$n = P / I + 1 .$$

Similarly, for patterns with $P/I \leq 1.0$,

$$n = I / P + 1 .$$

Also, define the weighted average flowing well pressures, for producers and injectors as follows:

$$P_{wfp} = \sum_{j=1}^{N_p} f_{(j)} \times P_{wfp(j)} , \quad (\text{A.28a})$$

and

$$P_{wfi} = \sum_{j=1}^{N_I} f_{(j)} \times P_{wfi(j)} , \quad (\text{A.28b})$$

where $f_{(j)}$ is the representation of the j th producing (or injection) well in the pattern element as a fraction of the total number of producing (or injection) wells represented by the pattern, and N_P and N_I are the number of producing and injection wells, respectively, contributing to the pattern element.

With the above definitions, Eq. A.27 can be written for $P/I \geq 1.0$ as:

$$\bar{p}_{pat} = \frac{p_{wfl} + P/I(p_{wfP})}{1 + P/I} \quad (\text{A.29a})$$

For $P/I \leq 1.0$, Eq. A.27 is

$$\bar{p}_{pat} = \frac{I/P(p_{wfl}) + p_{wfP}}{I/P + 1}, \quad (\text{A.29b})$$

which can be converted to Eq. A.29a when the right side numerator and denominator are multiplied by P/I .

Even though the above derivation has specifically used the inverted nine-spot pattern, the average reservoir pressure for the other ideal patterns, i.e. the line-drive, the five-spot, the inverted and normal seven-spot, and the normal nine-spot can also be shown to be described by Eq. 3.2.

This concludes the derivation of Eq. 3.2 of the main text.

APPENDIX B

MATHEMATICAL DEVELOPMENT OF NINE-SPOT

PATTERN DIMENSIONLESS PRESSURE

In this appendix, the dimensionless pressure that is consistent with the definition of dimensionless pressure given in Eq. 3.7 and the pressure drop term $\Delta P = p_{wfi} - p_{wfp}$ is derived, that is, the weighted average injection and production sand-face pressures as required for determining the average reservoir pressure in Eq. 3.2b.

In Table 3.1, the flow equations for the inverted nine-spot are shown (after Deppe²) as

$$q = \frac{0.003541kh(\Delta P_{i,c})}{\frac{1+R}{2+R} \left(\ln \frac{d}{r_w} - 0.272 \right) \mu}, \quad (3.13d)$$

and

$$q = \frac{0.007082kh(\Delta P_{i,s})}{\left[\frac{3+R}{2+R} \left(\ln \frac{d}{r_w} - 0.272 \right) - \frac{0.693}{2+R} \right] \mu}, \quad (3.13e)$$

where

R = ratio of producing rate of corner well to side well for nine-spot

$\Delta P_{i,c}$ = pressure difference between center well and corner well for nine-spot, psi, and

$\Delta P_{i,s}$ = pressure difference between center well and side well for nine-

spot, psi.

Since we want an expression for dimensionless pressure based on the pressure drop term

$\Delta P = p_{wfl} - p_{wfp}$, we can write for the inverted nine-spot based on Eq. A.28a

$$p_{wfp} = 2/3 p_{wfs} + 1/3 p_{wfc}, \quad (\text{B.1})$$

where

p_{wfs} = sand-face pressure of side-well producer, and

p_{wfc} = sand-face pressure of corner-well producer.

Combining Eq. 3.13d and Eq. 3.13e according to Eq. B.1, we can write

$$p_{D(inj)} = p_{D(prod)} = \frac{P/I}{1 + P/I} \frac{(p_{wfl} - p_{wfp})kh}{141.2q_{inj}\mu} =$$

$$\frac{2}{3} \times \left[\left(\frac{3+R}{2+R} \right) \left(\ln \frac{d}{r_w} - 0.272 \right) - \frac{0.693}{2+R} \right] + \frac{1}{3} \times \left[\left(\frac{1+R}{2+R} \right) \left(\ln \frac{d}{r_w} - 0.272 \right) \right] \quad (\text{B.2})$$

After some algebra, the right-hand side of Eq. B.2 can be written as

$$p_{D(inj)} = p_{D(prod)} = \ln \frac{d}{r_w} - 0.272 - \frac{1}{2} \times \frac{0.693}{2+R}, \quad (3.20f)$$

which is the result shown as Eq. 3.20f. This concludes the derivation of dimensionless pressure for the nine-spot pattern that is consistent with Eq. 3.2b.

APPENDIX C

EXAMPLE CALCULATIONS

In this appendix, the procedure for determining the highest conductivity pattern will be demonstrated using the equations and concepts presented in Chapters Four, Five, and Six, and the correlation for the total mobility ratio, M_T , versus the endpoint mobility ratio, M , for the pre-breakthrough period as presented in Chapter Seven.

C.1 – Determining Endpoint Mobility Ratio, M , and Pre-Breakthrough M_T

Figure C.1 shows the two-phase water-oil relative permeability curves using the correlation presented by Honarpour²⁴ for a water-wet sandstone reservoir with the following reservoir parameters:

$$S_{wirr} = 0.31$$

$$S_{orw} = 0.325$$

$$k = 10.0 \text{ md}$$

$$h = 25 \text{ ft}$$

$$\text{depth} = 5300 \text{ ft}$$

$$\text{spacing} = 20\text{-acres}$$

$$d = 933.4 \text{ ft for five-spot, nine-spot, or direct line-drive with } d/a = 1.0$$

$$d = 1.0745 \times 933.4 = 1002.9 \text{ ft for hexagonal seven-spot}$$

$$\text{wellbore radius} = 0.33 \text{ ft}$$

$$\phi = 0.12$$

$$\mu_o = 2.4 \text{ cp}$$

$$\mu_w = 0.80 \text{ cp}$$

Note how the oil relative permeability data was curve fit with Eq. 7.1 using an m exponent equal to 2.50, and an endpoint oil relative permeability $\alpha_1 = 1.0$. As exhibited by Fig. C.1, it is more important to match the oil relative permeability values at higher water saturations than at lower, as this region has a more significant influence on the total mobility of the water in the swept portion of the reservoir. The water relative permeability data was fit using Eq. 7.2 and an n exponent equal to 2.0, and an endpoint water relative permeability $\alpha_2 = 0.10$.

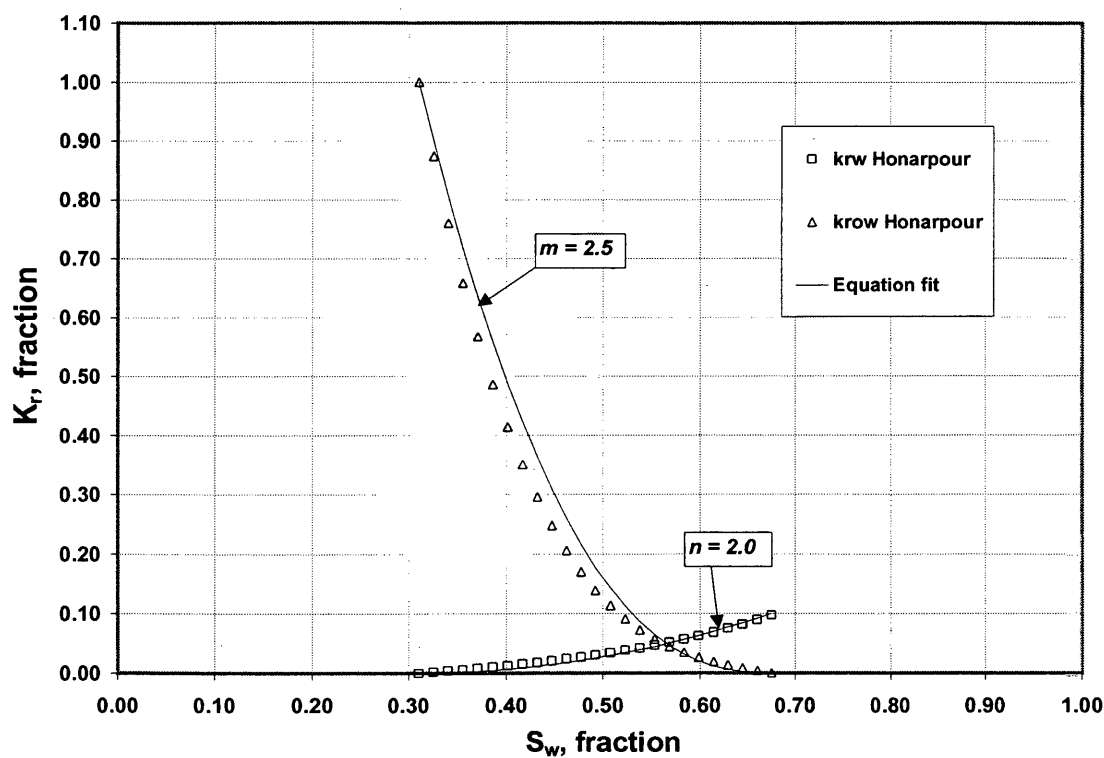


Fig. C.1 – Oil and water relative permeability curves using correlation of Honarpour²⁴ for a water-wet sandstone reservoir.

Furthermore, the endpoint mobility ratio M is calculated as follows:

$$M = \frac{k_{rw} / \mu_w}{k_{row} / \mu_o} = \frac{0.1/0.8}{1.0/2.4} = 0.30.$$

Using Table 7.1, we see that there are no tabulated values for this mobility ratio $M=0.3$ and at the exponent $m=2.5$. We can, however, interpolate a value of M_T for $M=0.3$ and $m = 3.0$ as follows. At $M=0.2$ and $m = 3.0$, we see that $M_T=0.1891$ for the inverted nine-spot, which is 95% of the value of M (note: we will use the value for the inverted nine-spot for all patterns because the error in flow rates using this value is minimized when applied to all patterns, as discussed in Chapter Seven). At $M=0.5$ and $m = 3.0$, we see that $M_T=0.4307$ for the inverted nine-spot, which is 86% of the value of M . Therefore, interpolating the percentage M_T/M between $M=0.2$ and $M=0.5$ we calculate M_T/M at $M = 0.3$ for $m = 3.0$ as

$$M_T / M = 0.95 + \frac{0.3 - 0.2}{0.5 - 0.2} (0.86 - 0.95) = 0.92.$$

In like manner, at $M=0.2$ and $m = 2.0$, we see that $M_T=0.2103$ for the inverted nine-spot, which is 105% of the value of M . At $M=0.5$ and $m = 2.0$, we see that $M_T=0.4849$ for the inverted nine-spot, which is 97% of the value of M . Therefore, interpolating the percentage M_T/M between $M=0.2$ and $M=0.5$ we calculate M_T/M at $M=0.3$ for $m = 2.0$ as

$$M_T / M = 1.05 + \frac{0.3 - 0.2}{0.5 - 0.2} (0.97 - 1.05) = 1.023.$$

Therefore, we calculate the total mobility ratio prior to water breakthrough at $M = 0.3$ and $m = 2.50$ as

$$M_T = (M_T / M) \times M = 0.5(0.92 + 1.023) \times 0.3 = 0.291.$$

C.2 – Determining Conductivity Ratio Relationship for $M_T = 0.291$

The conductivity relationship a system with $M_T = 0.291$ can be calculated using Eq. 5.5a, shown here for convenience:

$$\frac{\tilde{q}_{(1)}}{\tilde{q}_{(2)}} = \frac{(P/I)_1 (M_T + P/I)_2 (1 + P/I)_2}{(P/I)_2 (M_T + P/I)_1 (1 + P/I)_1}. \quad (5.5a)$$

We arbitrarily select a pattern, or producer/injector ratio, for $(P/I)_2$ as the base pattern that all other patterns will be compared in Eq. 5.5a, also using the value of $(M_T)_1 = (M_T)_2 = 0.291$. For example, comparing the pre-breakthrough conductivity for an inverted nine-spot ($P/I=3.0$) relative to a five-spot ($P/I=1.0$), we find that

$$\frac{\tilde{q}_{(Inv-9)}}{\tilde{q}_{(5-spot)}} = \frac{(3.0) (0.291 + 1.0) (1 + 1.0)}{(1.0) (0.291 + 3.0) (1 + 3.0)} = 0.59.$$

Therefore, developing the flood using the inverted nine-spot would be expected to have 59% of the conductivity of a full five-spot development within the same isotropic reservoir of uniform permeability-thickness, prior to water breakthrough. The normal seven-spot would be expected to have

$$\frac{\tilde{q}_{(Nor-7)}}{\tilde{q}_{(5-spot)}} = \frac{(0.50) (0.291 + 1.0) (1 + 1.0)}{(1.0) (0.291 + 0.50) (1 + 0.50)} = 1.09,$$

or 9% higher conductivity than the five-spot. The full conductivity relationship for $M_T = 0.291$ is shown on Fig. C.2, using $P/I=1.0$ as the reference producer/injector ratio. Note how the maximum reservoir flowrate is provided by the normal seven-spot pattern. The normal seven-spot also is $1.09/0.59$, or 85% more conductive than the inverted nine-spot. This result is also exhibited by Fig. C.2.

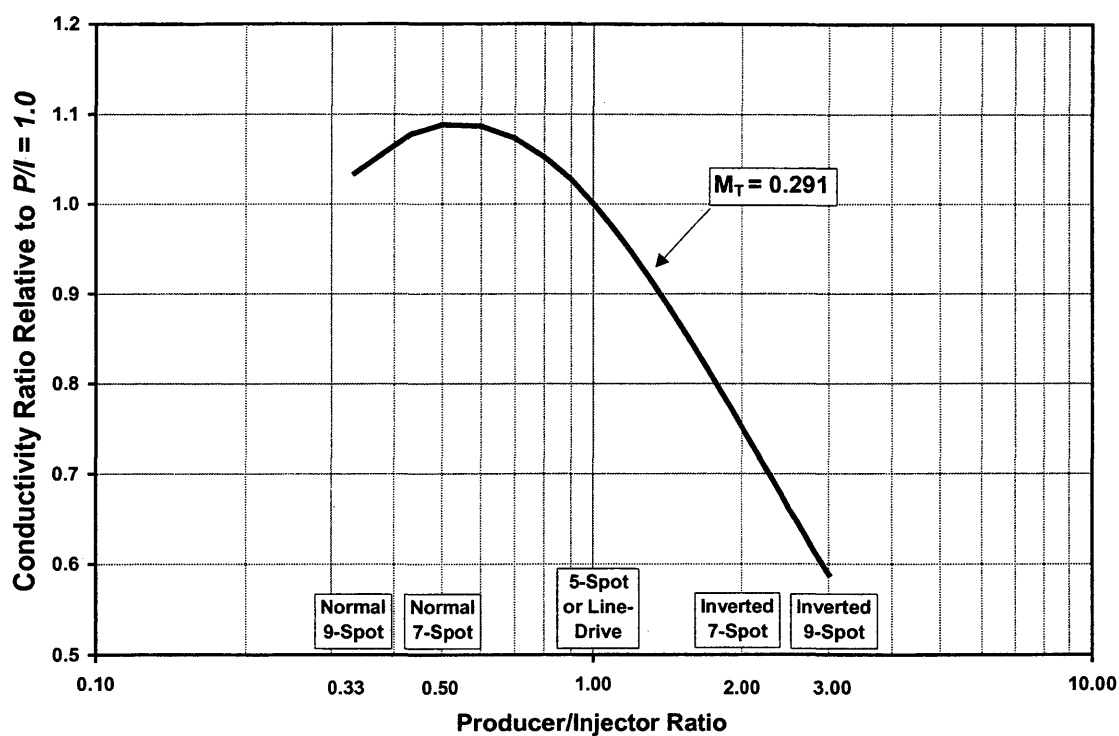


Fig. C.2 – Conductivity relationship for $M_T=0.291$.

C.3 – Calculating Absolute Well and Reservoir Flowrates for $M_T = 0.291$

We can also calculate the absolute flow rates that will be provided by the various patterns for the reservoir system discussed above with $M_T = 0.291$. As shown in Chapter Four, the equation for the injection well rate in any pattern is given by

$$q_{inj} = \bar{q}_{inj} = \bar{\lambda}_{TI} \frac{P/I}{M_T + P/I} \times \frac{\Delta P}{p_{D(pat)}} \times \frac{kh}{141.2}. \quad (4.18)$$

For an inverted nine-spot, the injection well rate can be calculated using the parameters given above, and also using $M_T = 0.291$. The average effective total mobility of the producing wells will be equal to the endpoint total mobility of the oil, assuming that the reservoir is at S_{wirr} . Thus, $\bar{\lambda}_{TP}$ is calculated using the information given above as

$$\bar{\lambda}_{TP} = \frac{k_{row}}{\mu_o} = \frac{1.0}{2.4} = 0.417.$$

The average effective injection well total mobility, $\bar{\lambda}_{TI}$, can be calculated knowing the total mobility ratio and the average effective producing mobility as

$$\bar{\lambda}_{TI} = M_T \bar{\lambda}_{TP} = 0.291 \times 0.417 = 0.121 \text{ cp}^{-1}.$$

Now, assuming a fracture pressure gradient of 0.80 psi/ft, the maximum injection well sandface pressure without parting the formation is calculated as

$$p_{wfl} = 0.80 \times 5300 = 4240 \text{ psi}.$$

The producing sandface pressure can be assumed to be 50 psi for a pumping well. Therefore, the total pressure drop, ΔP , is 4190 psi. The dimensionless pressure can be calculated for the inverted nine-spot can be calculated using Eq. 3.20f as

$$p_{D(inj)} = p_{D(prod)} = \ln \frac{d}{r_w} - 0.272 - \frac{1}{2} \times \frac{0.693}{2+R}, \quad (3.20f)$$

Since dimensionless pressure for the nine-spot is very insensitive to the value of R as discussed in Section 3.3, we can use $R = 0.91$ (see Fig. 3.3) for all times, even though R will change from this value after breakthrough (see also Table 3.3). Therefore, the dimensionless pressure for the nine-spot on 20-acres is calculated as

$$p_{D(inj)} = p_{D(prod)} = \ln \frac{933.4}{0.33} - 0.272 - \frac{1}{2} \times \frac{0.693}{2+0.91} = 7.55.$$

The dimensionless pressure for any pattern can also be calculated using Eq. 3.29, which is within 2.5% for any pattern

$$p_{D(inj)} = p_{D(prod)} = \ln \frac{d}{r_w} - 0.443. \quad (3.29)$$

The dimensionless pressure for the nine-spot using Eq. 3.29 is calculated as

$$p_{D(inj)} = p_{D(prod)} = \ln \frac{933.38}{0.33} - 0.443 = 7.50.$$

Thus, using the parameters given above, the injection well rate for the inverted nine-spot is calculated as

$$q_{inj} = \bar{q}_{inj} = 0.121 \frac{3.0}{0.291 + 3.0} \times \frac{4190}{7.55} \times \frac{(10.0)(25)}{141.2} = 101 \text{ rb/day},$$

which is, again, according to the conditions of Table 7.1, the average injection rate prior to water breakthrough. The normalized injection rate, as given by Eq. 5.2, is calculated as

$$\tilde{q} = \frac{q_{inj}}{1 + P/I} = \frac{101}{1 + 3.0} = 27 \text{ rb/day/well},$$

that is, the reservoir flowrate per pattern well,

The dimensionless pressure for the seven-spot is calculated according to Eq. 3.20c. As noted in Table 3.1, the interwell distance for the seven-spot must be greater than that of the nine-spot and five-spot patterns by a factor of 1.0745. Thus, the dimensionless pressure for the seven-spot is

$$P_{D(inj)} = P_{D(prod)} = \ln \frac{d}{r_w} - 0.569 = \ln \frac{(933.38)(1.0745)}{0.33} - 0.569 = 7.45. \quad (3.20c)$$

Once again, we can use this dimensionless pressure or simply use that given by Eq. 3.29 above as 7.50. The injection well rate for the normal seven-spot ($P/I = 0.5$) is likewise calculated according to Eq. 4.18 as

$$q_{inj} = \bar{q}_{inj} = 0.121 \frac{0.5}{0.291 + 0.5} \times \frac{4190}{7.45} \times \frac{(10.0)(25)}{141.2} = 76 \text{ rb/day}.$$

The normalized injection rate is calculated as

$$\tilde{q} = \frac{q_{inj}}{1 + P/I} = \frac{7.62}{1 + 0.5} = 50 \text{ rb/day/well.}$$

Thus, even though the individual injection well rate is lower for the normal seven-spot as compared to the inverted nine-spot, the normalized reservoir injection rate is 87% greater, as also predicted by the conductivity relationship discussed above, and also shown in Fig. C.2.

Note that the above calculations could be done using the equation for the producing wells, Eq. 4.17. It should be remembered that these equations are for flowrates at reservoir conditions, and the inclusion of the formation volume factor must be included to calculate surface production rates. The formation volume factor for water is usually sufficiently close to 1.0 such that it can be ignored when calculating water injection rates.

APPENDIX D

LISTING OF COMPUTER PROGRAM USED FOR EXTRACTING SIMULATOR RESULTS AND CALCULATING EFFECTIVE TOTAL MOBILITIES WITH RING METHOD

The computer program described in Chapter Six which calculates the cell areas in the rings, extracts the relative permeabilities and viscosities from the simulator output and calculates the effective total mobilities for each pattern well according to the ring method is shown below. The source code was written in C++.

```

*****

// file getpavg.cpp

// This program gets kr, vis, and average reservoir pressure data
// from a DRS output file, determines cell areas within rings,
// and determines the effective total mobility for each well, and the
// total mobility ratio.
// Note: prior to using the DRS .OUT file, all ( must be replaced by ( _
// and TIME= by TIME= _
// so that the program properly retrieves the rates and watercut data
// and goes beyond 10000 days

#include <fstream.h>
#include <string.h>
#include <math.h>

char * strpavg = new char [10];
double pavg = 0.0;
double time_days;
const int griddim = 41;
const int TOTRINGS = 20; // for average total mobility calculations
double DX = 23.33453; // DX for simulation run
double DY = 23.33453; // DY for simulation run
double rw = 0.333; // well radius from sim run

int trashi = 0;
int trashj = 0;
int trash_first_i = 0;
// read Pb pressures only for time 0
int Pbcounter = 0;

double Pwfi = 5000.0;
double Pwfp = 100.0;

```

```

int PATTERN_TYPE = 3; // = 1 5-spot; = 2 DLD; = 3 inv 9-spot; = 4 nor 9-spot
int MOBILITY_TYPE = 1; // = 1 oil+water = 2 oil+water+gas
double CONV_TIME = 4000; // conversion to new pattern at this time
int PATTERN_TYPE2 = 3; // pattern type after conversion
double PI = 0.0; // producer/ injector ratio (set later)
double Mtp = 0;
double Mti = 0;
double Mt = 0;
double Pbar_calc = 0;
double Skin_prod_ave = 0.0;
double Skin_inj_ave = 0.0;
double Skin1 = 20.0; // 1-1
double Skin2 = 10.0; // 1-41
double Skin3 = 5.0; // 41-1
double Skin4 = 0.0; // 41-41

double pD = 7.547;
double PI_tilde_mult = (pD + Skin_inj_ave)/(pD + Skin_prod_ave);

int AVERAGE_METHOD = 1; // ring method = 1 straight cell average = 2

int outflag_pbar = 0; // output pressure arrays 1 = yes 0 = no
int outflag_totmob_vs_r = 1; // output total mobility vs radius for SE well 1 = yes 0 = no
double out_days_min = 700.0; // min time at which to start prinout of arrays
double out_days_max = 800.0; // max time at which to start prinout of arrays

// prototypes *****

// ring factors
void calc_weights(double (*WRing)[griddim+1][griddim+1], double * Radius, double DX,
                 double DY, ostream & fout2);
void calc_Ring_Radius(double * Radius, double ro, int TOTRINGS, double DX, ostream & fout);
void init_3DArray(double (*WRing)[griddim+1][griddim+1], int griddim);
void init_3DArray2(double (*RingCellArea)[TOTRINGS+1][TOTRINGS+1], int TOTRINGS);
void init_ring_ow_mob(double * ring_ow_mob, int TOTRINGS);
void calc_NW_Cell(double (*NW_Cell)[TOTRINGS+1], double DX, double DY, int TOTRINGS);
void calc_SE_Cell(double (*SE_Cell)[TOTRINGS+1], double DX, double DY, int TOTRINGS);

// get data
void get_qo_and_qinj(char (*test_for_q)[150], char * qo, char * wcut, char * qinj,
                   ostream & fout, istream & fin);
void get_pavg_step1(istream & fin, char * test1, char * strpavg);
void get_time_days_step2(istream & fin, char * test1, double & time_days);
void get_to_data_step3(istream & fin, char * test1, ostream & fout, int & j, int & i, int & first_i);
void get_data_arr_step4(istream & fin, double (*pdoub)[griddim+1], char * test1, ostream & fout);
void get_back_to_arrdata(istream & fin, char * test1, ostream & fout, int & j, int & i, int & first_i);
void print_arr(double (*pdoub)[griddim+1], ostream & fout);

// calculations
void calc_oil_mob(double (*pdoub)[griddim+1], double (*pkro)[griddim+1], double (*pviso)[griddim+1],
                 ostream & fout);
void calc_water_mob(double (*pdoub)[griddim+1], double (*pkrw)[griddim+1], double (*pvisw)[griddim+1],
                   ostream & fout);
void calc_gas_mob(double (*pdoub)[griddim+1], double (*pkrg)[griddim+1], double (*pvisg)[griddim+1],
                  ostream & fout);
void calc_ow_totmob(double (*pdoub)[griddim+1], double (*poil_mob)[griddim+1], double
                   (*pwater_mob)[griddim+1], ostream & fout);
void calc_owg_totmob(double (*pdoub)[griddim+1], double (*poil_mob)[griddim+1], double

```

```

(*pwater_mob)[griddim+1], double (*pgas_mob)[griddim+1], ostream &
fout);
void calc_avgtot_ow_mob1(double & avetot_ow_mob1, double (*ptot_ow_mob)[griddim+1],
double * ring_ow_mob1, double
(*WRing)[griddim+1][griddim+1],
double * Radius, double rw, ostream & fout, double time_days);
void calc_avgtot_ow_mob2(double & avetot_ow_mob2, double (*ptot_ow_mob)[griddim+1],
double * ring_ow_mob2, double
(*WRing)[griddim+1][griddim+1],
double * Radius, double rw, ostream & fout, double time_days);
void calc_avgtot_ow_mob3(double & avetot_ow_mob3, double (*ptot_ow_mob)[griddim+1],
double * ring_ow_mob3, double
(*WRing)[griddim+1][griddim+1],
double * Radius, double rw, ostream & fout, double time_days);
void calc_avgtot_ow_mob4(double & avetot_ow_mob4, double (*ptot_ow_mob)[griddim+1],
double * ring_ow_mob4, double
(*WRing)[griddim+1][griddim+1],
double * Radius, double rw, ostream & fout, double time_days);

// *****

int main(void)
{
// inv 9 spot files
double weight_side = 0.333; // weighting factor on nine spot side well
mobilities
double weight_corner = 1.0 - 2*weight_side; // weighting factor on nine spot corner well mobility

// ifstream fin("C:\\Data\\Chris\\pattern_new\\YEAR2000\\M5\\2PHinv9-00M5.out");
// ofstream fout("C:\\Data\\Chris\\pattern_new\\YEAR2000\\M5\\2PHinv9-00M5.keh");
// ofstream fout2("C:\\Data\\Chris\\pattern_new\\YEAR2000\\M5\\2PHinv9-00M5.fac");
// ofstream fout3("C:\\Data\\Chris\\pattern_new\\YEAR2000\\M5\\2PHinv9-00M5.plt");

// ifstream fin("C:\\Data\\Chris\\pattern_new\\YEAR2000\\Mp2\\2PHinv9-00Mp2.out");
// ofstream fout("C:\\Data\\Chris\\pattern_new\\YEAR2000\\Mp2\\2PHinv9-00Mp2.keh");
// ofstream fout2("C:\\Data\\Chris\\pattern_new\\YEAR2000\\Mp2\\2PHinv9-00Mp2.fac");
// ofstream fout3("C:\\Data\\Chris\\pattern_new\\YEAR2000\\Mp2\\2PHinv9-00Mp2.plt");

// ifstream fin("C:\\Data\\Chris\\pattern_new\\YEAR2000\\Mp5\\2PHinv9-00Mp5.out");
// ofstream fout("C:\\Data\\Chris\\pattern_new\\YEAR2000\\Mp5\\2PHinv9-00Mp5.keh");
// ofstream fout2("C:\\Data\\Chris\\pattern_new\\YEAR2000\\Mp5\\2PHinv9-00Mp5.fac");
// ofstream fout3("C:\\Data\\Chris\\pattern_new\\YEAR2000\\Mp5\\2PHinv9-00Mp5.plt");

// Wilhite relk shape sensitivity to Mt

// ifstream fin("C:\\Data\\Chris\\pattern_new\\YEAR2000\\Wilhite_comparison\\M=0.2\\Inv9\\2PHinv9-
Mp2m1.out");
// ofstream fout("C:\\Data\\Chris\\pattern_new\\YEAR2000\\Wilhite_comparison\\M=0.2\\Inv9\\2PHinv9-
Mp2m1.keh");
// ofstream fout2("C:\\Data\\Chris\\pattern_new\\YEAR2000\\Wilhite_comparison\\M=0.2\\Inv9\\2PHinv9-
Mp2m1.fac");
// ofstream fout3("C:\\Data\\Chris\\pattern_new\\YEAR2000\\Wilhite_comparison\\M=0.2\\Inv9\\2PHinv9-
Mp2m1.plt");

```

```

//      ifstream fin("C:\\Data\\Chris\\pattern_new\\YEAR2000\\Wilhite_comparison\\M=0.2\\Inv9\\2PHinv9-
Mp2m2.out");
//      ofstream fout("C:\\Data\\Chris\\pattern_new\\YEAR2000\\Wilhite_comparison\\M=0.2\\Inv9\\2PHinv9-
Mp2m2.keh");
//      ofstream fout2("C:\\Data\\Chris\\pattern_new\\YEAR2000\\Wilhite_comparison\\M=0.2\\Inv9\\2PHinv9-
Mp2m2.fac");
//      ofstream fout3("C:\\Data\\Chris\\pattern_new\\YEAR2000\\Wilhite_comparison\\M=0.2\\Inv9\\2PHinv9-
Mp2m2.plt");

//      ifstream fin("C:\\Data\\Chris\\pattern_new\\YEAR2000\\Wilhite_comparison\\M=0.2\\Inv9\\2PHinv9-
Mp2m3.out");
//      ofstream fout("C:\\Data\\Chris\\pattern_new\\YEAR2000\\Wilhite_comparison\\M=0.2\\Inv9\\2PHinv9-
Mp2m3.keh");
//      ofstream fout2("C:\\Data\\Chris\\pattern_new\\YEAR2000\\Wilhite_comparison\\M=0.2\\Inv9\\2PHinv9-
Mp2m3.fac");
//      ofstream fout3("C:\\Data\\Chris\\pattern_new\\YEAR2000\\Wilhite_comparison\\M=0.2\\Inv9\\2PHinv9-
Mp2m3.plt");

//      ifstream fin("C:\\Data\\Chris\\pattern_new\\YEAR2000\\Wilhite_comparison\\M=0.2\\Inv9\\2PHinv9-
Mp2m4.out");
//      ofstream fout("C:\\Data\\Chris\\pattern_new\\YEAR2000\\Wilhite_comparison\\M=0.2\\Inv9\\2PHinv9-
Mp2m4.keh");
//      ofstream fout2("C:\\Data\\Chris\\pattern_new\\YEAR2000\\Wilhite_comparison\\M=0.2\\Inv9\\2PHinv9-
Mp2m4.fac");
//      ofstream fout3("C:\\Data\\Chris\\pattern_new\\YEAR2000\\Wilhite_comparison\\M=0.2\\Inv9\\2PHinv9-
Mp2m4.plt");

//      ifstream fin("C:\\Data\\Chris\\pattern_new\\YEAR2000\\Wilhite_comparison\\M=0.2\\Inv9\\2PHinv9-
Mp2m5.out");
//      ofstream fout("C:\\Data\\Chris\\pattern_new\\YEAR2000\\Wilhite_comparison\\M=0.2\\Inv9\\2PHinv9-
Mp2m5.keh");
//      ofstream fout2("C:\\Data\\Chris\\pattern_new\\YEAR2000\\Wilhite_comparison\\M=0.2\\Inv9\\2PHinv9-
Mp2m5.fac");
//      ofstream fout3("C:\\Data\\Chris\\pattern_new\\YEAR2000\\Wilhite_comparison\\M=0.2\\Inv9\\2PHinv9-
Mp2m5.plt");

// skin effect

//      ifstream fin("C:\\Data\\Chris\\pattern_new\\YEAR2000\\skin_effect\\M=2.0\\Inv9\\2PHinv9-M2m1.out");
//      ofstream fout("C:\\Data\\Chris\\pattern_new\\YEAR2000\\skin_effect\\M=2.0\\Inv9\\2PHinv9-M2m1.keh");
//      ofstream fout2("C:\\Data\\Chris\\pattern_new\\YEAR2000\\skin_effect\\M=2.0\\Inv9\\2PHinv9-M2m1.fac");
//      ofstream fout3("C:\\Data\\Chris\\pattern_new\\YEAR2000\\skin_effect\\M=2.0\\Inv9\\2PHinv9-M2m1.plt");

//      ifstream fin("C:\\Data\\Chris\\pattern_new\\YEAR2000\\skin_effect\\M=0.2\\2PHinv9-00mp2.out");
//      ofstream fout("C:\\Data\\Chris\\pattern_new\\YEAR2000\\skin_effect\\M=0.2\\2PHinv9-00mp2.keh");
//      ofstream fout2("C:\\Data\\Chris\\pattern_new\\YEAR2000\\skin_effect\\M=0.2\\2PHinv9-00mp2.fac");
//      ofstream fout3("C:\\Data\\Chris\\pattern_new\\YEAR2000\\skin_effect\\M=0.2\\2PHinv9-00mp2.plt");

if (fin.fail())
    cout << "file could not be opened" << endl;

// ring parameters
double * Radius = new double [TOTRINGS+1];

```

```

double (*WRing)[griddim+1][griddim+1] = new double [griddim+1][griddim+1][griddim+1];

if(AVERAGE_METHOD == 1)
{
    calc_weights(WRing, Radius, DX, DY, fout2); // calculate weight factors for ave mob calcs
}

char * test1 = new char[150];
char (*test_for_q)[150] = new char[25+1][150]; // this variable is to get qo, wtrcut, and qinj
char * qo = new char[10];
char * wcut = new char[10];
char * qinj = new char[10];

strcpy(test1, "Initial String");
double (*pSo)[griddim+1] = new double [griddim+1][griddim+1];
double (*pSg)[griddim+1] = new double [griddim+1][griddim+1];
double (*pSw)[griddim+1] = new double [griddim+1][griddim+1];
double (*pPr)[griddim+1] = new double [griddim+1][griddim+1];
double (*pPb)[griddim+1] = new double [griddim+1][griddim+1];
double (*pviso)[griddim+1] = new double [griddim+1][griddim+1];
double (*pvisg)[griddim+1] = new double [griddim+1][griddim+1];
double (*pvisw)[griddim+1] = new double [griddim+1][griddim+1];
double (*pkro)[griddim+1] = new double [griddim+1][griddim+1];
double (*pkrq)[griddim+1] = new double [griddim+1][griddim+1];
double (*pkrw)[griddim+1] = new double [griddim+1][griddim+1];

double (*poil_mob)[griddim+1] = new double [griddim+1][griddim+1];
double (*pwater_mob)[griddim+1] = new double [griddim+1][griddim+1];
double (*pgas_mob)[griddim+1] = new double [griddim+1][griddim+1];
double (*ptot_ow_mob)[griddim+1] = new double [griddim+1][griddim+1];
double (*ptot_owg_mob)[griddim+1] = new double [griddim+1][griddim+1];
double avetot_ow_mob1 = 0;
double avetot_ow_mob2 = 0;
double avetot_ow_mob3 = 0;
double avetot_ow_mob4 = 0;

double * ring_ow_mob1 = new double [TOTRINGS+1];
double * ring_ow_mob2 = new double [TOTRINGS+1];
double * ring_ow_mob3 = new double [TOTRINGS+1];
double * ring_ow_mob4 = new double [TOTRINGS+1];
init_ring_ow_mob(ring_ow_mob1, TOTRINGS);
init_ring_ow_mob(ring_ow_mob2, TOTRINGS);
init_ring_ow_mob(ring_ow_mob3, TOTRINGS);
init_ring_ow_mob(ring_ow_mob4, TOTRINGS);

//      fout << endl;
//      fout << "16 cell near well O+W total mobility average " << endl;
//      fout << "Time_days Sim_Pbar Mtp Mti Mt Pbarc Qo Wcut Qinj P/I lam1-1 lam1-41 lam41-1
lam41-41 Sprod Sinj " << endl;

while(!fin.eof())
{
//      fout << endl << endl << endl << endl;

if(Pbcounter == 2)
{
    get_qo_and_qinj(test_for_q, qo, wcut, qinj, fout, fin);
}
}

```

```

    get_pavg_step1(fin, test1, strpavg);
//    fout << "Average pressure = " << strpavg << endl;

    get_time_days_step2(fin, test1, time_days);
//    fout << "Time = " << time_days << endl;

    get_to_data_step3(fin, test1, fout, trashj, trash_i, trash_first_i);
    get_data_arr_step4(fin, pSo, test1, fout);
//    fout << "Time = " << time_days << endl;
//    fout << "Oil Saturations " << endl;
//    print_arr(pSo, fout);

    get_to_data_step3(fin, test1, fout, trashj, trash_i, trash_first_i);
    get_data_arr_step4(fin, pSg, test1, fout);
//    fout << "Time = " << time_days << endl;
//    fout << "Gas Saturations " << endl;
//    print_arr(pSg, fout);

    get_to_data_step3(fin, test1, fout, trashj, trash_i, trash_first_i);
    get_data_arr_step4(fin, pSw, test1, fout);
//    fout << "Time = " << time_days << endl;
//    fout << "Water Saturations " << endl;
//    print_arr(pSw, fout);

    get_to_data_step3(fin, test1, fout, trashj, trash_i, trash_first_i);
    get_data_arr_step4(fin, pPr, test1, fout);
//    fout << "Time = " << time_days << endl;
//    fout << "Pressures " << endl;
//    print_arr(pPr, fout);

    if(Pbcounter == 0)
    {
        get_to_data_step3(fin, test1, fout, trashj, trash_i, trash_first_i);
        get_data_arr_step4(fin, pPb, test1, fout);
//        fout << "Time = " << time_days << endl;
//        fout << "Pb Pressures " << endl;
//        print_arr(pPb, fout);
        Pbcounter = 1;
    }

    get_to_data_step3(fin, test1, fout, trashj, trash_i, trash_first_i);
    get_data_arr_step4(fin, pviso, test1, fout);
//    fout << "Time = " << time_days << endl;
//    fout << "Oil Viscosities " << endl;
//    print_arr(pviso, fout);

    get_to_data_step3(fin, test1, fout, trashj, trash_i, trash_first_i);
    get_data_arr_step4(fin, pvisg, test1, fout);
//    fout << "Time = " << time_days << endl;
//    fout << "Gas Viscosities " << endl;
//    print_arr(pvisg, fout);

    get_to_data_step3(fin, test1, fout, trashj, trash_i, trash_first_i);
    get_data_arr_step4(fin, pvisw, test1, fout);
//    fout << "Time = " << time_days << endl;
//    fout << "Water Viscosities " << endl;
//    print_arr(pvisw, fout);

    get_to_data_step3(fin, test1, fout, trashj, trash_i, trash_first_i);
    get_data_arr_step4(fin, pkro, test1, fout);
//    fout << "Time = " << time_days << endl;

```

```

//      fout << "Oil Relative Permeabilities " << endl;
//      print_arr(pkro, fout);

      get_to_data_step3(fin, test1, fout, trashj, trash_i, trash_first_i);
      get_data_arr_step4(fin, pkrg, test1, fout);
//      fout << "Time = " << time_days << endl;
//      fout << "Gas Relative Permeabilities " << endl;
//      print_arr(pkrg, fout);

      get_to_data_step3(fin, test1, fout, trashj, trash_i, trash_first_i);
      get_data_arr_step4(fin, pkrw, test1, fout);
//      fout << "Time = " << time_days << endl;
//      fout << "Water Relative Permeabilities " << endl;
//      print_arr(pkrw, fout);

//      fout << endl << endl << endl;

// calculate results

      // calculate individual phase mobilities
      calc_oil_mob(poil_mob, pkro, pviso, fout);
//      fout << "Time = " << time_days << endl;
//      fout << "Oil Total Mobilities " << endl;
//      print_arr(poil_mob, fout);

      calc_water_mob(pwater_mob, pkrw, pvisw, fout);
//      fout << "Time = " << time_days << endl;
//      fout << "Water Total Mobilities " << endl;
//      print_arr(pwater_mob, fout);

      calc_gas_mob(pgas_mob, pkrg, pvisg, fout);
//      fout << "Time = " << time_days << endl;
//      fout << "Gas Total Mobilities " << endl;
//      print_arr(pgas_mob, fout);

// calc oil + water total mobilities
      calc_ow_totmob(ptot_ow_mob, poil_mob, pwater_mob, fout);
//      fout << "Time = " << time_days << endl;
//      if(time_days == 3372)
//      {
//          fout << "Oil Sat " << endl;
//          print_arr(pSo, fout);
//      }

//      if(time_days == 3372)
//      {
//          fout << "Oil + Water Total Mobilities " << endl;
//          print_arr(ptot_ow_mob, fout);
//      }

// calc oil + water + gas total mobilities
      calc_owg_totmob(ptot_owg_mob, poil_mob, pwater_mob, pgas_mob, fout);
//      fout << "Time = " << time_days << endl;
//      fout << "Oil + Water + Gas Total Mobilities " << endl;
//      print_arr(ptot_owg_mob, fout);

// calculate average total o+w mobilities for wells
      if(MOBILITY_TYPE == 1)
      {

```

```

    calc_avgtot_ow_mob1(avetot_ow_mob1, ptot_ow_mob, ring_ow_mob1, WRing,
        Radius, rw, fout, time_days);
    calc_avgtot_ow_mob2(avetot_ow_mob2, ptot_ow_mob, ring_ow_mob2, WRing,
        Radius, rw, fout, time_days);
    calc_avgtot_ow_mob3(avetot_ow_mob3, ptot_ow_mob, ring_ow_mob3, WRing,
        Radius, rw, fout, time_days);
    calc_avgtot_ow_mob4(avetot_ow_mob4, ptot_ow_mob, ring_ow_mob4, WRing,
        Radius, rw, fout, time_days);
}

if(MOBILITY_TYPE == 2)
{
    calc_avgtot_ow_mob1(avetot_ow_mob1, ptot_owg_mob, ring_ow_mob1, WRing,
        Radius, rw, fout, time_days);
    calc_avgtot_ow_mob2(avetot_ow_mob2, ptot_owg_mob, ring_ow_mob2, WRing,
        Radius, rw, fout, time_days);
    calc_avgtot_ow_mob3(avetot_ow_mob3, ptot_owg_mob, ring_ow_mob3, WRing,
        Radius, rw, fout, time_days);
    calc_avgtot_ow_mob4(avetot_ow_mob4, ptot_owg_mob, ring_ow_mob4, WRing,
        Radius, rw, fout, time_days);
}

// check for pattern conversion parameters

if(time_days >= CONV_TIME)
{
    PATTERN_TYPE = PATTERN_TYPE2;
}

// calculate average producing O+W mobility
// inv 9 spot calculations
if(PATTERN_TYPE == 3)
{
    pD = 7.547;
    Skin_prod_ave =
(Skin1*avetot_ow_mob1/(pD+Skin1)+Skin2*avetot_ow_mob2/(pD+Skin2)+Skin3*avetot_ow_mob3/(pD+Skin3))
    /(avetot_ow_mob1/(pD+Skin1)+avetot_ow_mob2/(pD+Skin2)+avetot_ow_mob3/(pD+Skin3));

    Skin_inj_ave = Skin4;

    PI_tilde_mult=(pD + Skin_inj_ave)/(pD + Skin_prod_ave);

    PI = 3*PI_tilde_mult;
    Mtp = (avetot_ow_mob1*weight_corner + avetot_ow_mob2*weight_side +
        avetot_ow_mob3*weight_side);
    Mti = (avetot_ow_mob4)/1;

    Mt = Mti/Mtp;
}

// normal 9 spot calculations
if(PATTERN_TYPE == 4)
{
    PI = 0.333333*PI_tilde_mult;
    Mti = (avetot_ow_mob1 + avetot_ow_mob2 + avetot_ow_mob3)/3;
    Mtp = (avetot_ow_mob4)/1;

    Mt = Mti/Mtp;
}

```

```

// 5 spot calculations
// calculate average producing O+W mobility
if(PATTERN_TYPE == 1)
{
    PI = 1*PI_tilde_mult;
    Mtp = (avetot_ow_mob2 + avetot_ow_mob3)/2;
    Mti = (avetot_ow_mob1 + avetot_ow_mob4)/2;

    Mt = Mti/Mtp;
}

// direct line drive calculations
// calculate average producing O+W mobility
if(PATTERN_TYPE == 2)
{
    PI = 1*PI_tilde_mult;
    Mtp = (avetot_ow_mob1 + avetot_ow_mob3)/2;
    Mti = (avetot_ow_mob2 + avetot_ow_mob4)/2;

    Mt = Mti/Mtp;
}

// calculate average reservoir pressure

Pbar_calc = (Mt*Pwfi + PI*Pwfp)/(Mt + PI);

// output results
if(Pbcounter == 2)
{
    fout << " " << time_days << " " << strpavg << " " << Mtp << " " << Mti << " " <<
    Mt << " " << Pbar_calc << " " << qo << " " << wcut << " " << qinj << " " << PI <<
    " " << avetot_ow_mob1 << " " << avetot_ow_mob2 << " " << avetot_ow_mob3 << " " <<
    avetot_ow_mob4 << " " << Skin_prod_ave << " " << Skin_inj_ave << endl;
}

Pbcounter = 2;

if(outflag_pbar == 1)
{
    double pbhp = 0.0;
    if(time_days >= out_days_min && time_days <= out_days_max)
    {
        fout3 << "At time = " << time_days << " days, the pressure array is " << endl;
        fout3 << " X      Y      Pressure " << endl;

        for(int i = 1; i < griddim+1; i++)
        {
            for(int j = 1; j < griddim+1; j++)
            {
                if(i == 1 && j == 1
                ||
                i == 1 && j == 41
                ||
                i == 41 && j == 1
                ||
                i == 41 && j == 41)
                {
                    if (pPr[i][j] - Pwfp > Pwfi - pPr[i][j])
                    {
                        pbhp = Pwfi;
                    }
                }
            }
        }
    }
}

```

```

        if (pPr[i][j] - Pwfp < Pwfi - pPr[i][j])
        {
            pbhp = Pwfp;
        }

        fout3 << " " << i-0.5 << " " << j - 0.5 << " " << pbhp << endl;
    }
    else
    {
        fout3 << " " << i-0.5 << " " << j - 0.5 << " " << pPr[i][j] <<
endl;
    }
}
}
}

if(outflag_totmob_vs_r == 1) // printout array of radius vs. totmob for se well
{
    double delta_rad = sqrt(pow(DX,2)+pow(DY,2));
    double radius = rw;
    fout3 << "At time = " << time_days << " days, the tot mob from well4 is " << endl;
    fout3 << "Effective total mobility is on next line " << endl;
    fout3 << avetot_ow_mob4 << endl;
    fout3 << "xcoord ycoord radius totmob " << endl;
    // output well cell 41 41
    fout3 << " " << griddim << " " << griddim << " " << radius << " " <<
        ptot_ow_mob[griddim][griddim] << endl;

    for(int z = 1; z < griddim/2; z++)
    {
        radius = z*delta_rad;
        fout3 << " " << griddim-z << " " << griddim-z << " " << radius << " " <<
            ptot_ow_mob[griddim-z][griddim-z] << endl;
    }
    fout3 << endl;
}

} // while(!fin.eof()) closing bracket

return 0;
}

// *****
// ***** FUNCTIONS *****
// *****

// get qo, watercut and qinj
void get_qo_and_qinj(char (*test_for_q)[150], char * qo, char * wcut, char * qinj,
                    ostream & fout, istream & fin)
{
    int counter = 1;
    int flag_done = 1;
    int index = 0;

```

```

while(flag_done != 0)
{
    fin >> test_for_q[counter];

    if (!strcmp(test_for_q[counter], "*****"))
    {
        index = (counter+3-25)+(1-(counter+3-1)/25)*25;
        strcpy(qo, test_for_q[index]);

        index = (counter+5-25)+(1-(counter+5-1)/25)*25;
        strcpy(wcut, test_for_q[index]);

        index = (counter+7-25)+(1-(counter+7-1)/25)*25;
        strcpy(qinj, test_for_q[index]);

        flag_done = 0;

        //          fout << "qo = " << qo << endl;
        //          fout << "watercut = " << wcut << endl;
        //          fout << "qinj = " << qinj << endl;

    }

    if(counter == 25)
        counter = 0;
    counter++;
}

// get to X=
void get_pavg_step1(istream & fin, char * test1, char * strpavg)
{
    int counter = 0;
    int counterpavg = 0;

    while (!fin.eof() && counterpavg < 19)
    {
        fin >> test1;
        if (!strcmp(test1, "REGION"))
        {
            cout << "string " << test1 << " encountered " << endl;
            counter++;
            //          cout << counter << endl;
        }

        if (counter == 4)
        {
            //          cout << "REGION #4 encountered " << endl;
            if (++counterpavg == 19)
            {
                //          fin >> strpavg;
                //          cout << "Average Pressure = " << strpavg << endl;
                //          if(fin.fail())
                //          {
                //              cerr << "input of average pressure failed!" << endl;
                //              fin.clear();
                //              fin >> test1;
                //              EXIT.FAILURE();
                //          }
            }
        }
    }
}

```

```

    }
}

void get_time_days_step2(istream & fin, char * test1, double & time_days)
{
    int flag = 0;
    while (!fin.eof() && flag == 0)
    {
        fin >> test1;
        if (!strcmp(test1, "TIME="))
        {
            //          cout << "string " << test1 << " encountered " << endl;
            //          cout << test1 << endl;
            fin >> time_days;
            flag = 1;
        }
    }
}

// go to the next X=
void get_to_data_step3(istream & fin, char * test1, ostream & fout, int & j, int & i, int & first_i)
{
    int setflagZ = 0;
    int setflagXEQ = 0;
    int flag_start_data = 0;
    int index_i = 0;
    int index_j = 0;

    while (!fin.eof() && flag_start_data == 0)
    {
        fin >> test1;
        if (!strcmp(test1, "Z"))
        {
            //          setflagZ = 1;
            //          fout << "Z flag set " << endl;
        }

        if (setflagZ == 1)
        {
            if (!strcmp(test1, "X="))
            {
                //          setflagXEQ = 1;
                //          fout << "X = flag set " << endl;
                //          fin >> index_i;
                //          cout << "index_i = " << index_i << endl;
                //          first_i = index_i;
            }
        }

        if (setflagZ == 1 && setflagXEQ == 1)
        {
            if (!strcmp(test1, "="))
            {
                //          fin >> index_j;
                //          if (fin.fail())
                //              cerr << "input in get_to_data sub failed " << endl;
                //          cout << "end of line encountered - index_j = " << index_j << endl;
                //          flag_start_data = 1;
            }
        }
    }
}

```

```

        cout << "Start of Data Arrays " << endl;
    }
}
}
j = index_j;
}

// get data from array
void get_data_arr_step4(istream & fin, double (*pdoub)[griddim+1], char * test1,
                      ostream & fout)
{
    int first_i = 1;
    int trash = 0;
    int i = 0;
    int j = 0;
    int counter = 0;
    double temp_doub = 0.0;
    for(j = 1; j < griddim+1; j++)
    {
        for(i = 1; i < griddim+1; i++)
        {
            fin >> temp_doub;

            if(fin.fail())
            {
                //          fout << "input failed " << endl;
                //          cerr << "input failed " << endl;
                //          fin.clear();

                get_back_to_arrdata(fin, test1, fout, j, i, first_i); // bypass non data, reassign j
                i = first_i;
                //          cout << "j = " << j << endl;
                //          cout << "i = " << i << endl;
                //          fin >> temp_doub;
                //          cout << "correct input val is " << temp_doub << endl;
            }
            pdoub[i][j] = temp_doub;

            //          if(time_days == 3272)
            //          {
            //              //          fout << "arr[" << i << "]"[" << j << "] = " << pdoub[i][j] << endl;
            //          }
        }
    }
    //          fout << endl;
    //          for(j = 0; j < griddim+1; j++)
    //          {
    //              for(i = 0; i < griddim+1; i++)
    //              {
    //                  //          fout << pdoub[j][i] << " ";
    //                  //          counter++;
    //                  //          if(counter == 15)
    //                  //          {
    //                      //          fout << endl;
    //                      //          fout << "arr[" << j << "]"[" << i << "] = " << pdoub[j][i] << endl;
    //                      //          counter = 0;
    //                  }
    //              }
    //          }

    //          get_to_data_step3(fin, test1, fout, j, i, first_i);
}

```

```

}

// clear bad input and get to point of next array input value
void get_back_to_arrdata(istream & fin, char * test1, ostream & fout, int & j, int & i, int & first_i)
{
    int index_j = 0;
    fin >> test1;
    fout << "next test1 value = " << test1 << endl;
    if(!strcmp(test1, "Y"))
    {
        fin >> test1;
        fin >> index_j; // get input value (the j index number)
        // cout << "index_j = " << index_j << endl;
        j = index_j;

        // cout << "end of line encountered - test1 = " << test1 << endl;
    }

    if(!strcmp(test1, "PLANE"))
    {
        // get_to_data_step3(fin, test1, fout, j, i, first_i);
        // cout << "Z value encountered - now going to data" << endl;
    }
}

// *****
// *****
void print_arr(double (*pdoub)[griddim+1], ostream & fout)
{
    int j = 0;
    int i = 0;
    int counter = 0;
    fout << endl;
    for(i = 1; i < griddim+1; i++)
    {
        for(j = 1; j < griddim+1; j++)
        {
            fout << "arr[" << i << "][" << j << "] = " << pdoub[i][j] << endl;
        }
    }
}

// calculate oil mobility
void calc_oil_mob(double (*pdoub)[griddim+1], double (*pkro)[griddim+1], double (*pviso)[griddim+1],
                 ostream & fout)
{
    int j = 0;
    int i = 0;
    int counter = 0;
    for(j = 1; j < griddim+1; j++)
    {
        for(i = 1; i < griddim+1; i++)
        {
            pdoub[i][j] = pkro[i][j]/pviso[i][j];
        }
    }
}

```

```

    }
}

// calc water mobility
void calc_water_mob(double (*pdoub)[griddim+1], double (*pkrw)[griddim+1], double (*pvisw)[griddim+1],
                  ostream & fout)
{
    int j = 0;
    int i = 0;
    int counter = 0;
    for(j = 1; j < griddim+1; j++)
    {
        for(i = 1; i < griddim+1; i++)
        {
            pdoub[i][j] = pkrw[i][j]/pvisw[i][j];
        }
    }
}

// calc gas mobility
void calc_gas_mob(double (*pdoub)[griddim+1], double (*pkrw)[griddim+1], double (*pvisg)[griddim+1],
                  ostream & fout)
{
    int j = 0;
    int i = 0;
    int counter = 0;
    for(j = 1; j < griddim+1; j++)
    {
        for(i = 1; i < griddim+1; i++)
        {
            pdoub[i][j] = pkrw[i][j]/pvisg[i][j];
        }
    }
}

// calc total oil + water mobility
void calc_ow_totmob(double (*pdoub)[griddim+1], double (*poil_mob)[griddim+1], double
                  (*pwater_mob)[griddim+1], ostream & fout)
{
    int j = 0;
    int i = 0;
    int counter = 0;
    for(j = 1; j < griddim+1; j++)
    {
        for(i = 1; i < griddim+1; i++)
        {
            pdoub[i][j] = poil_mob[i][j] + pwater_mob[i][j];
        }
    }
}

// calc total oil + water + gas mobility
void calc_owg_totmob(double (*pdoub)[griddim+1], double (*poil_mob)[griddim+1], double
                  (*pwater_mob)[griddim+1], double (*pgas_mob)[griddim+1], ostream &
fout)
{
    int j = 0;
    int i = 0;

```

```

int counter = 0;
for(j = 1; j < griddim+1; j++)
{
    for(i = 1; i < griddim+1; i++)
    {
        pdoub[i][j] = poil_mob[i][j] + pwater_mob[i][j] + pgas_mob[i][j];
    }
}

// *****
// calculate average tot mobility for well 1
void calc_avgtot_ow_mob1(double & avetot_ow_mob1, double (*ptot_ow_mob)[griddim+1],
                        double * ring_ow_mob1, double
                        (*WRing)[griddim+1][griddim+1],
                        double * Radius, double rw, ostream & fout, double time_days)
{
    if(AVERAGE_METHOD == 2)
    {
        avetot_ow_mob1 = (ptot_ow_mob[1][1] + ptot_ow_mob[1][2] + ptot_ow_mob[2][2] +
                        ptot_ow_mob[2][1] //)/4;
                        + ptot_ow_mob[1][3] + ptot_ow_mob[2][3] +
                        ptot_ow_mob[3][3] + ptot_ow_mob[3][2] + ptot_ow_mob[3][1])/9;
//
//
//
                        ptot_ow_mob[1][4] + ptot_ow_mob[2][4] + ptot_ow_mob[3][4] +
                        ptot_ow_mob[4][4] + ptot_ow_mob[4][3] + ptot_ow_mob[4][2] +
                        ptot_ow_mob[4][1]) / 16;
    }

    if(AVERAGE_METHOD == 1)
    {
        double SumDenom = 0.0; // denominator summation term for calc of ave tot mobility in
        int k = 0;
        int j = 0;
        int i = 0;
        init_ring_ow_mob(ring_ow_mob1, TOTRINGS);

        for(k = 2; k < TOTRINGS + 1; k++) // k is index of each ring
        {
            for(i = 1; i < TOTRINGS + 1; i++) // i is index of x cell direction
            {
                for(j = 1; j < TOTRINGS + 1; j++) //
                {
                    ring_ow_mob1[k] = WRing[k][i][j]*ptot_ow_mob[i][j] + ring_ow_mob1[k];
                    if(time_days == 3372)
                    {
                        fout << "WRing[" << k << "][" << i << "][" << j << "]=" <<
                        fout << "ring_ow_mob1[" << k << "] = " << ring_ow_mob1[k] <<
                    }
                }
            }
        }

        ring_ow_mob1[1] = ptot_ow_mob[1][1];

        for(k = 2; k < TOTRINGS + 1; k++)
        {
            SumDenom = SumDenom + log(Radius[k]/Radius[k-1])/ring_ow_mob1[k];
        }
    }
}

```

```

SumDenom = SumDenom + log(Radius[1]/rw)/ring_ow_mob1[1];

avetot_ow_mob1 = log(Radius[TOTRINGS]/rw)/SumDenom;

//      if(time_days == 3372)
//      {
//          fout << "avetot_ow_mob1 = " << avetot_ow_mob1 << endl;
//      }

}

//      fout << "Ave O+W tot mobility Well 1-1 = " << avetot_ow_mob1 << endl;
//  }

// *****
// calculate average tot mobility for 9 cell near well for well 2
void calc_avgtot_ow_mob2(double & avetot_ow_mob2, double (*ptot_ow_mob)[griddim+1],
                        double * ring_ow_mob2, double
(*WRing)[griddim+1][griddim+1],
                        double * Radius, double rw, ostream & fout, double time_days)
{
    if(AVERAGE_METHOD == 2)
    {
        avetot_ow_mob2 = (ptot_ow_mob[1][41] + ptot_ow_mob[1][40] + ptot_ow_mob[2][40] +
                          ptot_ow_mob[2][41] // )/4;
                          + ptot_ow_mob[3][41] + ptot_ow_mob[3][40] +
                          ptot_ow_mob[3][39] + ptot_ow_mob[2][39] + ptot_ow_mob[1][39])/9;
//      ptot_ow_mob[1][38] + ptot_ow_mob[2][38] + ptot_ow_mob[3][38] +
//      ptot_ow_mob[4][38] + ptot_ow_mob[4][39] + ptot_ow_mob[4][40] +
//      ptot_ow_mob[4][41]) / 16;
    }

    if(AVERAGE_METHOD == 1)
    {
        double SumDenom = 0.0; // denominator summation term for calc of ave tot mobility in
        int k = 0;
        int j = 0;
        int i = 0;
        init_ring_ow_mob(ring_ow_mob2, TOTRINGS);

        for(k = 2; k < TOTRINGS + 1; k++) // k is index of each ring
        {
            for(i = 1; i < TOTRINGS + 1; i++) // i is index of x cell direction
            {
                for(j = 1; j < TOTRINGS + 1; j++) //
                {
                    ring_ow_mob2[k] = WRing[k][i][41-j+1]*ptot_ow_mob[i][41-j+1] +
                                      ring_ow_mob2[k];
//      if(time_days == 3372)
//      {
//          fout << "WRing[" << k << "]"[" << i << "]"[" << 41-j+1 << "] = " <<
//      WRing[k][i][41-j+1] << endl;
//          fout << "ring_ow_mob2[" << k << "] = " << ring_ow_mob2[k] <<
//      endl;
//      }
                }
            }
        }
    }
}

```

```

ring_ow_mob2[1] = ptot_ow_mob[1][41];

for(k = 2; k < TOTRINGS + 1; k++)
{
    SumDenom = SumDenom + log(Radius[k]/Radius[k-1])/ring_ow_mob2[k];
}

SumDenom = SumDenom + log(Radius[1]/rw)/ring_ow_mob2[1];

avetot_ow_mob2 = log(Radius[TOTRINGS]/rw)/SumDenom;

//
// if(time_days == 3372)
// {
//     fout << "avetot_ow_mob2 = " << avetot_ow_mob2 << endl;
// }

}

//
// fout << "Ave O+W tot mobility Well 1-41 = " << avetot_ow_mob2 << endl;
//
}

// *****
// calculate average tot mobility for 9 cell near well for well 3
void calc_avgtot_ow_mob3(double & avetot_ow_mob3, double (*ptot_ow_mob)[griddim+1],
                        double * ring_ow_mob3, double
                        (*WRing)[griddim+1][griddim+1],
                        double * Radius, double rw, ostream & fout, double time_days)
{
    if(AVERAGE_METHOD == 2)
    {
        avetot_ow_mob3 = (ptot_ow_mob[41][1] + ptot_ow_mob[40][1] + ptot_ow_mob[40][2] +
                        ptot_ow_mob[41][2] //)/4;
                        + ptot_ow_mob[41][3] + ptot_ow_mob[40][3] +
                        ptot_ow_mob[39][3] + ptot_ow_mob[39][2] + ptot_ow_mob[39][1])/9;
//
// ptot_ow_mob[38][1] + ptot_ow_mob[38][2] + ptot_ow_mob[38][3] +
// ptot_ow_mob[38][4] + ptot_ow_mob[39][4] + ptot_ow_mob[40][4] +
// ptot_ow_mob[41][4]) / 16;
    }

    if(AVERAGE_METHOD == 1)
    {
        double SumDenom = 0.0; // denominator summation term for calc of ave tot mobility in
        int k = 0;
        int j = 0;
        int i = 0;
        init_ring_ow_mob(ring_ow_mob3, TOTRINGS);

        for(k = 2; k < TOTRINGS + 1; k++) // k is index of each ring
        {
            for(i = 1; i < TOTRINGS + 1; i++) // i is index of x cell direction
            {
                for(j = 1; j < TOTRINGS + 1; j++) //
                {
                    ring_ow_mob3[k] = WRing[k][41-i+1][j]*ptot_ow_mob[41-i+1][j] +
                    ring_ow_mob3[k];
                    if(time_days == 3372)
                    {
                        fout << "WRing[" << k << "][" << 41-i+1 << "][" << j << "] = " <<
                        WRing[k][41-i+1][j] << endl;
                    }
                }
            }
        }
    }
}

```

```

endl; //                                     fout << "ring_ow_mob3[" << k << "]" = " << ring_ow_mob3[k] <<
//                                     }
//                                     }
}
ring_ow_mob3[1] = ptot_ow_mob[41][1];
for(k = 2; k < TOTRINGS + 1; k++)
{
    SumDenom = SumDenom + log(Radius[k]/Radius[k-1])/ring_ow_mob3[k];
}
SumDenom = SumDenom + log(Radius[1]/rw)/ring_ow_mob3[1];
avetot_ow_mob3 = log(Radius[TOTRINGS]/rw)/SumDenom;

//     if(time_days == 3372)
//     {
//         fout << "avetot_ow_mob3 = " << avetot_ow_mob3 << endl;
//     }
}

//     fout << "Ave O+W tot mobility Well 41-1 = " << avetot_ow_mob3 << endl;
}

// *****
// calculate average tot mobility for 9 cell near well for well 4
void calc_avgtot_ow_mob4(double & avetot_ow_mob4, double (*ptot_ow_mob)[griddim+1],
                        double * ring_ow_mob4, double
(*WRing)[griddim+1][griddim+1],
                        double * Radius, double rw, ostream & fout, double time_days)
{
    if(AVERAGE_METHOD == 2)
    {
        avetot_ow_mob4 = (ptot_ow_mob[41][41] + ptot_ow_mob[40][41] + ptot_ow_mob[40][40] +
                        ptot_ow_mob[41][40] // )/4;
                        + ptot_ow_mob[41][39] + ptot_ow_mob[40][39] +
                        ptot_ow_mob[39][39] + ptot_ow_mob[39][40] + ptot_ow_mob[39][41])/9;
//     ptot_ow_mob[38][41] + ptot_ow_mob[38][40] + ptot_ow_mob[38][39] +
//     ptot_ow_mob[38][38] + ptot_ow_mob[39][38] + ptot_ow_mob[40][38] +
//     ptot_ow_mob[41][38]) / 16;
    }

    if(AVERAGE_METHOD == 1)
    {
        double SumDenom = 0.0; // denominator summation term for calc of ave tot mobility in
        int k = 0;
        int j = 0;
        int i = 0;
        init_ring_ow_mob(ring_ow_mob4, TOTRINGS);

        for(k = 2; k < TOTRINGS + 1; k++) // k is index of each ring
        {

```



```

double dA = 0;

double increment = 0.001;      // divide up numerical integration into this

init_3DArray(WRing, griddim);
double * RingArea = new double [TOTRINGS+1];
double (*RingCellArea)[TOTRINGS+1][TOTRINGS+1] = new double [TOTRINGS+1][TOTRINGS+1][TOTRINGS+1];
init_3DArray2(RingCellArea, TOTRINGS);
double (*NW_Cell)[TOTRINGS+1] = new double[TOTRINGS+1][TOTRINGS+1];
double (*SE_Cell)[TOTRINGS+1] = new double[TOTRINGS+1][TOTRINGS+1];

double ro = 0.28*pow((pow(DX,2) + pow(DY,2)),0.5)/2;

calc_Ring_Radius(Radius, ro, TOTRINGS, DX, fout2);
calc_NW_Cell(NW_Cell, DX, DY, TOTRINGS);
calc_SE_Cell(SE_Cell, DX, DY, TOTRINGS);

// calculate ring areas
for(k = 1; k < TOTRINGS + 1; k++)
{
    if(k == 1)
        RingArea[k] = 3.14159*(pow(Radius[k],2))/4;    // quarter circle
    else
        RingArea[k] = 3.14159*(pow(Radius[k],2) - pow(Radius[k-1],2))/4;
    fout2 << "RingArea[" << k << "] = " << RingArea[k] << endl;
}

for(k = 2; k < TOTRINGS + 1; k++)    // k is index of each ring
{
    for(i = 1; i < TOTRINGS + 1; i++)    // i is index of x cell direction
    {
        for(j = 1; j < TOTRINGS + 1; j++)    //
        {
            // case tests in 1, 2, 3 order

            if( (SE_Cell[i][j] >= Radius[k-1] && Radius[k] >= SE_Cell[i][j])
                ||
                (NW_Cell[i][j] >= Radius[k-1] && Radius[k] >= NW_Cell[i][j])
                ||
                (Radius[k-1] >= NW_Cell[i][j] && Radius[k] <= SE_Cell[i][j]) )
            {
                dA = 0;

                XMAX_Cell = (i-1)*DX + DX/2;
                YMAX_Cell = (j-1)*DY + DY/2;

                if(i == 1)
                    XMIN_Cell = 0.0;
                if(j == 1)
                    YMIN_Cell = 0.0;
                if(i == 2)
                    XMIN_Cell = DX/2;
                if(j == 2)
                    YMIN_Cell = DY/2;
                if(i > 2)
                    XMIN_Cell = (i - 2)*DX + DX/2;
                if(j > 2)
                    YMIN_Cell = (j - 2)*DY + DY/2;
            }
        }
    }
}

```

```

// case 3 - both contours of ring lie within cell
if(Radius[k-1] > NW_Cell[i][j] && Radius[k] < SE_Cell[i][j])
{
    fout2 << "Cell [" << i << "]"[" << j << "] meets case 3 criteria for
    cout << "Cell [" << i << "]"[" << j << "] meets case 3 criteria for

    for(m = 1; m < 1.0/increment; m++)
    {
        if(i == 1)
            X = XMIN_Cell + m*increment*DX/2;
        else
            X = XMIN_Cell + m*increment*DX;
        Y_RMIN = pow((pow(Radius[k-1],2) - pow(X,2)),0.5);
        Y_RMAX = pow((pow(Radius[k],2) - pow(X,2)),0.5);

        if(Y_RMIN <= YMIN_Cell)
            YMIN_Calc = YMIN_Cell;
        if(Y_RMIN > YMIN_Cell && Y_RMIN <=
YMAX_Cell)
            YMIN_Calc = Y_RMIN;
        if(Y_RMIN > YMAX_Cell)
            YMIN_Calc = YMAX_Cell;
        if(Y_RMAX <= YMAX_Cell && Y_RMAX >=
YMIN_Cell)
            YMAX_Calc = Y_RMAX;
        if(Y_RMAX <= YMIN_Cell)
            YMAX_Calc = YMIN_Cell;
        if(Y_RMAX > YMAX_Cell)
            YMAX_Calc = YMAX_Cell;

        if(i == 1)
            dA = increment*DX/2*(YMAX_Calc -
YMIN_Calc);
        else
            dA = increment*DX*(YMAX_Calc -
YMIN_Calc);

        RingCellArea[k][i][j] = RingCellArea[k][i][j] + dA;
    }
}

// case 1 - SE corner only of cell lies within ring
if(SE_Cell[i][j] >= Radius[k-1] && Radius[k] >= SE_Cell[i][j])
{
    fout2 << "Cell [" << i << "]"[" << j << "] meets case 1 criteria for
    cout << "Cell [" << i << "]"[" << j << "] meets case 1 criteria for

    for(m = 1; m < 1.0/increment; m++)
    {
        if(i == 1)
            X = XMIN_Cell + m*increment*DX/2;

```

```

else
    X = XMIN_Cell + m*increment*DX;
    Y_RMIN = pow((pow(Radius[k-1],2) - pow(X,2)),0.5);

    YMAX_Calc = YMAX_Cell;
    if(Y_RMIN >= YMAX_Cell)
        YMIN_Calc = YMAX_Cell;
    if(Y_RMIN > YMIN_Cell && Y_RMIN <
YMAX_Cell)
        YMIN_Calc = Y_RMIN;
    if(Y_RMIN <= YMIN_Cell)
        YMIN_Calc = YMIN_Cell;

    if(i == 1)
        dA = increment*DX/2*(YMAX_Calc -
YMIN_Calc);
    else
        dA = increment*DX*(YMAX_Calc -
YMIN_Calc);

    //
    //
    //
    Y_RMIN << endl;
    //
    << " YMAX_Calc = " << YMAX_Calc <<
    //
    //

    if(m == 75)
    {
        fout << "X = " << X << " Y_RMIN = " <<
        fout << "YMIN_Calc = " << YMIN_Calc
        " dA = " << dA << endl;
    }

    RingCellArea[k][i][j] = RingCellArea[k][i][j] + dA;
}

}

// case 2 - NW corner only of cell lies within ring
if(NW_Cell[i][j] >= Radius[k-1] && Radius[k] >= NW_Cell[i][j])
{
    fout2 << "Cell [" << i << "]" << j << "]" meets case 2 criteria for
    cout << "Cell [" << i << "]" << j << "]" meets case 2 criteria for

    for(m = 1; m < 1.0/increment; m++)
    {
        if(i == 1)
            X = XMIN_Cell + m*increment*DX/2;
        else
            X = XMIN_Cell + m*increment*DX;

        Y_RMAX = pow((pow(Radius[k],2) - pow(X,2)),0.5);

        YMIN_Calc = YMIN_Cell;
        if(Y_RMAX >= YMAX_Cell)
            YMAX_Calc = YMAX_Cell;
        if(Y_RMAX > YMIN_Cell && Y_RMAX <=
YMAX_Cell)
            YMAX_Calc = Y_RMAX;
        if(Y_RMAX <= YMIN_Cell)
            YMAX_Calc = YMIN_Cell;

```

```

YMIN_Calc);

YMIN_Calc);

//
//
//
<< " YMIN_Cell = " << YMIN_Cell << endl;
//
<< Y_RMAX << endl;
//
<< " YMAX_Calc = " << YMAX_Calc <<
//
//

if(i == 1)
    dA = increment*DX/2*(YMAX_Calc -
else
    dA = increment*DX*(YMAX_Calc -

if(m == 50)
{
    fout2 << "YMAX_Cell = " << YMAX_Cell
    fout2 << "X = " << X << " Y_RMAX = "
    fout2 << "YMIN_Calc = " << YMIN_Calc
    " dA = " << dA << endl;
}

RingCellArea[k][i][j] = RingCellArea[k][i][j] + dA;
}
}
}

// calculate weighting factors
for(k = 2; k < TOTRINGS + 1; k++) // k is index of each ring
{
    for(i = 1; i < TOTRINGS + 1; i++) // i is index of x cell direction
    {
        for(j = 1; j < TOTRINGS + 1; j++) //
        {
            WRing[k][i][j] = RingCellArea[k][i][j]/RingArea[k];

            // transpose to other grid corners
            WRing[k][41-i+1][j] = WRing[k][i][j];
            WRing[k][41-i+1][41-j+1] = WRing[k][i][j];
            WRing[k][i][41-j+1] = WRing[k][i][j];
        }
    }
}

// printout results of Areas
for(k = 1; k < TOTRINGS + 1; k++) // k is index of each ring
{
    for(i = 1; i < TOTRINGS + 1; i++) // i is index of x cell direction
    {
        for(j = 1; j < TOTRINGS + 1; j++) //
        {
            cout << " RingCellArea[" << k << "][" << i << "][" << j << "] = " <<
                RingCellArea[k][i][j] << endl;
            fout2 << " RingCellArea[" << k << "][" << i << "][" << j << "] = " <<
                RingCellArea[k][i][j] << endl;
        }
    }
}

```

```

// printout results of Weighting factors
for(k = 1; k < TOTRINGS + 1; k++) // k is index of each ring
{
    for(i = 1; i < TOTRINGS + 1; i++) // i is index of x cell direction
    {
        for(j = 1; j < TOTRINGS + 1; j++) //
        {
            cout << " WRing[" << k << "]"[" << i << "]"[" << j << "] = " <<
                WRing[k][i][j] << endl;
            fout2 << " WRing[" << k << "]"[" << i << "]"[" << j << "] = " <<
                WRing[k][i][j] << endl;
        }
    }

    for(i = 1; i < TOTRINGS + 1; i++) // i is index of x cell direction
    {
        for(j = 1; j < TOTRINGS + 1; j++) //
        {
            cout << " WRing[" << k << "]"[" << 41-i+1 << "]"[" << j << "] = " <<
                WRing[k][41-i+1][j] << endl;
            fout2 << " WRing[" << k << "]"[" << 41-i+1 << "]"[" << j << "] = " <<
                WRing[k][41-i+1][j] << endl;
        }
    }

    for(i = 1; i < TOTRINGS + 1; i++) // i is index of x cell direction
    {
        for(j = 1; j < TOTRINGS + 1; j++) //
        {
            cout << " WRing[" << k << "]"[" << i << "]"[" << 41-j+1 << "] = " <<
                WRing[k][i][41-j+1] << endl;
            fout2 << " WRing[" << k << "]"[" << i << "]"[" << 41-j+1 << "] = " <<
                WRing[k][i][41-j+1] << endl;
        }
    }

    for(i = 1; i < TOTRINGS + 1; i++) // i is index of x cell direction
    {
        for(j = 1; j < TOTRINGS + 1; j++) //
        {
            cout << " WRing[" << k << "]"[" << 41-i+1 << "]"[" << 41-j+1 << "] = " <<
                WRing[k][41-i+1][41-j+1] << endl;
            fout2 << " WRing[" << k << "]"[" << 41-i+1 << "]"[" << 41-j+1 << "] = " <<
                WRing[k][41-i+1][41-j+1] << endl;
        }
    }
}

void calc_Ring_Radius(double * Radius, double ro, int TOTRINGS, double DX,
                    ostream & fout)
{
    for(int i = 0; i < TOTRINGS+1; i++)
    {
        Radius[i] = DX*(i-1)+DX/2;
    }
}

```

```

        fout << "Radius[" << i << "] = " << Radius[i] << endl;
    }
}

void init_3DArray(double (*WRing)[griddim+1][griddim+1], int griddim)
{
    for(int k = 0; k < griddim+1; k++)
    {
        for(int i = 0; i < griddim+1; i++)
        {
            for(int j = 0; j < griddim+1; j++)
            {
                WRing[k][i][j] = 0.0;
            }
        }
    }
}

void init_3DArray2(double (*RingCellArea)[TOTRINGS+1][TOTRINGS+1], int TOTRINGS)
{
    for(int k = 0; k < TOTRINGS+1; k++)
    {
        for(int i = 0; i < TOTRINGS+1; i++)
        {
            for(int j = 0; j < TOTRINGS+1; j++)
            {
                RingCellArea[k][i][j] = 0.0;
            }
        }
    }
}

void init_ring_ow_mob(double * ring_ow_mob, int TOTRINGS)
{
    for(int i = 0; i < TOTRINGS + 1; i++)
    {
        ring_ow_mob[i] = 0.0;
    }
}

// calculate NW corners of each cell
void calc_NW_Cell(double (*NW_Cell)[TOTRINGS+1], double DX, double DY, int TOTRINGS)
{
    double XCALC = 0;
    double YCALC = 0;

    for(int i = 0; i < TOTRINGS+1; i++)
    {
        for(int j = 0; j < TOTRINGS+1; j++)
        {
            if(i == 1)
                XCALC = 0.0;
            if(j == 1)
                YCALC = 0.0;
            if(i == 2)
                XCALC = DX/2;
            if(j == 2)

```

```

        YCALC = DY/2;
    if(i > 2)
        XCALC = (i - 2)*DX + DX/2;
    if(j > 2)
        YCALC = (j - 2)*DY + DY/2;

    NW_Cell[i][j] = pow((pow(XCALC,2) + pow(YCALC,2)),0.5);
    }
}

// calculate SW corners of each cell
void calc_SE_Cell(double (*SE_Cell)[TOTRINGS+1], double DX, double DY, int TOTRINGS)
{
    double XCALC = 0;
    double YCALC = 0;

    for(int i = 0; i < TOTRINGS+1; i++)
    {
        for(int j = 0; j < TOTRINGS+1; j++)
        {
            XCALC = (i-1)*DX + DX/2;
            YCALC = (j-1)*DY + DY/2;
            SE_Cell[i][j] = pow((pow(XCALC,2) + pow(YCALC,2)),0.5);
        }
    }
}

```